Characterisation of Amyloid β Membrane Interaction Using Nanodiscs as a Model Membrane System

Inaugural-Dissertation

zur Erlangung des Doktorgrades
der Mathematisch-Naturwissenschaftlichen Fakultät
der Heinrich-Heine-Universität Düsseldorf

vorgelegt von

Maren Thomaier
aus Stuttgart

Düsseldorf, Januar 2016

Aus dem Institut für Physikalische Biologie
der Heinrich-Heine-Universität Düsseldorf

Gedruckt mit der Genehmigung der
Mathematisch-Naturwissenschaftlichen Fakultät der
Heinrich-Heine-Universität Düsseldorf

Referent: Prof. Dr. Dieter Willbold

Korreferent: Prof. Dr. Karl-Erich Jäger

Tag der mündlichen Prüfung: 09.02.2016

Fairy tales are more than true:

not because they tell us that dragons exist,

but because they tell us that dragons can be beaten

-G.K. Chesterton

Table of contents

List of Figures

List of Tables

1. Introduction

1.1 Alzheimer´s Disease

Alzheimer's disease (AD) is the most prominent neurodegenerative disease. It was first described by the German psychiatrist Alois Alzheimer in 1906 and subsequently named after him (Alzheimer 1911). Back then, Alzheimer already described characteristic symptoms such as confusion and cognitive decline as well as characteristic changes properties of AD-affected (Alzheimer 1911).

Despite extensive research over more than 100 years, the underlying molecular mechanism causing AD is still unknown. Furthermore, neither a definite *pre-mortem* diagnosis nor a medication to slowdown or cure the disease is available. Currently, only symptoms can be treated. In a continuously aging society AD is an increasing serious issue as the biggest risk factor is aging itself (Assoc 2015). Most cases of AD occur in patients older than 65 years. Only 4% of the AD patients are younger than 65 years (Assoc 2015).

AD is the most common form of dementia with 60 to 80 % of all cases (Katz, Lipton et al. 2012; Assoc 2015). The World Alzheimer Report 2015 states that worldwide 46.8 million people live with dementia and this number is expected to double every 20 years (Prince, Bryce et al. 2013). This tremendous increase in people suffering from dementia does not only have a high impact on patients and their relatives but is also a global public health challenge (Assoc 2015).

According to the WHO International Statistical Classification of Diseases and Related Health Problem (ICD-10) there are two types of AD: Type 1 is characterised by a late onset of the disease, after the age of 65. Type 2 is defined by an early onset of the disease, before the age of 65.

In addition to the differentiation according to the age of disease onset, there is familial AD and sporadic AD. While the first form is rather rare with a prevalence of 1% and caused by mutations in different genes, the cause of the sporadic AD is not known yet (Blennow, de Leon et al. 2006). The course of the disease varies considerable between patients and the life expectancy after the onset of Alzheimer´s disease is between three and eleven years (Helzner 2009; Rountree, Chan et al. 2012).

1.1.1 Neuropathology

Already Alois Alzheimer described neuropathological features of the disease such as military bodies (plaques) and dense bundles (tangles) in the brain of deceased AD patients (figure 1.1), which are today known as the hallmarks of the disease and allow its *post-mortem* diagnosis (Alzheimer 1911; Terry, Gonatas et al. 1964; Perl 2010). Synaptic and neuronal loss associated with volume reduction

(atrophy) in the hippocampus and cortex is a macroscopic feature of AD patients (Fox, Cousens et al. 2000; Kril, Hodges et al. 2004; Fotuhi, Hachinski et al. 2009).

The amyloid plaques, also known as senile or neuritic plaques, are extracellular, insoluble deposits mainly composed of the peptide amyloid beta (Aβ) (Perl 2010; Serrano-Pozo, Frosch et al. 2011). Amyloid plaques can be divided in diffuse and dense-core plaques by their morphology and negative or positive staining with Congo red and Thioflavin-S. While diffuse plaques are thought to occur in healthy elderly people, dense-core plaques are associated with deleterious effects on the neurons (Knowles, Wyart et al. 1999; Serrano-Pozo, Frosch et al. 2011).

Neurofibrillar tangles (NFT) are intraneuronal aggregates of the hyperphosphorylated protein tau. Tau is an essential factor in microtubule assembly (Weingarten, Lockwood et al. 1975) and its function is tightly regulated by phosphorylation (Stoothoff and Johnson 2005). NFTs also occur in the brains of healthy aging elderly people, but to a lower extend than in AD patients (Price and Morris 1999).

Both amyloid plaques and NFTs are first found in entorhinal cortex and hippocampal formations and spread to parietal, temporal and frontal association cortices at later stages of the disease. First lesions are found hippocampus and the association cortex, in the areas of poorly myelinated neurons. Both areas are associated with memory and learning. Highly myelinated neurons are affected at later stages of the disease (Braak, Del Tredici et al. 2000; Jahn 2013). The relationship of amyloid plaques and NFTs is not completely clear yet, but results indicate that a certain amyloid species triggers the formation of NFTs (King, Kan et al. 2006; Nussbaum, Schilling et al. 2012).

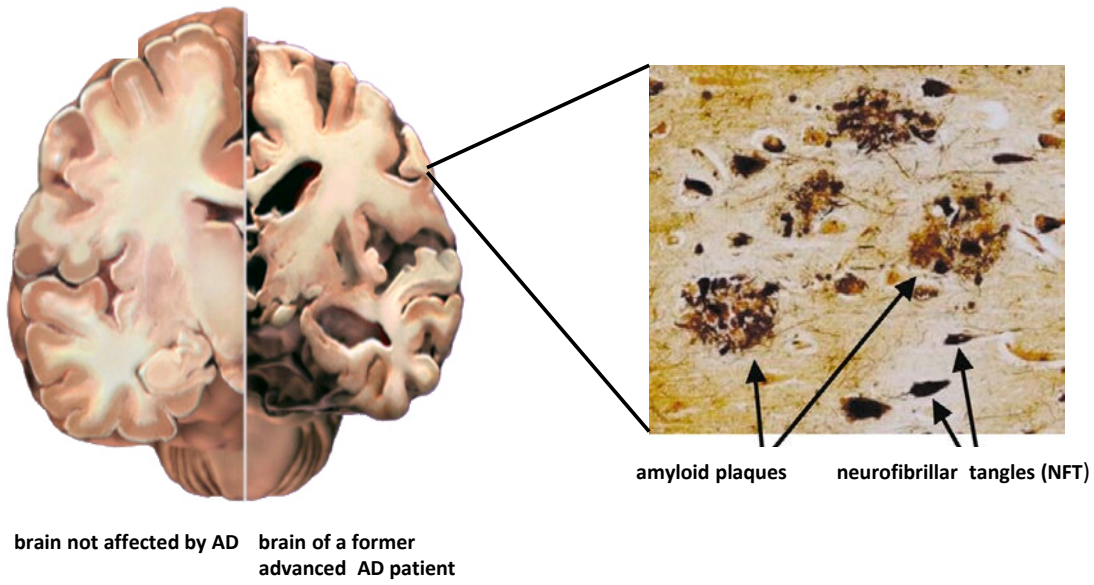

Figure 1.1: Schematic representation of AD pathology

Shown is a brain of an individual, not diseased of AD, in comparison to the brain of an advanced former AD patient. The AD affected brain is characterised by cerebral atrophy, amyloid plaques and neurofibrillar tangles (NFTs). Amyloid plaques and NFTs are marked with arrows. Modified from www.alz.org and (Blennow, de Leon et al. 2006).

1.1.2 From the Amyloid Precursor Protein to Amyloid β

In 1984, finding and determination of a partial amino acid sequence of a peptide, today known as amyloid beta (Aβ), together with determination of the full sequence one year later made the identification of the amyloid precursor protein (APP) possible (Glenner and Wong 1984; Masters, Simms et al. 1985; Kang, Lemaire et al. 1987).

APP is a glycosylated integral transmembrane protein encoded on chromosome 21. APP is ubiquitously expressed and different splice variants and posttranslational modifications are found (Kang, Lemaire et al. 1987; Selkoe 1998).

Two different APP processing pathways are known notably the anti-amyloidogenic and amyloidogenic pathway (figure 1.2). For the first one α-secretase(s) cleaves between residue 16 and 17 of the Aβ region resulting in a soluble APPs-α fragment and a membrane bound C-terminal fragment (CTF), C83. Further cleavage of the C83 by γ-secretase(s) results in 3 kDa fragment, p3 (Esch, Keim et al. 1990; Selkoe 1998). In the amyloidogenic pathway APP is cleaved in an analogous fashion by β-secretase generating the N-terminus of Aβ and by γ-secretase(s) generating the C-terminus of Aβ. γ-secretase cleavage occurs within the transmembrane region of CTF C99 resulting in different Aβ isoforms, the most common ones are Aβ(1-40) and Aβ(1-42). The mechanism is not fully understood but thought to occur by imprecise stepwise cleavage of the γ-secretases, a complex containing either presenilin 1 or 2 (Edbauer, Winkler et al. 2003; Takami, Nagashima et al. 2009). Moreover, several N-terminal truncated as well as modified versions are known, the two most

familiar ones are Aβ(4-42) and pEAβ(3-42) (Portelius, Bogdanovic et al. 2010; Kumar and Walter 2011). Their truncation is suspected to be caused by several secretory proteases (Leissring, Lu et al. 2003; Kummer and Heneka 2014).

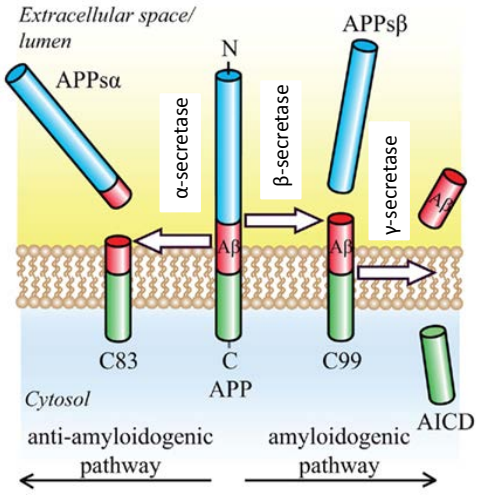

Figure 1.2: Schematic representation of anti-amyloidogenic and amyloidogenic processing of APP

In the anti-amyloidogenic pathway APP (displayed as a cylinder) is cleaved within the region of Aβ (red) by the α-secretase resulting in a soluble APPsα fragment and a membrane (brown) bound C-terminal fragment, C83. In the amyloidogenic pathway cleavage by γ- and β-secretase results in APPsβ, Aβ and a C-terminal fragment, AICD. All secretases are displayed as white arrows. Modified from (Dislich and Lichtenthaler 2012).

1.1.3 Physiological Role of Aβ and Aβ Aggregation

Expression and processing of APP to Aβ is a normal physiological pathway, therefore Aβ is found in liquor and in the brain of healthy people as well as AD patients (Haass, Schlossmacher et al. 1992; Shoji, Matsubara et al. 1998).

Several groups report a physiological role of Aβ in healthy humans. An antimicrobial activity has been shown for Aβ (Soscia, Kirby et al. 2010) as well as a physiological role in gene expression as a transcription factor for its own feedback regulation (Bailey, Maloney et al. 2011) and as repressor of two genes, *LRP1* and *KAI1*, (Barucker, Harmeier et al. 2014). Moreover, Aβ might be involved in cholesterol trafficking (Igbavboa, Sun et al. 2009).

Aβ has an amphipathic character with a hydrophilic N-terminus and a hydrophobic C-terminus, which is part of the membrane spanning domain of the precursor protein. Its propensity to aggregate is dependent on different factors such as temperature, pH and concentration but also on the isoform (chapter 1.1.2) (Stine, Dahlgren et al. 2003) and has been analysed *in vitro* by various groups (El-Agnaf, Mahil et al. 2000; Finder and Glockshuber 2007; Dammers, Gremer et al. 2015). Aβ(1-42) has a higher propensity to aggregate than Aβ(1-40), as the it has two additional hydrophobic amino acids at the C-terminus(El-Agnaf, Mahil et al. 2000). pEAβ(3-42) and pEAβ(3-40), which are lacking the first two amino acids and have a pyroglutamate at the N-terminus, show in turn a higher aggregation

propensity than Aβ(1-42) and Aβ(1-40) (Schlenzig, Manhart et al. 2009; Dammers, Gremer et al. 2015; Dammers, Gremer et al. 2015).

The analysis of the aggregation pathway of Aβ from the monomeric form over oligomeric species to Aβ fibrils is rather challenging (figure 1.3). Several species are only present in low concentrations in addition to a fast interconversion of the different species (Bruggink, Muller et al. 2012).

Despite the challenging task, several Aβ species have been detected *in vitro* as well as *in vivo* (Finder and Glockshuber 2007). Dependent on the isoform and the environment, monomers have been found in random coil, α-helical and β-sheet form. At physiological pH Aβ(1-42) adopts significantly faster a β-sheet structure from an initial random coil form than Aβ(1-39) (Barrow and Zagorski 1991). α-helical structures of Aβ have been detected in water alcohol mixtures or micelle solution (Shao, Jao et al. 1999; Crescenzi, Tomaselli et al. 2002; Dammers, Gremer et al. 2015). From monomers intracellular dimers (Walsh, Tseng et al. 2000) as well as small oligomers are formed. Latter ones are soluble and thought to exhibit the most neurotoxic effects (McLean, Cherny et al. 1999; Cleary, Walsh et al. 2005).

Next in size are rod like, soluble and with a high β-sheet content protofibrils. Those are found *in vitro* and thought to be the precursor molecules of fibrils (Harper and Lansbury 1997; Harper, Wong et al. 1997; Walsh, Hartley et al. 1999). Aβ fibrils, as other amyloid fibrils, have been characterised as thermodynamically stable, insoluble and composed of repeating β-sheet units (Ross and Poirier 2005). Fibrils found *in vitro* resemble those extracted from amyloid plaques in brains of AD patients (Kirschner, Inouye et al. 1987; Hilbich, Kisterswoike et al. 1992).

Different mechanisms are discussed for the aggregation of Aβ (Finder and Glockshuber 2007). A nucleation-dependent mechanism, in which an ordered nucleus or seed is required, is the most favoured one (figure 1.3). According to this mechanism Aβ molecules are incorporated after formation of the seed, which leads to growth. The rate limiting step is the formation of the seed, which is in accordance with an observed lag-phase in the formation of fibrils (Harper and Lansbury 1997; Harper, Wong et al. 1997; Petkova, Leapman et al. 2005).

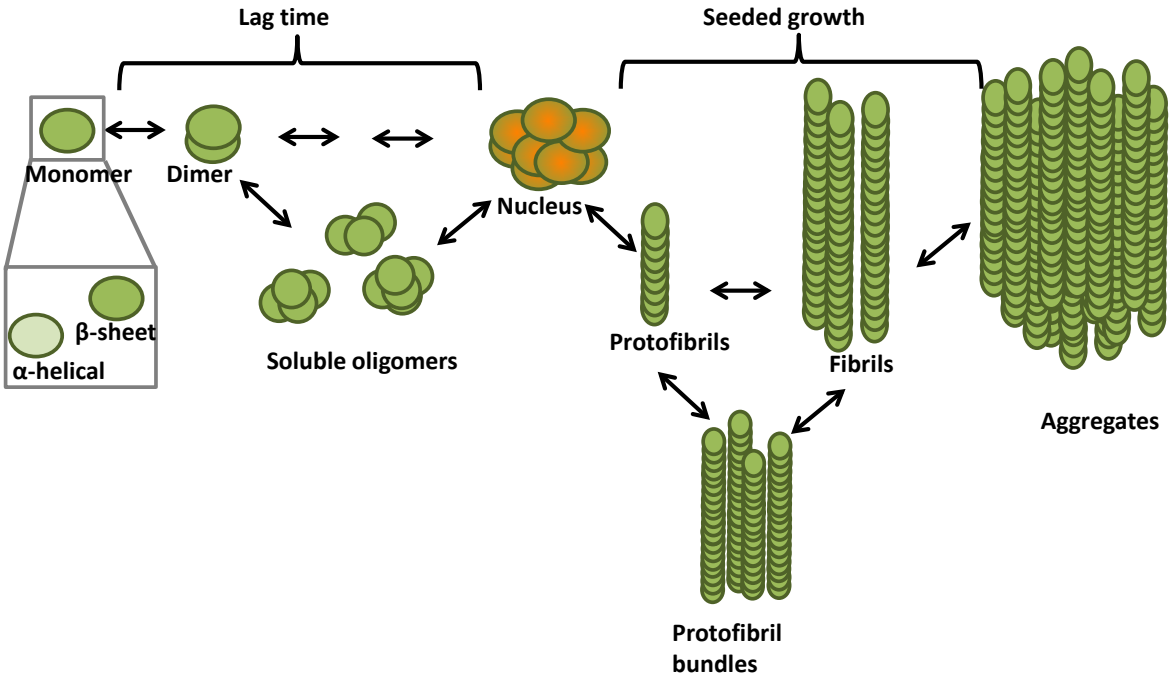

Figure 1.3: Schematic representation of Aβ aggregation

Aβ monomer is assumed to have an α-helical as well as a β-sheet conformation in solution. β-sheet structured Aβ is thought to favour the formation of dimers and soluble oligomers. After a lag phase, a nucleus is formed, which accelerates the generation of protofibrils and fibrils by a seeding mechanism. Modified from (Finder and Glockshuber 2007).

1.1.4 The Amyloid Cascade Hypothesis

The amyloid cascade hypothesis was first postulated by Hardy and Higgins in 1992 (Hardy and Higgins 1992). Since then, the hypothesis has been refined and updated as well as modified to the so-called amyloid hypothesis (Klein 2002). Originally, amyloid plaques were thought to be the most toxic agent, causing neurofibrillary tangles and neurodegeneration. Later results did not find a correlation of the amount of plaques with the disease (Klein 2002). Nowadays, soluble oligomeric Aβ species are thought to be the most toxic molecules (McLean, Cherny et al. 1999; Hardy and Selkoe 2002).

The imbalance between production and clearance of Aβ, causing an increase in the amount of Aβ, is the starting point of the disease according to the amyloid cascade hypothesis (figure 1.4). In case of familial AD mutations in the *APP* or presenilin genes and in case of sporadic AD ageing together with other risk factors lead to the increase in Aβ. In both cases the amount of oligomers as well as amyloid plaques increases. Whereby, the amount of soluble oligomers correlates with the loss of synapses and the severity of the disease (McLean, Cherny et al. 1999). Hyperphosphorylation of tau and the subsequent formation of NFTs as well as inflammatory response and oxidative stress are, according to this model, a downstream event of the increase in Aβ.

One has to keep in mind that the amyloid cascade hypothesis is a hypothesis supported by various results. Yet, an exact molecular mechanism for Aβ toxicity has not been found.

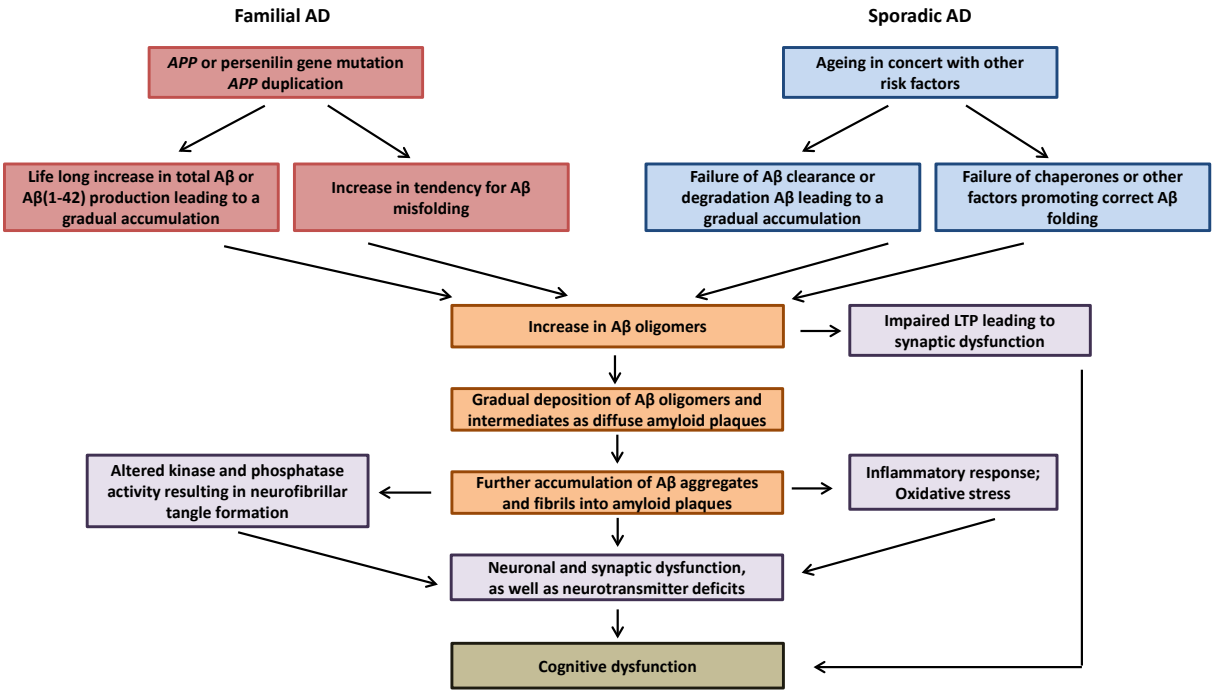

Figure 1.4: The amyloid cascade hypothesis

According to this hypothesis, the increase in Aβ oligomer concentration in familial AD as well as in sporadic AD is caused by an imbalance in production and clearance of Aβ or a misfolding of Aβ leading to a higher tendency of oligomerisation. All other symptoms such as amyloid plaques and NFTs, synaptic dysfunction, inflammatory response and oxidative stress are a result of the increase in Aβ oligomer concentration. Modified from (Blennow, Hampel et al. 2010).

1.1.5 Aβ Membrane Interaction

One possible explanation for Aβ toxicity is Aβ´s ability to interact with cell membranes. The mechanism of Aβ membrane interaction has not been completely elucidated yet. On the one hand the membrane can serve as starting point for Aβ nucleation and on the other hand the membrane is a target for toxic Aβ species, which disturb the cell ion homeostasis either by membrane pore formation or disrupting cell membranes (Kotler, Walsh et al. 2014; Yanagisawa 2015).

1.1.5.1 The Channel Hypothesis

Arispe and co-workers first demonstrated Aβ´s ability to form ion channels across bilayers *in vitro* (figure 1.5) (Arispe, Rojas et al. 1993). The features of the channel are cation selectivity and blockage by Zn^{2+}, suggesting a specific structure of the channel as well as explaining Ca^{2+} influx and dyshomeostasis as seen in AD pathogenesis (Arispe, Rojas et al. 1993; Lin, Zhu et al. 1999; Quist, Doudevski et al. 2005). The features are independent from chirality and stereospecificity, indicating a membrane protein independent mechanism. Not only L-peptides but also by D-peptides did form pores and exhibited ion channel behaviour as shown by electrophysiological recordings and atomic

force microscopy (Arispe, Rojas et al. 1993; Capone, Jang et al. 2012; Connelly, Jang et al. 2012). Furthermore, Aβ induced Ca^{2+} influx in fibroblasts, which led to their subsequent death. The dying of cells was inhibited by Zn^{2+} (Rhee, Quist et al. 1998; Zhu, Lin et al. 2000).

The Aβ species forming the channel has been biochemically analysed, revealing a predominantly monomeric species and forming stable trimers or hexamers after membrane insertion (Lin, Bhatia et al. 2001). Yet, little is known about the structure of Aβ forming the pore within the membrane. Modelling studies indicate a β-sheet rich conformation, in particular a U-shaped motif found in amyloid structures (Jang, Zheng et al. 2008; Strodel, Lee et al. 2010; Connelly, Jang et al. 2012).

1.1.5.2 The Role of Charged Lipid Head Groups in Aβ Membrane Interaction

The above mentioned channel formation was analysed in mixed anionic phosphatidylserine (PS) and neutral phosphatidylethanolamine (PE) lipid bilayers by electrophysiological recordings and AFM. Aβ was pre-incorporated in liposomes by mixing lipids with Aβ. Those liposomes were either composed of pure PS or a mixture of PS and PE (Arispe, Rojas et al. 1993; Capone, Jang et al. 2012).

Binding of Aβ preferentially to lipid membranes with anionic head groups is a recurring finding (Terzi, Holzemann et al. 1995; McLaurin, Franklin et al. 1997; Terzi, Holzemann et al. 1997; Ege and Lee 2004). Furthermore, CD analysis of liposomes with anionic headgroups titrated with Aβ reveals secondary structure changes in Aβ, induced by Aβ membrane interaction. A random coil to β-sheet transition upon interaction with negatively charged lipids has been observed (Terzi, Holzemann et al. 1995; McLaurin and Chakrabartty 1997; Terzi, Holzemann et al. 1997). The random coil to β-sheet transition was observed at low lipid to peptide ratio while at high lipid to peptide ratio a random coil to α-helix transition was found (figure 1.5). Together with other findings, this suggest membranes, especially negative charged ones, can accelerate fibrillisation at low lipid to peptide ratio or inhibit fibrillisation at high lipid to peptide ratio (Terzi, Holzemann et al. 1997; Butterfield and Lashuel 2010).

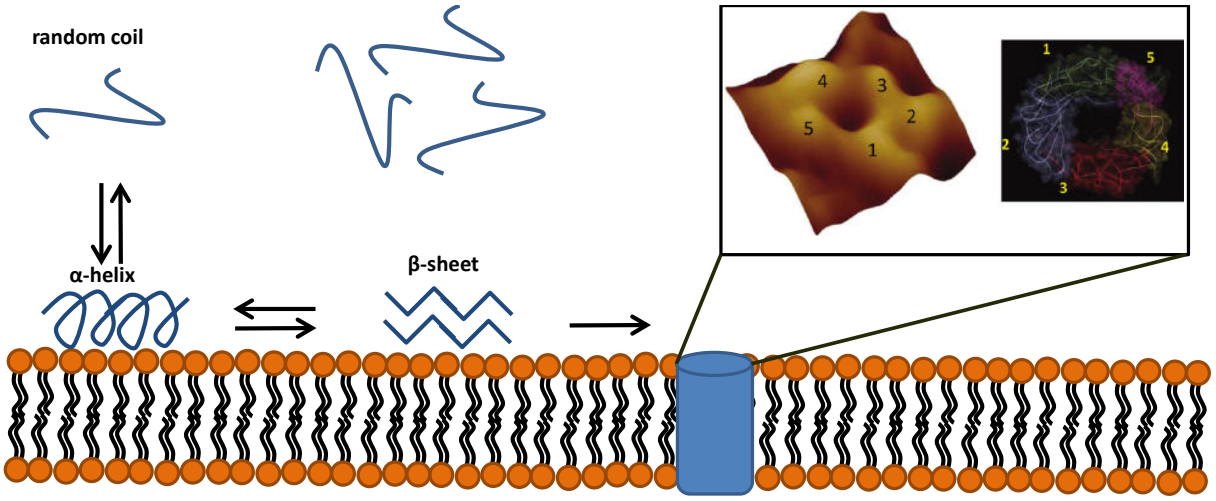

Figure 1.5: Schematic representation of a possible Aβ membrane interaction

Upon binding to membranes Aβ is thought to undergo a structural transition from random coil to α-helical conformation at a low peptide to lipid ratio whereas a transition to β-sheets is preferred at high ratios. Aβ is able to form pores in membranes (displayed by the blue cylinder). The exact mechanism of the pore formation as well as the structure of the pore are not yet elucidated. Yet, AFM images (brown) and modelled structures (coloured) are available. Modified from (Connelly, Jang et al. 2012).

Lee and co-workers showed, by using X-ray- and neutron-scattering techniques, that Aβ inserts spontaneously in anionic phosphatidylglycerol monolayers but not in neutral phosphatidylcholine monolayers. They further revealed that at a pH above 7.4 the interaction of anionic Aβ was abolished (Ege and Lee 2004; Chi, Ege et al. 2008). However, they and others further demonstrate interaction and insertion of Aβ with neutral and cationic lipid membrane, suggesting Aβ membrane interaction is not only driven by electrostatic interaction but also by hydrophobic interactions (Kremer, Sklansky et al. 2001).

Studies using a fluorescent labelled Aβ found an interaction of Aβ with anionic and cationic lipids at acidic and alkaline pH, respectively. Yet, under neutral conditions no interaction was observed indicating a mainly electrostatic interaction. In contrast, Aβ interaction with ganglioside GM1 containing liposomes was present at all conditions, suggesting a hydrogen-bonding as well as hydrophobic interactions of the sugar groups with Aβ lead to membrane binding (Ikeda and Matsuzaki 2008).

1.1.5.3 The Role of Ganglioside GM1

Gangliosides are a class of glycolipids with an anionic sialic acid headgroup. They cluster together with sphingomyelin and cholesterol in lipid rafts in the outer membrane leaflet. Gangliosides are predominantly found in neuronal cells (Tamai, Matsukaw.S et al. 1971; Allen, Halverson-Tamboli et al. 2007).

Yanagisawa *et al*. discovered in 1995 GM1-ganglioside-bound Aβ (GAβ) in AD patients brains. The altered unique molecular characteristics of GAβ led to the hypothesis that GAβ can serve as a seed for amyloid fibril formation (Yanagisawa, Odaka et al. 1995; Hayashi, Kimura et al. 2004; Yanagisawa 2015). CD experiments conducted by different groups revealed α-helical structure content of Aβ through binding to ganglioside containing liposomes at low Aβ to ganglioside ratio, 1:30 (Kakio, Nishimoto et al. 2001; Utsumi, Yamaguchi et al. 2009), while high Aβ to ganglioside ratio, 1:20, led to a mix of α-helical and β-sheet secondary structures (McLaurin, Franklin et al. 1998; Kakio, Nishimoto et al. 2001; Ikeda, Yamaguchi et al. 2011). A transition from α-helices to β-sheets is thought to be a crucial step in the formation of amyloid fibrils and a study from Lashuel and co-workers has shown that an "ongoing nucleated polymerisation process" is required for neurotoxicity (Jan, Adolfsson et al. 2011).

Kato and colleagues further conducted nuclear magnetic resonance (NMR) experiments of Aβ bound to GM1 gangliosides in micelles at low Aβ to ganglioside ratio (Utsumi, Yamaguchi et al. 2009; Yagi-Utsumi, Matsuo et al. 2010). The structure was not determined but backbone chemical shifts indicate that the ganglioside bound region forms partial α-helices (Utsumi, Yamaguchi et al. 2009). NMR titration experiments by Williamson *et al.* also revealed binding to GM1 ganglioside micelles, yet they propose a N-terminally driven binding which appears to contradict the C-terminally driven binding of Utsumi *et al*. (Williamson, Suzuki et al. 2006; Utsumi, Yamaguchi et al. 2009). However, one can explain this by a combined mechanism: an electrostatic N-terminal driven binding and a hydrophobic C-terminal binding of Aβ to ganglioside GM1 membranes (Utsumi, Yamaguchi et al. 2009; Kotler, Walsh et al. 2014).

A recent study from Sciacca *et al.* is bridging the GAβ and the amyloid channel hypothesis. They propose a two-step mechanism which is enhanced in the presence of gangliosides (i) formation of an ion selective pore by amyloid oligomers (ii) ongoing amyloid fibrillisation is disrupting the membrane in a detergent like manner (Sciacca, Kotler et al. 2012).

1.2 Lipid Model Membrane Systems

Cell membranes are complex systems composed of a lipid bilayer with regions of varying fluidity. Within the bilayer globular proteins, ion channels, glycoproteins and receptors are integrated. The complexity of the cell membrane reflects its various functions such as communication between intra- and intercellular compartments and selective transport in and out of the cell (Singer and Nicolson 1972).

Due to the complexity of biological membranes, scientists rely on less complex organised model membrane systems. These model systems allow systematically rearrangements of chemical composition as well as the fluidity in order to follow changes in protein membrane interaction and protein activity.

1.2.1 Vesicles, Micelles and Bicelles

Vesicles, also known as liposomes, are spherical lipid bilayers which are water-filled (figure 1.6). Three types of different size are common: 1) small unilamellar vesicles (SUV) with a diameter ranging from 20-50 nm 2) large unilamellar vesicles (LUV) with a diameter around 100 nm 3) giant unilamellar vesicles (GUV) with a diameter range of 1-10 µm (Chan and Boxer 2007; Butterfield and Lashuel 2010). All three types offer the possibility to introduce dyes in the water-filled interior, which makes them suitable for permeabilisation assays. Alternatively they can be used for Ca^{2+} leakage or Ca^{2+} uptake studies (Lin and Zhu 1999)

Micelles are detergent or lipid aggregates of a relatively small size of 5 nm, which are formed above the critical micelle concentration (CMC) of an amphiphilic molecule (figure 1.6). Their interior is formed by hydrocarbon tails of the lipid or detergent. Due to their relatively small size they are suitable for solution NMR spectroscopy. However, their high curvature is a potential disadvantage as it may impose not physiological relevant structures. In case of α-synuclein the peptide exhibits an extended α-helix when bound to LUV, whereas a binding to micelles leads to helix-turn-helix conformation (Ulmer, Bax et al. 2005; Jao, Hegde et al. 2008; Trexler and Rhoades 2009).

The high curvature of micelles can be diminished by mixing lipids in a specific molar ratio with a detergent in order to generate bicelles (bilayer micelle) (figure 1.6). Bicelles are disk like shaped with a flat lamellar surfaces and regions of high curvature. They may offer a more biological membrane mimetic than micelles. Truly, in case of α-synuclein, electron spin resonance (ESR) measurments revealed an extended α-helix upon bicelle binding (Georgieva, Ramlall et al. 2008). Bicelles are sufficiently small for solution NMR spectroscopy but they are heterogeneous in size, shape and combination of lipid and detergent (Prosser, Evanics et al. 2006; Raschle, Hiller et al. 2010).

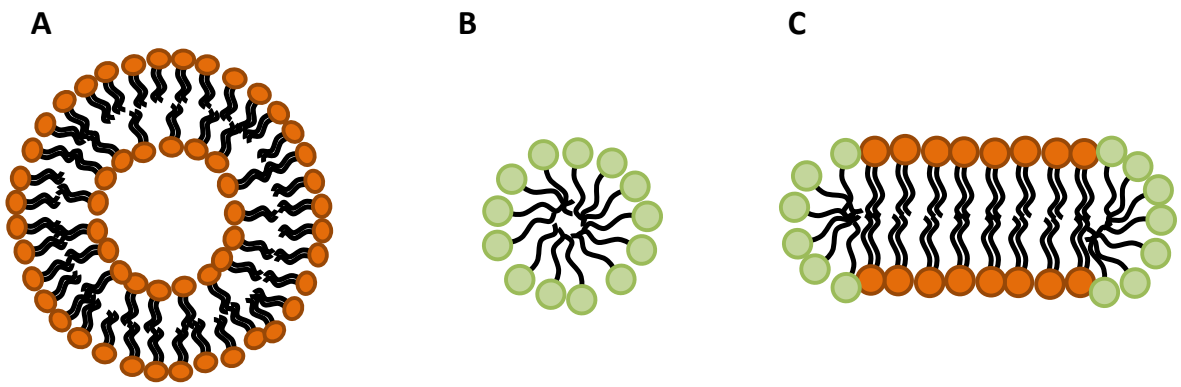

Figure 1.6: Schematic representation of model membrane systems

Lipid (orange) and detergent (green) molecules have a hydrophilic headgroup (circle) and a hydrophobic tail (black lines). A) unilamellar liposome B) detergent micelle C) bicelles. The proportions are not consistent with reality.

1.2.2 Nanodiscs

Nanodiscs are self-assembled discoidal model membrane systems composed of two copies of the membrane scaffold protein (MSP), which is surrounding a lipid bilayer (figure 1.7) (Bayburt, Grinkova et al. 2002). The MSP originates from the apolipoprotein A-I (Apo-A-I) (Bayburt, Carlson et al. 1998). The human Apo-A-I is an amphiphilic α-helical protein, which is part of the reverse cholesterol-transport from peripheral organs back to the liver. Two copies of the protein form together with phospholipids the nascent discoidal high density lipoprotein (ndHDL) particles, in which cholesterol is integrated and esterified by lecithin:cholesterol esterase resulting in the HDL (Ohashi, Mu et al. 2005).

Nanodisc are formed in a self-assembly process, therefore the MSP protein is mixed in a certain ratio with detergent solubilised lipids (figure 1.7). Upon slow removal of the detergent, the nanodisc is spontaneously formed. For the generation of the MSP, the globular N-terminal domain of Apo-A-I was deleted and a His-tag following a tobacco etch virus (TEV) protease cleavage site was introduced. One of the first synthetic genes constructed on the basis of Apo-A-I encodes MSP1, which forms a nanodisc with a diameter of approximately 10 nm (Bayburt and Sligar 2002; Denisov, Grinkova et al. 2004). By deletion of the DNA sequence encoding for 11 N-terminal amino acids of MSP1 the MSP1D1 constructs was generated (Denisov, Grinkova et al. 2004). Based on the MSP1D1 construct further smaller MSP variants were generated. One of them is the MSP1D1ΔH5. The protein is missing helix 5 and has a diameter of 9.2 nm according to Hagn *et al*. 2013. Further recombinant MSP variants, forming nanodiscs in a size range of 7 to 17 nm, were generated (Grinkova, Denisov et al. 2010; Hagn, Etzkorn et al. 2013).

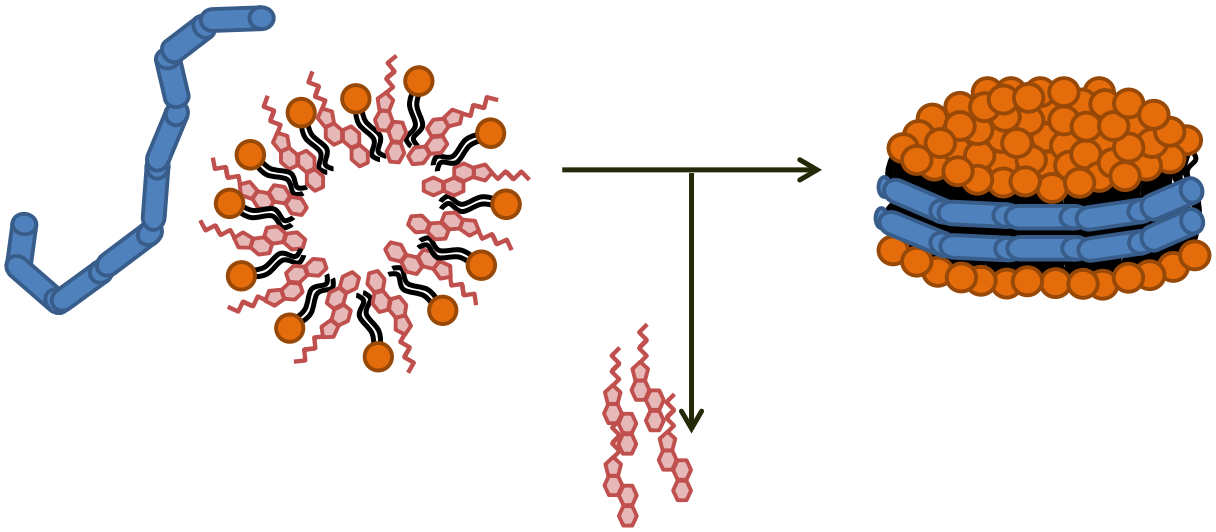

Figure 1.7: Schematic representation of nanodisc assembly

The nanodisc composed of two copies MSP (blue) surrounding a lipid bilayer (orange/black) is formed in a self-assembled process. Therefore detergent (pink) solubilised lipids are mixed in a certain ratio; upon slow removal of the detergent the nanodisc is formed.

Nanodiscs have several advantages in comparison to other membrane model systems. They provide a detergent free lipid bilayer and due to the surrounding MSP, they are homogenous in size and shape. In comparison to detergent micelles and bicelles they offer a more physiological membrane environment and have an improved homogeneity (Shaw, McLean et al. 2004). Moreover, due to the different available variants the size is adjustable and changes in lipid mixtures are easily achievable. Nanodiscs are stable over a wide temperature range and allow an analysis at higher temperature than liposomes (Nath, Atkins et al. 2007; Hagn, Etzkorn et al. 2013). In comparison to liposomes nanodisc have the advantage of a from both sides available lipid bilayer, yet they do not allow permeabilisation studies or analysis of ion channel activity.

Nanodiscs made several functional and structural methods, which were restricted to soluble proteins, available for membrane proteins (Borch and Hamann 2009). Several membrane proteins incorporated in nanodiscs have been shown to be suitable for solution NMR spectroscopy (Gluck, Wittlich et al. 2009; Ma, Mohrluder et al. 2010; Raschle, Hiller et al. 2010). Further, nanodiscs can be used to analyse interaction kinetics between a soluble ligand and a membrane protein by Surface Plasmon Resonance (SPR) (Borch and Hamann 2009; Gluck, Koenig et al. 2011).

1.3 Nuclear Magnetic Resonance Spectroscopy

Nuclear magnetic resonance (NMR) spectroscopy is a physical method, which can be used for the analysis of biomolecules. Atom nuclei with a magnetic dipole moment, which is energetically

separable in an external, static magnetic field, are used. The magnetic moment of atoms was first discovered by Otto Stern and Walther Gerlach (Gerlach and Stern 1922; Gerlach and Stern 1922). They discovered the deflection of silver atoms in an inhomogeneous magnetic field. This orientation of the magnetic moment of atom nuclei is used in NMR spectroscopy so that in 1946 first NMR spectroscopy experiments were conducted (Bloch, Hansen et al. 1946; Purcell, Torrey et al. 1946). Several improvements since the first NMR spectroscopy experiments have been introduced namely multidimensional NMR-Experiments and the Fourier-transformation-NMR-Spectroscopy (Aue, Bartholdi et al. 1976). Therefore, it is possible nowadays to resolve the structure of biological macromolecules. After alignment of the magnetic moments in the magnetic field, a radio frequency pulse is applied causing a disturbance of the alignment. After the pulse the spin systems return over time to the equilibrium state, measured in NMR spectroscopy. The NMR signal in the time domain can be observed as a superposition of sinewaves. Fourier transformation allows transforming the NMR signal of the time domain in to the frequency domain.

1.3.1 The Chemical Shift

Details as well as the definition of physical values and parameters are found in chapter 2.2.16.2.

The resonant frequency of an NMR active nucleus in relation to a standard substance is the chemical shift. As a first approximation one expects that for one isotope e.g. protons one resonance frequency (Larmor frequency) in a given magnetic field B_0. Yet, in a ^{1}H-spectrum of a protein one can observe in practice that the ^{1}H-NMR signals are distributed over a near frequency band and they differ several parts per million (ppm) from the Larmor frequency of a chosen reference substance. This distribution is caused by the local shielding of the nuclei from the external magnetic field B_0, which is due to the different electronic environment of a single nucleus. This means that all ^{1}H-nuclei of a protein with a similar environment have a comparable chemical shift. A one-dimensional (1D) proton spectrum of a folded protein shows in general a dispersion of -1 to 12 ppm. Signals of strongly shielded protons have low ppm values while high values are detected from weakly shielded protons.

In a 1D-spectrum of a folded globular protein the signals of H^{α}-protons are found between 4 and 6 ppm and the signals of the sidechains H^N are between 5.5 and 7.5 ppm. Additionally the signals of aromatic protons are found between 6 and 8 ppm besides the protons of the protein backbone, which are found between 6 and 10 ppm. This can cause overlay of signals. Analysis on an atomistic level is in most cases not possible; therefore two or three dimensional NMR spectroscopy is applied in order to separate signals from one dimensional NMR spectroscopy.

1.3.2 NMR Spectroscopy with Model Membrane Systems

In order to analyse a membrane protein or a membrane bound protein one has to use model membranes, such as SUV, micelles or nanodiscs. However, the size of the model membrane systems in addition to the size of the protein of interest as well as stability and homogeneity of the system makes structural analysis considerably more difficult than for a soluble protein of similar molecular weight.

Size is still a limiting factor in solution NMR spectroscopy. With size the temperature dependent rotational correlation time of a molecule increases. This causes an increased transversal relaxation rate, which leads to line broadening and eventually to a complete loss of the detected resonance signal. A 6 kDa complex for example has a rotational correlation time of 3.9 ns at 25 °C while a 95 kDa MSP1D1ΔH5 nanodisc at 45 °C has a rotational correlation time of 34 ns (Bobby, Medini et al. 2013; Hagn, Etzkorn et al. 2013).

However, usage of TROSY-pulse sequences (transverse relaxation optimized spectroscopy) allows an analysis of proteins with a molecular weight of 100 kDa and more (Pervushin, Riek et al. 1997). Several proteins in nanodiscs were analysed by solution NMR spectroscopy (Gluck, Wittlich et al. 2009; Ma, Mohrluder et al. 2010; Raschle, Hiller et al. 2010), yet it has been shown that high-resolution NMR structures are still difficult to obtain. Only through usage of the smaller MSP1D1ΔH5 nanodisc it was possible to achieve the structure of the transmembrane protein OmpX in a lipid bilayer by solution NMR spectroscopy (Hagn, Etzkorn et al. 2013).

The transverse relaxation time T2 is shorter in large molecules. This is caused by dipol-dipol couplings (DD) and the anisotropy of the chemical shift (CSA). The relaxation mechanisms DD and CSA are stronger in larger molecules than in small molecules, as their influence on relaxation is dependent on the Brownian motion (Pervushin, Riek et al. 1997). At high field strength, the frequency of the rotational diffusion is close to the Larmor frequency of ^{15}N-nuclei and the influence of DD and CSA on the relaxation increases. The four components of a detected correlation signal of a small protein without decoupling are of identical line width, due to the fast rotational diffusion. Upon decoupling a sharp signal is detected. For a large molecule however, the four components of the quartet are influenced differently by the relaxation mechanisms due to the slow rotational diffusion and the connected converge to the Larmor frequency. Therefore their *R2*-rates are different which leads to a broad signal upon decoupling which can disappear in the noise of the spectrum. By using a TROSY pulse sequence, only one of the four components is chosen. For this component the relaxation mechanisms almost cancel each other out and it has the slowest relaxation. This results in sharper signals, which increases the quality of spectra from proteins or molecules with a slow rotational diffusion.

1.4 Experimental Approach

As pointed out above interaction of Aβ with neuronal cell membranes plays a crucial role in the Alzheimer´s disease, the most common form of dementia. Upon binding to membranes the secondary structure of Aβ changes from random coil to α-helical or β-sheet depending amongst others on the lipid to peptide ratio. This structural change is thought to be a pivotal step in the formation of a toxic Aβ species and has been extensively studied by using liposomes. As liposomes and bicelles have several drawbacks regarding homogeneity and stability the aim of this work was to test nanodiscs for their suitability of Aβ interaction with membranes and characterise the interaction. Nanodiscs have an improved homogeneity and a higher stability than liposomes.

For studying Aβ membrane interaction two approaches were followed. On the one hand the assembly of nanodiscs with Aβ and on the other hand the assembly of empty nanodiscs with a subsequent incubation of Aβ. For the latter approach the assembly of nanodiscs with novel lipid raft mixtures, varying in their GM1 content was established. Those and nanodiscs with neutral as well as anionic phospholipids were used to study and compare Aβ membrane interactions with differently composed membranes by NMR spectroscopy, fluorescence titration (FT) and BioLayer Interferometry (BLI).

From FT and BLI experiments overall equilibration dissociation constants (K_D) for Aβ(1-40) binding to nanodiscs with different GM1 concentrations were obtained and compared. In order analyse possible differences in binding for Aβ(1-40) to Aβ(1-42) BLI studies were extended to Aβ(1-42). Of special interest is question which Aβ species binds to membranes. Therefore not only monomeric Aβ but also a defined oligomeric species were applied in BLI experiments in order to analyse the binding to GM1 nanodiscs.

2. Materials and Methods

2.1 Materials

2.1.1 Instruments

Table 2.1: List of used instruments

Instrument	Source
-80 °C freezer, HERAfreeze	Thermo Fischer Scientific, Massachusetts, USA
-20 °C freezer, no frost	Liebherr, Bergheim, Germany
4 °C fridge	Liebherr, Bergheim, Germany
30 °C/37 °C incubator, Unitron	Infors-HT, Bottmingen, Switzerland
ÄKTA purifier system	GE Healthcare, Freiburg, Germany
Centrifuges	
- 5417R	Eppendorf, Hamburg, Germany
- 5702R	Eppendorf, Hamburg, Germany
- 5804R	Eppendorf, Hamburg, Germany
- Avanti J-20 XP	Beckman Coulter, Brea, USA
- Optima MAX-XP benchtop ultracentrifuge	Beckman Coulter, Brea, USA
Cool trap	ZEA-1, FZJ, Germany
DynaPro dynamic light scattering system	Protein Solutions, Lakewood, USA
Gel documentation system ChemiDoc MP	Bio-Rad Laboratories Inc. ,Hercules, USA
Lyophyliser	
- Lyophile Alpha 1-4	Christ, Osterode am Harz, Germany
- Lyophile Alpha 2-4 LD plus	Christ, Osterode am Harz, Germany
LC 1200 series HPLC system	Agilent Technologies, Böblingen, Germany
LiposoFast-Basic extruder	Avestin, Mannheim, Germany
LKB FPLC system	GE Healthcare, Freiburg, Germany
Milli-Q-Biocell system	Merck, Darmstadt, Germany
ph-meter and pH-electrode	Mettler TOLEDO, Greifensee, Switzerland
Octet RED96 instrument	fortéBIO, PALL Life Science, Menlo Park, USA
Semi-micro balance CP225D	Sartorius, Göttingen, Germany
Shaker Unitron	Infors-HT, Bottmingen, Switzerland
Sonifier Branson 250	Branson Ultrasonics Corporation, Danbury, USA
Spectrometer	
- UV/VIS spectrophotometer Lambda 25	PerkinElmer Inc. Waltham, MA, USA
- UV/VIS spectrophotometer UV-1800	Shimadzu, Kyoto, Japan
- QuantaMaster40 spectrofluorometer	PTI, Birmingham, USA
Power supply EPS 1001	Amersham, San Francisco, USA
Trans Blot Turbo	Bio-Rad Laboratories Inc. ,Hercules, USA
Vacuum pump, D25E	Leybold, Cologne, Germany

2.1.2 Software Tools

Table 2.2: List of used software

Software	Source
ChemStation	Agilent, Böblingen, Germany
CorelDRAW X6	Corel Corporation, Ottawa, Canada
Dynamic V6	Protein Solutions, Lakewood, NJ, USA
FelixGX	Photon Technology International, Birmingham, USA
fortéBIO Data acquisition 8.1	fortéBIO, PALL Life Science, Menlo Park, USA
fortéBIO Data analysis 8.1	fortéBIO, PALL Life Science, Menlo Park, USA
Microsoft Office 2010	Microsoft Corporation, Redmond, USA
nmrDraw	(Delaglio, Grzesiek et al. 1995); 8.1
nmrPipe	(Delaglio, Grzesiek et al. 1995); 8.1
Origin 9.0G	OriginLab Corporation, Northhampton, USA
SigmaPlot for Windows Version 11.0	Systat Software GmbH, Erkrath, Germany
Unicorn 5.0	GE Healthcare, Little Chalfont, UK

2.1.3 Chemicals & Additives

In table 2.3 not listed chemicals were purchased from the companies AppliChem (Darmstadt, Germany), Sigma-Aldrich (Steinheim,Germany), Fluka (Neu-Ulm, Germany),Merck (Darmstadt, Germany) und Roth (Karlsruhe, Germany) in *pro analysis* or comparable quality.

Table 2.3: List of chemicals and additives

Chemical	Source
Acrylamid 4K solution (30 %) mix 29:1	AppliChem, Darmstadt, Germany
D_2O [99,990 %]	Sigma-Aldrich,Steinheim,Germany
Dithiothreitol (DTT)	AppliChem, Darmstadt, Germany
Isopropyl-β-D-Thiogalaktosid (IPTG)	Boehringer, Mannheim, Germany
Formaldehyde (36.5 %, p.a.)	Honeywell Specialty Chemicals Seelze GmbH, Seelze, Germany
Ni^{2+}-NTA-Agarose	Qiagen, Hilden, germany
β-Mercaptoethanol	Sigma-Aldrich, Steinheim, Germany

2.1.4 Consumable Supplies

Table 2.4: List of consumable supplies

Consumable	Source
Eppendorf UVette cuvettes Sigma-Aldrich, Munich	Sigma-Aldrich, Munich, Germany
Hamilton air-tight syringe	Hamilton, Reno, USA
Nuclepore track-etched polycarbonate membranes	GE Healthcare, Freiburg, Germany
Nitrocellulose membrane, protran BA83	GE Healthcare, Buckinghamshire, GB
Polyallomer Centrifuge Tubes (11x34 mm)	Beckman coulter, Passadena, USA
Quartz cuvette QS-105.251	Helma, Mülheim, Germany
Quartz cuvette QS-104F	Helma, Mülheim, Germany
Shigemi 5 mm symetric NMR micro tubes matched with ^2D_2O	Sigma Aldrich, Steinheim, Germany
Spectra/Pro Dialyseschlauch	Spectrumlabs, Los Angeles, USA
Super Streptavidin Biosensors (SSA)	fortéBIO, PALL Life Science, Menlo Park, USA
VIVAspin 20	Satorius, Göttingen, Germany
Whatman chromatography paper (3 mm)	GE Healthcare, Buckinghamshire, GB

2.1.5 Media & Buffers

If not stated otherwise MilliQ water (genetrated by MilliQ-system; water resistance 18,2 MΩ*cm) was used.

All buffers and media are listed in the following tables. Solutions and agar marked with an asterisk were autoclaved for 20 min at 121 °C.

Table 2.5: List of used media

Name	Components
LB-Media (Lysogenic Broth) *	10 g/l trypton, 5 g/l yeast extract, 5 g/l NaCl
LB-Agar*	10 g/l trypton, 5 g/l yeast extract, 5 g/l NaCl, 20g/l agar

Table 2.6: List of general buffers

Name	Components
PBS*	137 mM NaCl, 2.7 mM KCl, 1.8 mM KH_2PO_4, 10 mM Na_2HPO_4 x 2 H_2O
Tris pH 7.0*	1.5 mM Tris, pH adjusted with HCl
Tris pH 8.8*	1.5 mM Tris, pH adjusted with HCl
TBS*	136 mM NaCl, 2.7 mM KCl, 24.7 mM Tris, pH 7.4

Table 2.7: List of solutions for TEV protease purification

Name	Components
TEV-lysis buffer	20 mM Tris-HCl pH 8, 500 mM NaCl, 10 mM imidazole
TEV-elution buffer I	20 mM Tris-HCl pH 8, 500 mM NaCl, 10 % glycerol, 100 mM imidazole
TEV-elution buffer II	20 mM Tris-HCl pH 8, 500 mM NaCl, 10 % glycerol, 300 mM imidazole
TEV-elution buffer III	20 mM Tris-HCl pH 8, 500 mM NaCl, 10 % glycerol, 750 mM imidazole
TEV-SEC buffer	25 mM NaH_2PO_4/Na_2HPO_4, pH 8, 200 mM NaCl, 10 % glycerol, 2 mM EDTA, 10 mM DTT
TEV-storage buffer	50 mM Tris-HCl pH 8, 25 mM NaCl, 10 % glycerol, 0,5 mM EDTA, 2 mM DTT

Table 2.8: List of solutions MSP purification

Name	Components
MSP-lysis buffer	20 mM NaH_2PO_4/Na_2HPO_4, pH 7.4, Roche protease inhibitor, 1 % triton, 100 µg/ml lysozyme, DNase I
MSP wash buffer I	40 mM Tris-HCl pH 8, 300 mM NaCl, 1 % triton
MSP wash buffer II	40 mM Tris-HCl pH 8, 300 mM NaCl, 50 mM sodium cholate
MSP wash buffer III	40 mM Tris-HCl pH 8, 300 mM NaCl,
MSP wash buffer IV	40 mM Tris-HCl pH 8, 300 mM NaCl, 10 mM imidazole
MSP elution buffer I	40 mM Tris-HCl pH 8, 300 mM NaCl, 300 mM imidazole
MSP elution buffer II	40 mM Tris-HCl pH 8, 300 mM NaCl, 750 mM imidazole
TEV-cleavage buffer	50 mM Tris-HCl pH 8, 0.5 mM EDTA, 1 mM DTT
Ni-NTA-batch buffer	20 mM Tris-HCl pH 8, 150 mM NaCl, 50 mM sodium cholate
Ni-NTA-batch elution buffer	20 mM Tris-HCl pH 8, 150 mM NaCl, 50 mM sodium cholate, 750 mM imidazole

Table 2.9: List of solutions for SDS-PAGE after Laemmli (Laemmli 1970)

Name	Components
Stacking gel (5 %)	4.85 % (w/v) acrylamide , 0.15 % (w/v) N,N'-methyldisacrylamid, 125 mM Tris-HCl pH 6.8, 0.1 % (w/v) SDS, 0.1 % (v/v) APS, 0.1 % (v/v) TEMED
Running gel (12 %)	11.64 % (w/v) acrylamide , 0.36 % (w/v) N,N'-methyldisacrylamid, 375 mM Tris-HCl pH 6.8, 0.1 % (w/v) SDS, 0.1 % (v/v) APS, 0.1 % (v/v) TEMED
Running gel (15 %)	14.55 % (w/v) acrylamide, 0.45 % (w/v) N,N'-methyldisacrylamid, 375 mM Tris-HCl pH 6.8, 0.1 % (w/v) SDS, 0.1 % (v/v) APS, 0.1 % (v/v) TEMED
4 x Sample buffer	200 mM Tris-HCl pH 7.4, 40 % (v/v) glycerol, 8 % (w/v) SDS, 0.05 (w/v) bromphenolblue, 8 % β-mercaptoethanol
SDS-running buffer	50 mM Tris-HCl, pH 8.3, 0.1 % (w/v) SDS
Coomassie staining solution	25 % (v/v) isopropanol, 10 % (v/v) acetic acid, 0.5 g/l coomassie brilliant blue R-250

Table 2.10: List of solutions for SDS-PAGE after Schagger (Schagger 2006)

Name	Components
Stacking gel (4 %)	3.88 % (w/v) acrylamide, 0.12 % (w/v) N,N'-methyldisacrylamide, 1 M Tris-HCl pH 8.45, 0.1 % (w/v) SDS, 0.1 % (v/v) APS, 0.1 % (v/v) TEMED
Running gel (16.5 %)	16 % (w/v) acrylamide , 0.51 % (w/v) N,N'-methyldisacrylamide, 1 M Tris-HCl pH 8.45, 0.1 % (w/v) SDS, 0.1 % (v/v) APS, 0.1 % (v/v) TEMED
4 x Tris-Tricine sample buffer	4 % (w/v) SDS, 12 % (v/v) glycerol, 50 mM Tris-HCl, 2 % (v/v) β-mercaptoethanol, 0.01 % (w/v) SERVA BlueG, pH adjusted to 6.8
3 x Gel buffer	3 M Tris , 0.3 % (w/v) SDS; pH adjusted to 8.45
10 x Anode buffer	2 M Tris; pH adjusted to 8.9
10 x Cathode buffer	1 M Tris, 1M tricine, 1 % (w/v) SDS; pH adjusted to 8.25

Table 2.11: List of solutions for silver staining

Name	Components
Fixation solution	50 % (v/v) ethanol, 10 % (v/v) acetic acid
SDS-removing solution	10 % (v/v) ethanol, 5 % (v/v) acetic acid
Farmers reagent	4.72 mM Na_2CO_3, 4.07 mM $K_3Fe(CN)_6$, 18.97 mM $Na_2S_2O_3$
Staining solution	12 mM $AgNO_3$
Developing solution	280 mM Na_2CO_3, 0.05 % (v/v) formaldehyde
Stop-solution	1 % (v/v) acetic acid

Table 2.12: List of buffers used for Western Blot and Dot Blot

Name	Components
Anode buffer I	300 mM Tris-HCl, 10 % methanol pH 10.4 (add Methanol directly before use)
Anode buffer II	25 mM Tris-HCl, 10 % Methanol pH 10.4 (add Methanol directly before use)
Cathode buffer	25 mM Tris-HCl, 40 mM glycine pH 9.4
TBS*	136 mM NaCl, 2.7 mM KCl, 24.7 mM Tris, pH 7.4
Blocking buffer	TBS pH 7.4, 2 % BSA
Wash buffer	TBS, 0.1 % Tween 20

Table 2.13: List of solutions for nanodisc assembly

Name	Components
Lipid buffer	20 mM Tris-HCl pH 7.4, 100 mM sodium cholate
Assembly buffer	20 mM Tris-HCl pH 7.4, 100 mM NaCl, 0,5 mM EDTA
Nanodisc SEC buffer I	10 mM NaH_2PO_4/Na_2HPO_4, pH 7.4, 150 mM NaCl
Nanodisc SEC buffer II	10 mM NaH_2PO_4/Na_2HPO_4, pH 7.4, 50 mM NaCl
Nanodisc SEC buffer III	10 mM KH_2PO_4/K_2HPO_4, pH 7.2 0.5 mM EDTA

Table 2.14: List of IMAC buffers for Aβ nanodisc separation

Name	Components
Nanodisc SEC buffer I	10 mM NaH_2PO_4/Na_2HPO_4, pH 7.4, 150 mM NaCl
Aβ-IMAC wash buffer I	10 mM NaH_2PO_4/Na_2HPO_4, pH 7.4, 150 mM NaCl, 10 mM imidazole
Aβ-IMAC elution buffer I	10 mM NaH_2PO_4/Na_2HPO_4, pH 7.4, 150 mM NaCl, 300 mM imidazole
Aβ-IMAC elution buffer II	10 mM NaH_2PO_4/Na_2HPO_4, pH 7.4, 150 mM NaCl, 600 mM imidazole

Table 2.15: List of FT buffers

Name	Components
FT-high-salt-buffer	150 mM NaCl, 2 mM CaCl, 10 mM Tris pH 7.4 at 37 °C
FT-low-salt-buffer	30 mM KH_2PO_4/K_2HPO_4, pH 7.2, 0.5 mM EDTA

Table 2.16: List of BLI solutions

Name	Components
Running buffer	30 mM KH_2PO_4/K_2HPO_4, pH 7.2, 0.5 mM EDTA
Quenching solution	50 µg/ml biotin in PBS
Monomer wash solution	0.5 mM NaOH
Oligomer wash solution	1 mM guadinium-HCl

Table 2.17: List of NMR buffers

Name	Components
NMR-buffer I	50 mM NaCl, 10 mM NaH_2PO_4/Na_2HPO_4, pH 7.4
NMR-buffer II	10 mM KH_2PO_4/K_2HPO_4, pH 7.2 0.5 mM EDTA

2.1.6 Size Standards

Following size standards were used for SDS-PAGE. Size standards were obtained from Thermo Fisher Scientiffic, Massachusetts, USA or Sigma, Aldrich, Steineheim, Germany.

Table 2.18: List of size standards

Marker	Molecular weights
Unstained Protein Molecular Weight Marker	116; 66.2; 45; 35; 25; 18.4; 14.4 kDa
Multicolour Low Range Protein Ladder	40; 25; 10; 4.6; 1.7 kDa
Colour Marker Ultra Low Range	26.6; 17; 14.2; 6.5; 3.5; 1.06 kDa

2.1.7 Antibodies & Kits

Following antibodies were used for Western Blot experiments. For detection the Super Signal West Pico Kit from Themo Fischer Scientific, Massachusetts, USA was used.

Table 2.19: List of used antibodies

Description	Antigen specificity	Specificity	Conjugate	Source
Beta Amyloid, 1-16 (6E10) monoclonal antibody	human Aβ	mouse anti-Aβ	none	Covance Inc., Princeton, USA
Goat anti mouse IgG-HRP	whole mouse IgG	mouse IgG	HRP	Santa Cruz Biotechnology, Inc.,Dallas, USA

2.1.8 Chromatography Materials and Columns

All size exclusion chromatograpy (SEC) columns were obtained from GE Healthcare Life Sciences, Freiburg, Germany. The column used for reversed phase high performance liquid chromatography (RP-HPLC) was a Zorbax 300SB-C8 from Agilent, Böblingen, Germany.

Table 2.20: List of used gravity chromatography materials

Material	Source
Ni^{2+}-NTA-Agarose	Qiagen, Hilden, Germany
Ni^{2+}-NTA-Agarose	Cube Biotech, Monheim, Germany

Table 2.21: List of used SEC columns

Column	Material
SD 75 XK 26/600 pg	Cross-linked agarose and dextran
SD 75 10/300 GL	Cross-linked agarose and dextran
HiLoad SD 200 XK 16/600 pg	Cross-linked agarose and dextran
SD 200 10/300 GL	Cross-linked agarose and dextran
SD200 increase 5/15	Cross-linked agarose and dextran

2.1.9 Bacterial Strains & Plasmids

Bacterial strains and plasmids used are listed in the following two tables.

Table 2.22: List of bacterial strains

Strain	Genotype	Source
***E. coli* BL21 (DE3) $T1^R$**	*E. coli* B, F-, *dcm*, *omp*T, *hsd*S(r_{B^-},m_{B^-}), *gal*, λ(DE3),*ton*A	Novagen, Darmstadt, Germany
***E. coli* BL21 (DE3) Codon Plus RIL $T1^R$**	*E. coli* B, F-, *dcm*, *omp*T, *hsd*S(r_B,m_{B^-}), *gal*, λ(DE3),*end*A, Hte, [argU, ileY, leuW, Camr], *ton*A	Stratagene Europa, Amsterdam, Netherlands

Table 2.23: List of plasmids

Plasmid	Lab.Nr.	Description	Resistance	Source
pET28a_MSP1	9/1/E*	pET28a vector carrying *MSP1D1*;product His-MSP1D1	kanamycin	Addgene, Rockeville, USA
pET28a_MSP1D1ΔH5		pET28a vector carrying *MSP1D1ΔH5*;product His-MSP1D1ΔH5	kanamycin	AG Wagner, Harvard Medical School, USA
pRK793	7/6/D	pRK793 vector carrying *TEV_S219V-Arg5*; plasmid #8827; product His-TEV	ampicillin	Addgene, Rockeville, USA

2.1.10 Peptides & Lipids

Aβ(1-42), N-terminally biotinylated Aβ(1-40) and (7-dimethylaminocoumarin-3yl)-carbonyl Aβ(1-40) were purchased from Bachem (Heidelberg, Germany). N-terminally biotinylated Aβ(1-42) and Aβ(1-40) was purchased from JPT (Berlin, Germany) and Innovagen (Lund, Sweden), respectively. Peptides were purchased as RP-HPLC purified lyophilisates with a MALDI-TOF-MS stated purity of at least 95 %. Storage conditions were -20 °C.

Recombinant expressed and purified Cys0-Aβ(1-42) and [U-^{15}N]-Aβ(1-42) was obtained from Dr. L. Gremer, AG Willbold, University of Düsseldorf, Germany.

All lipids were purchased as lyophylised powder from AvantiPolarLipids, Inc., Alabaster, USA with one exception Folch extract 1 lipids were obtained from Sigma-Aldrich, Steinheim, Germany.

The fluorescent labelled lipid DMPE Atto633 was purchased from ATTO-Tec GmbH, Siegen, Germany.

2.2 Methods

2.2.1 Bacterial Plate & Liquid Cultures

For *E.coli* growth agar plates were incubated over night at 37 °C.

Aerobic liquid precultures were inoculated with 1 to 100 colonies from an agar plate. The media was supplemented with appropriate antibiotics. Cultures were shaken over night at 170 rpm and 37 °C. Main cultures were supplemented with the appropriate additives and inoculated 1:100 with the preculture.

2.2.2 Preparation of $CaCl_2$ Competent *E. coli* Cells

Starting from a colony of *E. coli* BL21(DE3), a preculture (5 ml LB) was generated by incubation over night at 200 rpm and 37 °C. 200 ml LB were inoculated 1:100 with the preculture. Cells were grown at 200 rpm and 37 °C until they reach an optical density ($OD_{580\ nm}$) of 0.6 to 0.8. After cooling on ice for

10 min, the culture was centrifuged for 10 min at 4 °C and 5,500 x g. The precipitated cells were resuspended in 40 ml ice cold, sterile 100 mM $CaCl_2$ and incubated on ice for 20 to 30 min. After centrifugation for 15 min at 5,500 x g and 4 °C the pellet was resuspended in 8 ml ice cold, sterile 100 mM $CaCl_2$ and incubated on ice for 15 min. 840 µl ice cold, sterile 80 % glycerol were added and stored in 200 µl aliquots at -80 °C.

2.2.3 Transformation of $CaCl_2$ Competent *E. coli* Cells

100 ng plasmid DNA was mixed with an aliquot of competent *E. coli* cells. The cells were heat shocked for 30 s at 42 °C. After a few seconds on ice, 1 ml LB was added and cells were incubated for 1 h at 300 rpm and 37 °C. 10 to 100 µl of cells were spread on a LB-medium agar plate with the appropriate antibiotics and incubated over night at 37 °C.

2.2.4 Heterologous Protein Expression in *E. coli*

For recombinant protein production, competent cells of *E. coli* strain BL21 (DE3) were transformed with the appropriate plasmid.

2.2.4.1 Heterologous TEV Protease Expression in E. coli

In order to cleave the N-terminal His-tag of the MSP variants, tobacco etch virus (TEV)-protease with the mutation S219V was used (Kapust, Tozser et al. 2001). The resulting strain was grown at 37 °C in 50 ml LB supplemented with 100 µg/ml ampicillin and 34 µg/ml chloramphenicol. 2 x 1 l LB with appropriate antibiotics were inoculated 1:100 with the preculture and grown at 170 rpm and 30 °C until and $OD_{580\ nm}$ of 0.6 to 0.8 was reached. By adding IPTG to a final concentration of 1 mM the heterologous protein expression was induced. After 4 to 5 h incubation, the cells were centrifuged for 20 min at 5,000 x g and 10 °C. The pellet was resuspended in 25 ml 1 x PBS and centrifuged again. The pellet was stored at -20 °C until protein purification.

2.2.4.2 Heterologous MSP Variants Expression in E. coli

The resulting strain was grown at 37 °C in 50 ml LB supplemented with 50 µg/ml kanamycin. 4 x 1 l LB with 25 µg/ml of the appropriate antibiotic were inoculated 1:100 with the preculture and grown at 170 rpm and 37 °C until an $OD_{580\ nm}$ of 0.6 to 0.8 was reached. By adding IPTG to a final concentration of 1 mM, the heterologous protein expression was induced. After 4 to 5 h incubation, the cells were centrifuged for 20 min at 5,000 x g and 10 °C. The pellet was resuspended in 25 ml 1 x PBS and centrifuged again. The pellet was stored at -20 °C until protein purification.

2.2.5 Protein Purification

2.2.5.1 Chromatographies

Purification of proteins tagged with polyhistidine-tag (His-tag) is performed in general with Ni^{2+}-NTA-agarose. This chromatography method is also called immobilised metal affinity chromatography (IMAC)(Porath, Carlsson et al. 1975). The polyhistidine tag interacts with a metal ion chelating ligand. In case of Ni^{2+}-NTA-agarose, the chelating ligand is nitrilotriacetic acid (NTA), which is a tetradentate chelator that binds nickel ions strongly. The polyhistidine tag binds with micromolar affinity to nickel ions. Proteins lacking the tag can be washed away by 10 to 40 mM imidazole. The protein of interest can be eluted by higher imidazole concentrations (350 mM), which outcompetes the binding between nickel ions and the polyhistidine tag.

Size exclusion chromatography (SEC) is a method for separation of molecules by their hydrodynamic radius. A mixture of molecules passes through a column packed with a gel media composed of e.g. cross-linked agarose and dextran (Superdex column) or a different porous material. The matrix has pores of different size, in which the molecules can diffuse. Particles smaller than the smallest pore can diffuse in all pores of the column matrix, while bigger molecules diffuse into a few pores only and elute therefore. Molecules bigger than the biggest pore in the column matrix elute in the void volume.

The SEC columns Superdex 200 10/300 GL and Superdex HiLoad200 XK 16/600 pg were calibrated with a protein standard by a ICS-6 co-worker (AG Willbold, ICS-6, FZJ Jülich, Germany) in order to estimate the hydrodynamic radius of the molecule of interest from the elution volume.

2.2.5.2 TEV Protease Purification

Buffers used for TEV protease purification are listed in table 2.7. For protein purification, cell pellets from 2 l expression culture were used. Each pellet was resuspended in 25 ml TEV-lysis buffer. Cell disruption occurred by using sonication for 4 min 25 s with an amplitude of 50 % in an 45 s on 60 s off interval. After adding polyethylenimin to a final concentration of 0.1 % (v/v), the cell debris was removed by centrifugation for 30 min at 50,000 x g and 10 °C.

The protein purification was performed by IMAC and SEC. The supernatant was added on an equilibrated Ni^{2+}-NTA-column. The column was washed with 15 column volumes (CV) TEV-lysis buffer. The protein was eluted by washing with 1 CV TEV-elution buffer I, 3 CV TEV-elution buffer II and 1 CV TEV-elution buffer III. The elution fractions were placed immediately on ice, 1 mM EDTA and 1 mM DTT were added. After SDS-PAGE analysis (chapter 2.2.7), TEV proteasecontaining fractions were united and, by using amicon filtration chambers (10,000 Da MCOW) the volume was reduced to 10 ml. For further purification SEC was performed. A HiLoad 26/60 Superdex 75pg column

was used with a flow rate of 1.5 ml/min and TEV-SEC-buffer. Before loading the sample it was filtered (0.45 µm). Fractions containing TEV proteasewere dialysed against TEV-storage buffer and stored at -80 °C after adding glycerol to a final concentration of 20 %. The concentration was determined using an extinction coefficient at $A_{280\,nm}$ of ε = 32220 $M^{-1}cm^{-1}$. The molecular weight is 28617.5 Da.

2.2.5.3 MSP Variants Purification

The two used MSP variants (table 2.23) in this work were urified after the same protocol. Buffers used for MSP purification are listed in table 2.8. For protein purification, cell pellets from 2 l expression culture were used. Each pellet was resuspended in 25 ml lysis buffer. Cell disruption occurred by using sonication for 4 min 25 s with amplitude of 50 % in a 45 s on 60 s off interval. The cell debris was removed by centrifugation for 30 min at 50,000 x g and 10 °C.

For the fusion protein IMAC was used. Therefore, the supernatant was added to Ni^{2+}-NTA coated agarose, which was equilibrated before with lysis buffer without lysozyme, DNase I and triton. After an incubation of 30 min the column was washed with 4 CV of each MSP-wash buffer I-IV. The elution of the fusion protein was achieved by washing with 4 CV MSP-elution buffer I and 3 CV MSP-elution buffer II.

Before and after sonication, after centrifugation and after each washing step, samples were taken for SDS-PAGE analysis (chapter 2.2.7). Elution fractions containing MSP were dialysed (3,500 Da) against 1 l TEV-cleavage buffer. The cleavage of the N-terminal His-tag was performed using TEV protease(chapter 2.2.5.2), added directly in the dialysis tube. The dialysis tube was transferred to 4 l cleavage buffer and the cleavage duration was 48 to 64 h. The ratio of TEV proteaseto MSP was 1:100.

The cleaved MSP protein was separated from TEV proteaseand His-tag by using a Ni^{2+}-NTA-column. Therefore the cleavage products were dialysed against Ni^{2+}-NTA-batch buffer without sodium cholate for 2 x 1 h and 1 l. Sodium cholate was added to a final concentration of 50 mM and the solution was incubated with 10 ml Ni^{2+}-NTA material for 1 h. The column was washed with 2 x 2 CV Ni^{2+}-NTA-batch buffer. The cleaved MSP protein was in the flow through and the first wash fraction. The TEV proteaseand the His-tag were eluted with 3 CV Ni^{2+}-NTA-batch elution buffer. The fractions containing MSP were united and dialysed against nanodisc assembly buffer. The protein was concentrated to 1.5 to 2.5 mg/ml by the usage of centriprep centrifuge-filterunits. 1 ml aliquots were lyophylised and stored at -80 °C. The theoretical extinction coefficient and the molecular weight of the different MSP variants are listed in table 2.23.

Table 2.24: List of MSP variants

	MSP1E3D1	MSP1D1	MSP1D1ΔH5
Molecular weight [g/mol]	29,981.9	22,043.9	19,488
Extinction coefficient [M^{-1} cm^{-1}] at 280 nm	26,930	18,450	18,450

2.2.6 Protein Concentration Determination

2.2.6.1 Protein Concentration Determination by Absorbance at 280 nm

Protein concentration was determined by absorbance of ultra violet (UV) light at a wavelength of 280 nm ($A_{280\ nm}$) through the protein. This concentration determination is possible because the amino acids tryptophan and tyrosine and to a lesser extend phenylalanine absorb UV light at 280 nm. The concentration of proteins can be calculated by using the Lambert-Beer law:

$$c = \frac{\mathrm{A}_{280\ \mathrm{nm}}}{\mathrm{d} * \varepsilon_{280\ \mathrm{nm}}}$$

c = concentration (M)
A_{280} = measured absorbance at 280 nm
d = cuvette (cm)
ε= molar extinction coefficient (M^{-1} cm^{-1}) at 280 nm

Extinction is based on the physical processes scattering and absorbance. As diluted solutions are measured, the scattering can be neglected. The molar extinction coefficient of proteins can be calculated by the theoretical molar extinction coefficient of the amino acids. The online programme ExPASy-ProtParam (http://web.expasy.org/protparam/) was used to calculate molar extinction coefficients.

2.2.6.2 Aβ Concentration Determination by Reversed Phase High Performance Liquid Chromatography

Reversed phase chromatography allows separation of molecules according to their hydrophobic properties on a stationary apolar silica gel in a polar mobile phase.

Aβ is lacking the amino acids tryptophan and tyrosine and has therefore a very low molar extinction coefficient. Aβ concentrations were quantified by isocratic reversed phase high performance liquid chromatography (RP-HPLC). A Zorbax 300SB-C8 column connected to a 1260 Infinity HPLC system was used. 20 µl sample were injected and run with 1 ml/min in aqueous 30 % (v/v) acetonitrile/0.1 % (v/v) trifluoric acid buffer as mobile phase. The column was kept at 80 °C and UV absorption was measured at 214 nm. The data was recorded and analysed with the ChemStation software. In order to generate a calibration equation Aβ samples of known concentrations were used to plot peak area

versus Aβ concentration. The molar concentration of samples was determined using the calibration equation.

2.2.7 SDS-Polyacrylamide Gel Electrophoresis Analysis

Separation of proteins was achieved by polyacrylamide gel electrophoresis (PAGE) either after Laemmli or Schagger (Laemmli 1970; Schagger 2006). All used buffers und gel compositions are listed in table 2.10 and 2.11. The samples were mixed with the corresponding 4 x sample buffer down to a solution of 1 x and boiled for 5 min at 95 °C. Heating with β-mercaptoethanol reduces disulphide bonds and denatures the proteins. The anionic detergent SDS binds to the protein backbone and causes an overall negative charge, allowing protein separation in the electric field by size. The use of protein markers allows an estimation of the size of the proteins. Used markers are listed in table 2.17.

Gels were run at 40 mA for 45 min, stained for 30 min in Coomassie solution and destained by boiling in water, when SDS-PAGE was performed after Laemmli. PAGE after Schagger was performed at 45 mA for 1 h 30 min and gels were stained by silver staining. For silver staining, gels were fixed for minimum 1 h in fixation solution, SDS was removed for 10 min in SDS-removing solution, followed by 3 x 30 s washing and 1 min step in Farmer´s reagent. Gels were stained in staining solution for 20 min, leading to an accretion of silver ions to the negatively charged side chains. After washing, incubation with developer solution visualised the protein bands. After the desired intensity was reached, gels were incubated in an aqueous 1 % acetic acid solution for 10 min to stop the reaction and stored in tap water until detection. Detection of the bands was carried out for both methods with the gel documentation system ChemiDoc MP.

2.2.8 Western Blot & Dot Blot

Western Blot is an analytical technique, whereby proteins are transferred, after being separated by SDS-PAGE, from a gel onto a membrane and subsequently identified by detection with a specific antibody. For Dot Blot the protein sample is directly applied on the membrane in form of a little dot. Buffers used for both methods are listed in table 2.12.

For the Western Blot protein samples were separated by SDS-PAGE (2.2.7). The Colour Ultra Low Range Marker was used (table 2.17).

Nine pieces of Whatman paper and one piece of nitrocellulose membrane were cut out in the size of the gel. Each 3 pieces of Whatman paper were incubated in anode buffer I (ABI), anode buffer II (ABII) and cathode buffer (CB), respectively. 3 pieces of Whatman paper incubated in ABI, 3 pieces of Whatman paper incubated in ABII, the membrane, the gel and 3 pieces of Whatman paper incubated

in CB were placed in the blotter. A Turbo Trans-Blot Turbo system at 10 V, 0.2 A for 1 h was used for the protein transfer from the gel onto the membrane.

After blocking the membrane, either from Western Blot or Dot Blot, for 1 h in blocking buffer and washing for 1 min in wash buffer, the primary antibody was added (1:10,000 in TBS) and incubated over night at 4 °C. The next day, the membrane was washed 5 x 5 min with wash buffer before the secondary antibody was added (1:10000 in TBS). After 1 h at 4 °C, the membrane was washed again 5 x 5 min with wash buffer. The membrane was incubated with a 1:1 mix of the stable peroxide and luminol enhancer solution from the SuperSignal West Pico kit for 5 to 10 min. Detection and documentation was performed with the ChemiDoc MP-system.

2.2.9 Nanodisc Preparation

2.2.9.1 Lipid Preparation

Phospholipids and cholesterol were dissolved in chloroform, sphingomyelin and gangliosides were dissolved in a chloroform:methanol 2:1 solution. The solvent was removed under a stream of nitrogen. The residual lipid film, after drying overnight in a cool trap, was resolved in a lipid buffer (table 2.13) to a concentration of 50 mM or 25 mM. The lipid to detergent ratio was constantly 1:2.

2.2.9.2 Empty Nanodisc Assembly and Purification

For preparation of MSP stock solutions in assembly buffer (1.5 to 2.5 mg/ml), lyophylised MSP was resuspended in the original volume sterile MiliQ water. For analytical samples 125-500 µg MSP were used, while for preparative samples 4 to 10 mg were used. The MSP solution was mixed in the appropriate ratio with lipids in lipid buffer (table 3.2). Subsequently, the samples were incubated on ice following an incubation for 5 x 20 min at a temperature depending on the respective lipid (table 3.2). The removal of sodium cholate, by dialysis (1,000 Da) against assembly buffer (table 2.13) for 1 h 0.5 l, 3 to 4 h 1.5 l and over night 3 l at 4 °C, induces nanodisc assembly. Analysis and purification of the nanodisc solution was achieved by SEC. For analytical runs a Superdex200 10/300 GL column or a Superdex200 5/15 increase column was used. For preparative runs a HiLoad 16/600 Superdex 200 pg column was used. All columns were connected to an ÄKTApurifier system. Flow rates were used according to the manufacturer instructions. The elution of unlabelled proteins was detected by a wavelength of 280 nm and 214 nm. The elution of lipids can be also followed by 214 nm or when labelled with a fluorescent dye at the respective absorption wavelength. After SEC, nanodisc peaks were pooled and concentrated. The concentration was achieved with VivaSpin6 concentrators (MCOW 30,000 Da) at very low numbers of revolutions (300 to 500 x g). Concentration was determined by absorbance at 280 nm using 2 x the molar extinction coefficient of the MSP variant (chapter 2.2.6.1), as nanodiscs are composed of two copies of MSP and lipids, which do not absorb at

a wavelength of 280 nm. After concentration, quality of nanodiscs was checked by SEC using the Superdex200 5/15 increase column.

2.2.9.3 Nanodisc Assembly in the Presence of Aβ

For the assembly of nanodiscs in the presence of Aβ, Aβ was dried together with lipids. Aβ, solubilised in HFIP for minimum 24 h, was mixed with lipids in chloroform and dried as described in chapter 2.2.9.1.

After rehydration of the lipid-Aβ mixture in lipid buffer the MSP was added and the assembly was performed as described in chapter 2.2.9.1.

2.2.9.4 Separation of free Aβ from Aβ-Nanodiscs

In order to separate free Aβ from possibly Aβ loaded nanodiscs using IMAC. Empty nanodiscs, possibly Aβ loaded nanodiscs and Aβ were each added to Ni^{2+}-NTA coated agarose, which was equilibrated before with nanodisc SEC bufferI (table 2.14). After an incubation of 30 min the column was washed with 4 CV of Aβ-IMAC-wash buffer I(table 2.14). The elution of His-tagged nanodiscs was achieved by washing with 4 CV MSP-elution buffer I and 3 CV MSP-elution buffer II (table 2.14).

2.2.10 Liposome Preparation

Liposomes are spherical, water or buffer filled lipid bilayers. They exist in different sizes, which can be regulated by extrusion through a membrane. Liposomes are model membrane systems which allow protein membrane interaction analysis by different methods. In this study they were used for NMR spectroscopy experiments and fluorescence titration experiments.

Phospholipids were dissolved in chloroform. Gangliosides and sphingomyelin were dissolved in a chloroform:methanol 2:1 (v/v) solution. The desired lipid solution was dried under a stream of N_2 and, in order to remove residual organic solvents, the lipids were further placed for a minimum of 3 h in a cool trap. The dried lipids were dissolved in the respective buffer in the desired concentration. After a freeze-thaw cycle, five times each, the lipids were either stored at -20°C or directly used for liposome preparation. Therefore the lipid mixtures were extruded through a 50 nm membrane in case of NMR experiments or a 100 nm membranes in case of fluorescence titration experiments. The liposomes were analysed by dynamic light scattering in order to check the dispersity and size (2.2.12).

2.2.11 Aβ Preparation

Aβ samples were prepared and handled in Protein LowBinding tubes. For monomerisation Aβ was dissolved in 1,1,1,3,3,3,-hexafluoro-2-propanol (HFIP) for at least 24 h at room temperature before aliquots were lyophilised.

2.2.11.1 Aβ Preparation for BioLayer Interferometry

In order to obtain monomeric N-terminally biotinylated Aβ, Aβ was purified and immobilised as described before with minor adjustments (Frenzel, Gluck et al. 2014). HFIP pretreated and lyophilised aliquots were dissolved in buffer (30 KH_2PO_4/K_2HPO_4, pH 7.2, 0.5 mM EDTA) to a final concentration of 160 µg/ml and purified by SEC on a Superdex75 10/300 GL column to yield pure monomeric Aβ. SEC was operated at RT and a flow rate of 0.5 ml min^{-1} on an Äkta purifier system using 30 mM KH_2PO_4/K_2HPO_4, pH 7.2, 0.5 mM EDTA as running buffer.

For Aβ oligomer preparation, suitable for coupling on BLI sensor tips, N-terminally biotinylated Aβ and non-biotinylated Aβ were mixed in a 1:10 ratio prior to lyophilisation. Aβ samples with a monomer-related concentration of 80 µM were incubated at 22°C and 600 rpm for 2.5 h [Aβ(1-42)] and overnight [Aβ (1-40)], respectively. 100 µl were used for density gradient centrifugation as described in the following (Frenzel, Gluck et al. 2014). Density gradient centrifugation allows matrix-free separation and fractionation of different Aβ species according to their sedimentation coefficients, which depend on particle size and shape. The gradient consists of 260 µl of 50 % iodixanol at the bottom of an 11x34 mm polyallomer centrifuge tube, overlaid by 260 µl of 40 % iodixanol, 260 µl of 30 % iodixanol, 780 µl of 20 % iodixanol, 260 µl of 10 % iodixanol and 100 µl of 5 % iodixanol. The samples were centrifuged for 3 h at 259,000 x g and 4 °C (TLS-55 rotor, OptimaXP centrifuge). 14 fractions of 140 µl each were collected from top to bottom. Tris-Tricine-SDS-PAGE analysis was performed followed by silver staining. Oligomers were obtained from fraction 5 (Brener, Dunkelmann et al. 2015).

2.2.12 Dynmic Light Scattering

Dynamic light scattering (DLS) was used to analyse nanodiscs and liposomes. DLS gives information about the size distribution of particles in a sample. Temporal fluctuations of the scattered laser light are analysed by means of the intensity. Measurements were performed with a DynaPro dynamic light scattering system using a 45 µl quartz cuvette with 3 mm path length (QS-105-251). Measurements were recorded at 20 °C with a fixed angle of 90 °. Data were recorded for 5 min with 10 s acquisition time using a 655.6 nm (13 mW) laser. Analysis of the data was performed with the software Dynamic V6. The size distribution profile was obtained by a regularisation fit using calculated autocorrelation functions.

2.2.13 Fluorescence Titration

Fluorescence titrations (FT) were performed in order to analyse interaction of (7-dimethyl-aminocoumarin-3yl)-carbonyl-Aβ(1-40) (DAC-Aβ(1-40)) with nanodiscs composed of different lipid mixtures. DAC is a solvatochromic dye, which has low fluorescent yield in aqueous solution but

increases fluorescence intensity upon increased hydrophobicity of the surrounding environment e.g. when bound to a membrane (Demchenko, Mely et al. 2009).

Fluorescence measurements were recorded on a recorded with the QuantaMaster40 spectrofluorometer using a quartz cuvette (104F-QS) in a cuvette halter tempered at 37 °C. Spectra were corrected by using the spectrum correction attachment of the manufacturer. Buffer correction was performed manually afterwards. Fluorescence emission spectra were recorded at an excitation wavelength of 430 nm. All buffers used for FT experiments are listed in table 2.15.

Firstly 1 ml of a 109 nM DAC-Aβ(1-40) was titrated with aliquots of liposomes or nanodiscs in FT-high-salt-buffer in order to establish the method from Matzusaki and co-workers (Kakio, Nishimoto et al. 2002).

Secondly the buffer was changed to FT-low-salt-buffer and further experiments were conducted. 1 ml of a 109 nM DAC-Aβ(1-40) was titrated with aliquots of concentrated nanodiscs. The titration dilution was below 5 %. The titration interval was 3 min.

The relative fluorescence enhancement R = $(F-F_0)/F_0$ of each titration step was plotted against ND concentrations in order to determine overall apparent equilibration dissociation constants (K_D) values. Data were fitted according to Langmuir´s 1:1 binding model (Hill function with n = 1, OriginPro 8.5G). K_D values represent means ± SD (standard deviation) of minimum three independent experiments.

$$y = \frac{V_{max} * x^n}{k^n + x^n}$$

V_{max} = maximum fluorescence enhancement R
x = concentration of the ligand (nanodiscs)
k = overall apparent equilibration dissociation constants (K_D)

2.2.13.1 Labelling of the Tripeptide Glutathione with DACIA

The solvatochromic dye [N-(7-dimethylamino-4-methylcoumarin-3-yl)iodoacetamide] (DACIA), a thiolreactive labelling agent is insoluble in water or buffer. For the generation of a negative control for the titration experiments the tripeptide gluthatione was labelled with DACIA. The tripeptide is highly water soluble and no membrane binding is known.

Iodoacetamid reacts with sulfhydryl groups at physiological pH. The reaction is a nucleophilic substitution of iodine with a sulphur atom from the sulfhydryl group resulting in a stable thioether linkage. Sulfhydryl group selectivity is achieved by a pH above 8.3 and an excess of the iodoacetamid group over the sulfhydrylgroup.

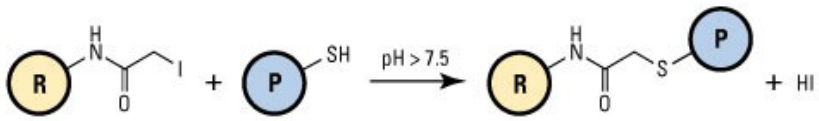

Iodoacetamid reagent | Protein with a sulfhydryl group | Conjugate

Figure 2.1: Schematic representation of Iodoacetamide reaction chemistry

The iodoacetamid reagent (R) reacts with the sulfhydryl group of a protein (P) by nucleophilic substitution, resulting in a conjugate with a stable thioether bond. Modified from www.thermofischer.com.

The reaction buffer contained 40 % DMSO to ensure solubilty of DACIA for the reaction. The reaction mixture was: 5 mM GSH, 1 mM DACIA, 40 % DMSO, 40 mM NaCl and 20 mM Tric-HCl at pH 8.4. The reaction was performed in darkness for 1 h.

The reaction was followed by RP-HPLC. A Zorbax SB-300-C8 column connected to a 1260 Infinity HPLC system was used. 20 µl sample were injected and run with 1 ml/min in a gradient from aqueous 10 % (v/v) acetonitrile/0.1 % (v/v) trifluoric acid buffer to 100 % (v/v) acetonitrile/0.1 % (v/v) trifluoric acid buffer over 35 min as mobile phase. The column was tempered at 80 °C and UV absorption at 376 nm and 214 nm was detected. The data was recorded and analysed with the ChemStation software.

The peaks containing DAC-gluthatione were collected and lyophylised for further use.

2.2.13.2 Labelling of the Cys0-Aβ(1-42) with DACIA

In order to obtain DAC labelled Aβ(1-42) an Aβ variant, which has at the N-terminus a cysteine residue was used and labelled with DACIA. In principle the same protocol as in 2.2.13.2 was used. However, as it was not possible to dissolve the required reagents in 40 % DMSO a 80 % DMSO solution was used with additional TCEP to avoid dimer formation of Cys0-Aβ(1-42). The ratio 20:4.5:1 DACIA:TCEP:Cys0-Aβ(1-42) was used. The concentration of Cys0-Aβ(1-42) was 44 µM.

2.2.14 BioLayer Interferometry

BioLayer Interferometry (BLI) is an optical analytical method allowing real-time analysis of molecule binding. For this purpose the interference pattern of white light form two surfaces is analysed. The two surfaces are an internal references layer and the biosensor surface with the bound molecules. Binding or dissociating of molecules from the sensor tip causes changes in the interference pattern and can be directly measured.

Purified Aβ monomers or Aβ oligomers were immobilised immediately after preparation (chapter 2.2.11) on the sensor surface of Super Streptavidin biosensors (SSA) to a final level of 2 nm using an

Octet RED96 instrument. Ligand and reference biosensors were quenched with 50 µg/ml biotin for 7 min.

Experiments were performed in a volume of 180 µl at 26 °C and 300 rpm vertical shaking. K_D determinations of nanodiscs to Aβ(1-42) and Aβ(1-40) were carried out in multi cycle kinetics. Association of nanodiscs in running buffer (table 2.16) on ligand and reference biosensors was recorded for 300 s, followed by a dissociation phase of 300 s. After each cycle, a regeneration step of 30 s was performed. 0.5 mM NaOH was used in case of monomers and 1 M guadinium-HCl was used for oligomers.

Sensorgrams were double referenced using the reference biosensors and a buffer cycle. Evaluation was performed by plotting the respective response levels against nanodisc concentrations. The curves were fitted using Langmuir´s 1:1 binding model (Hill function with n = 1, OriginPro 8.5G) (chapter 2.2.13.1).

2.2.15 Ultracentrifugation

2.2.15.1 Liposome Floating Assay

The liposome floating assay was used to analyse the binding of Aβ to liposomes. Aggregated Aβ will pellet during the centrifugation, while monomeric Aβ, liposomes and Aβ bound to liposomes will float up.

Sucrose solutions were prepared with the appropriate buffer. From bottom to top following solutions were carefully pipetted: 500 µl 55 % (w/w) sucrose, 380 µl 27 % (w/w) sample in sucrose, 900 µl 19 % (w/w) sucrose and 200 µl 10 % (w/w) sucrose. After centrifugation for 4 h at 259,000 x g using a TLS-55 rotor, 200 µl fractions were taken from top to bottom.

2.2.15.2 Sucrose Gradient

A sucrose gradient was used to analyse binding of Aβ to nanodiscs. Aβ-nanodisc mixtures are layered on top of a sucrose gradient. During centrifugation, aggregated Aβ will pellet while soluble Aβ, nanodiscs and Aβ bound to nanodiscs will be found in the top fractions separated according to their sedimentation coefficients which depend on particle size and shape.

Sucrose solutions were prepared in the appropriate buffer and from bottom to top following layers were pipetted: 300 µl 50 % (w/w) sucrose, 400 µl 41.5 % (w/w) sucrose, 400 µl 43.3% (w/w) sucrose, 400 µl 25 % (w/w) sucrose, 150 µl 16.5 % (w/w) sucrose, 150 µl 48.3 % (w/w) sucrose and 150 µl sample. After centrifugation for 3 h at RT and 259,000 x g using a TLS-55 rotor, 150 µl fractions were taken from top to bottom.

2.2.15.3 Sample Concentration by UC

Ultracentrifugation was performed in order to sediment and thereby concentrate Aβ bound to nanodiscs. Samples were centrifuged for 6 h at RT and 160,000 x g using a TLA-55 rotor. Subsequently, fractions were taken from top to bottom.

2.2.16 Nuclear Magnetic Resonance Spectroscopy

Nuclear magnetic resonance (NMR) spectroscopy is an analytical method to characterise structures and dynamics of proteins. While most spectroscopic methods use the electric part of electromagnetic waves, NMR uses the magnetic part. For NMR spectroscopy, nuclei with a magnetic dipole moment μ are required. μ is defined as μ = γ * I, whereby γ is the gyromagenetic ratio, a characteristic constant for any isotope, and I is the intrinsic angular momentum (spin). All nuclei that do not have an even number of protons and neutrons at the same time have a spin that is different from zero and are therefore active in NMR spectroscopy. The most important nuclei for protein NMR spectroscopy are ^{1}H, ^{15}N and ^{13}C, each with a spin ½. In a static magnetic field B_0 the energy levels of the nuclei ^{1}H, ^{15}N and ^{13}C will be split in two, m = + ½ and m = - ½, according to the following formula:

$$E_m = -\mu \cdot B_0 = -\frac{m \cdot h \cdot \gamma \cdot B_0}{2 \cdot \pi}$$

h = Planck´s constant

The occupation ratio of the two states can be described by the Boltzman-distribution

$$\frac{N(+\frac{1}{2})}{N(-\frac{1}{2})} = e^{\frac{-h \cdot \gamma \cdot B_0}{2\pi \cdot T \cdot k_B}}.$$

B_k = Boltzman constant

The energy difference between the both levels can be described by

$$\Delta E = \frac{h \cdot \gamma \cdot B_0}{2 \cdot \pi}.$$

The equation reveals why ^{1}H is the most sensitive isotope in NMR spectroscopy as it has the highest gyromagnetic ratio. The nuclei with the energetically favourable m = + ½ spin will be parallel to the external magnetic field B_0, while spins with an unfavourable m = - ½ will be antiparallel to the external magnetic field. The nuclei precess along the B_0-axis with their Larmor frequencies ω_0, dependent on the strength of the magnetic field B_0 and the gyromagnetic ratio γ, $\omega_0 = B_0 \gamma$.

Due to the higher occupation of the energy level m = + ½, according to the Boltzman-distribution, and the precession along the B_0-axis, there is a macroscopic magnetisation (M_0) along the magnetic field axis. By applying a second magnetic field B_1 e.g by a 90° radiofrequency pulse (RF pulse) with the

Larmor frequency of the isotope of interest along the x-axis, a disturbance of the magnetic moments of all spins of the respective isotope will occur. At the end of the 90° RF pulse along the x-axis there will be a macroscopic magnetisation along the –y-axis (M_{-y}). After switching off the B_1 field, the spins will precess in phase along the z-axis. The signal detection is achieved by a radiofrequency coil in the spectrometer probe in which a change of voltage is induced by the transversal precessing magnetisation. This process is called free induction decay, as the spin system turns back to the ground state by relaxation and the induced voltage decays. In doing so the spins dephase in the x-y-plane through T_2-relaxtion (spin-spin-relaxation) and through T_1-relaxation (spin-lattice-relaxation) the spins go back and align with or against M_0 magnetisation. Processing with Fourier transformation allows displaying the time domain signal in a frequency domain signal, independent on the strength of the magnetic field B_0, in parts per million (ppm).

2.2.16.1 The Chemical Shift (δ)

The chemical shift δ is a small difference in the Larmor frequency ω of nuclei from one istotope in an external the magnetic B_0 field, which arises from different magnetic shielding of the nuclei in the molecule. This shielding is caused by the atomic shell of the nuclei of interest and there neighbouring nuclei. The B_0 field induces an electron current in the atomic shell thus an additional local magnetic field at the nuclei. The local magnetic field is shielding the nuclei from B_0, thereby causing a minor change in the Larmor frequency. The degree of shielding is defined by the shielding constant σ. A big impact on the shielding, hence the chemical shift, has the chemical environment of a nucleus. The nuclei are in a non-symmetric environment; therefore they are not equally shielded in all directions from B_0. The chemical shift of a given nucleus depends on the relative orientation of the molecule to the magnetic field B_0. This effect is called chemical shift anisotropy, CSA. Furthermore the chemical shift depends strongly on secondary and tertiary structures of a protein. Temperature and pH also influence the chemical shift as well as protein interactions.

The chemical shift δ refers to a reference Larmor frequency ($\omega_{reference}$), which is most often the ^1H frequency of the methylgroup of tetramethylsilane,TMS, or 2,2-dimethyl-2-silapentane-5-sulfonic acid, DSS. The chemical shift is defined as

$$\delta = \frac{\omega_{signal} - \omega_{reference}}{\omega_{reference}} \cdot 10^6$$

2.2.16.2 Two Dimensional NMR

One dimensional protein NMR spectroscopy leads to an overlap of signals due to the high number of protons. Analysis on an atomistic level is in most cases not possible; therefore two or three

dimensional NMR spectroscopy is applied in order to separate signals from one dimensional NMR spectroscopy.

A 2D-experiment is composed of four parts preparation: evolution with an increment time *t1*, mixing and detection. After preparation, in which the sample is excited with one or more pulses, the magnetisation is allowed to precess and evolve for a time *t1* during evolution. In the following mixing period, the magnetisation can be transferred between nuclei by scalar or dipolar coupling. During detection the FID is detected as a function of time *t2*. Fourier transformation of the direct time *t2* results in a 1D-spectrum in the frequency domain. Through incrementing of *t1* by the time *Δt1*, the time dependent evolution of the spin system is detected. After fourier transformation of all FIDs along the direct time *t2,* one gets a series of 1D-spectra, showing snap shots of the spin systems at different magnetisation states. The series of 1D-spectra is also a series of FIDs along the indirect time *t1*. A fourier transformation along these FIDs results in the 2D-spctrum.

2.2.16.3 Sample Preparation, NMR Spectrometer and Data analysis

For NMR experiments lyophilised HFIP pretreated [U-^{15}N]-Aβ(1-42) was dissolved either in the appropriate buffer or model membrane systems were directly added. Table 2.25 lists the prepared samples. Buffers contained 10 % D_2O and 0.2 % NaN_3. 5 mm Shigemi tubes (BMS-005V) were used for the experiments.

Table 2.25: List of prepared NMR samples for 2D [^{1}H, ^{15}N]-TROSY experiments

NMR sample	Buffer
25 µM Aβ(1-42)	50 mM NaCl, 10 mM NaH_2PO_4/Na_2HPO_4, pH 7.4
25 µM Aβ(1-42) DMPC-liposome (14.75 mM)*	50 mM NaCl, 10 mM NaH_2PO_4/Na_2HPO_4, pH 7.4
25 µM Aβ(1-42) PC/PG/Chol-liposome (13.7 mM)*	50 mM NaCl, 10 mM NaH_2PO_4/Na_2HPO_4, pH 7.4
50 µM Aβ(1-42) DMPC-MSP1D1-ND (28 µM)	50 mM NaCl, 10 mM NaH_2PO_4/Na_2HPO_4, pH 7.4
50 µM Aβ(1-42) PC/PG/Chol-MSP1D1-ND (50 µM)	50 mM NaCl, 10 mM NaH_2PO_4/Na_2HPO_4, pH 7.4
50 µM Aβ(1-42) Folch1-MSP1D1-ND (45 µM)	50 mM NaCl, 10 mM NaH_2PO_4/Na_2HPO_4, pH 7.4
56 µM Aβ(1-42) Low-GM1-MSP1D1-ND (62.9 µM)	50 mM NaCl, 10 mM NaH_2PO_4/Na_2HPO_4, pH 7.4
144 µM Aβ(1-42)	10 mM KH_2PO_4/K_2HPO_4, pH 7.2 0.5 mM EDTA
144 µM Aβ(1-42) GM1-micelle (4.33 mM)	10 mM KH_2PO_4/K_2HPO_4, pH 7.2 0.5 mM EDTA
185 µM total GM1 MSP1D1ΔH5 ND	10 mM KH_2PO_4/K_2HPO_4, pH 7.2 0.5 mM EDTA
100 µM Aβ(1-42) total GM1 MSP1D1ΔH5 ND (185 µM)	10 mM KH_2PO_4/K_2HPO_4, pH 7.2 0.5 mM EDTA
100 µM Aβ(1-42)	10 mM KH_2PO_4/K_2HPO_4, pH 7.2 0.5 mM EDTA
103 µM Aβ(1-42) total-GM1 MSP1D1-ND (95 µM)	10 mM KH_2PO_4/K_2HPO_4, pH 7.2 0.5 mM EDTA

*Liposome concentration was calculated on the starting concentration before liposome extrusion

The NMR experiments were conducted on Bruker spectrometers operated with 14.1 T and 16.4 T as well as on a Varian VNMRS-NMR spectrometer operated with 21.2 T. The Varian spectrometer is equipped with a 5 mm Z-PFG ^{1}H[^{13}C,^{15}N] cryoprobe while the Bruker spectrometers are equipped with a 5 mm CPTCI ^{1}H-^{13}C/^{15}N/D Z-GRD cryoprobe.

All spectra were processed with nmrPipe (Delaglio, Grzesiek et al. 1995), visualized with nmrDraw and analysed with CcpNmr analysis (Vranken, Boucher et al. 2005).

All spectra were recorded with 256 complex points in the first and 3072 in the second dimension. The experiments were repeated 40 to 64 with a relaxtion time of 1.25 s between two experiments. The spectral width was 29 to 33 ppm for the first dimension and 16 ppm for the second dimension. The real points after processing were 3897 for the first and 4096 for the second dimension.

3. Results

3.1 Heterologous Protein Expression and Purification

3.1.1 Heterologous TEV Expression and Purification

The TEV protease was recombinantly produced in *E. coli* and purified by immobilised metal affinity chromatography (IMAC) and size exclusion (SEC) as described in chapter 2.2.4.1 and 2.2.5.2 and analysed by SDS-PAGE on 15 %(v/v) polyacrylamide gel (fig. 3.1)

Expression and purification of the His-tagged protein were successful. After sonication for cell disruption and centrifugation for the removal of insoluble fragments, the recombinant protein was mainly found in the supernatant (SN). The TEV protease has a molecular weight of 28.6 kDa. A strong band of the expected size was detected by SDS-PAGE analysis on 15 % (v/v) polyacrylamide gel after comassie brilliant blue (CBB) staining in the elution fractions (EII-EIII). For the removal of impurities a SEC was performed, the pooled fractions (fig. 3.1 SEC) with a concentration of 17.2 µM were aliquoted with 3 % glycerol and stored at -80 °C until further use.

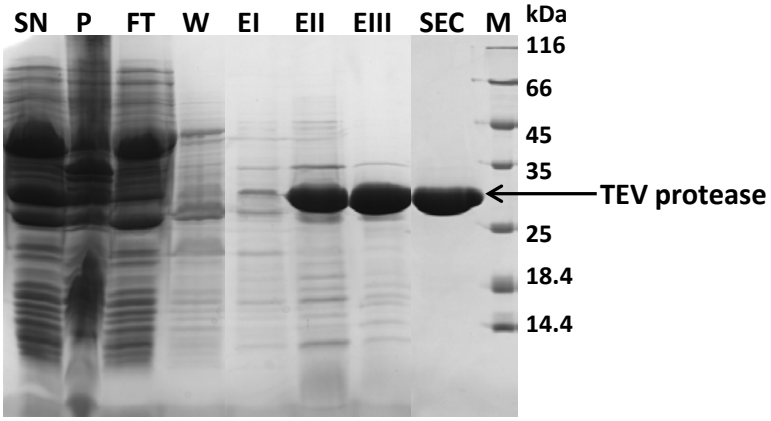

Figure 3.1: Analysis of heterologously expressed TEV protease in *E. coli* by SDS-PAGE using a 15 % polyacryamide gel

15 % polyacrylamide gel stained with CBB. SN: supernatant after cell disruption and centrifugation; P: pellet after cell disruption and centrifugation; FT: flow through IMAC; W: wash fraction; EI-EIII: elution fractions; SEC: pooled fractions after SEC; M: molecular weight marker.

3.1.2 Heterologous MSP Variants Expression and Purification

The different MSP variants (MSP1D1ΔH5, MSP1D1) were recombinant produced in *E. coli* and purified by IMAC as described in chapter 2.2.4.2 and 2.2.5.3. If not stated otherwise the His-tag was removed by TEV protease cleavage (chapter 2.2.5.3).

Expression and purification of the different His-tagged proteins and subsequent TEV protease cleavage were successful. Exemplarily, the recombinant expression and purification of MSP1D1 and removal of the His-tag by TEV protease cleavage are shown in figure 3.2 and 3.3.

4 h after induction with IPTG a band of the expected size, 24.66 kDa, which was not present before induction, was detected by SDS-PAGE analysis on 15 % (v/v) polyacrylamide gel after CBB staining (fig. 3.2 lane i). After cell disruption by sonication and removal of insoluble fragments by centrifugation the supernatant was loaded on an equilibrated Ni^{2+}-NTA column. Neither in the flow through nor in the four washing fractions (WI-IV) the recombinant His-tagged protein was found. The His-MSP1D1 was found in the elution fractions (EI-EII fig. 3.2).

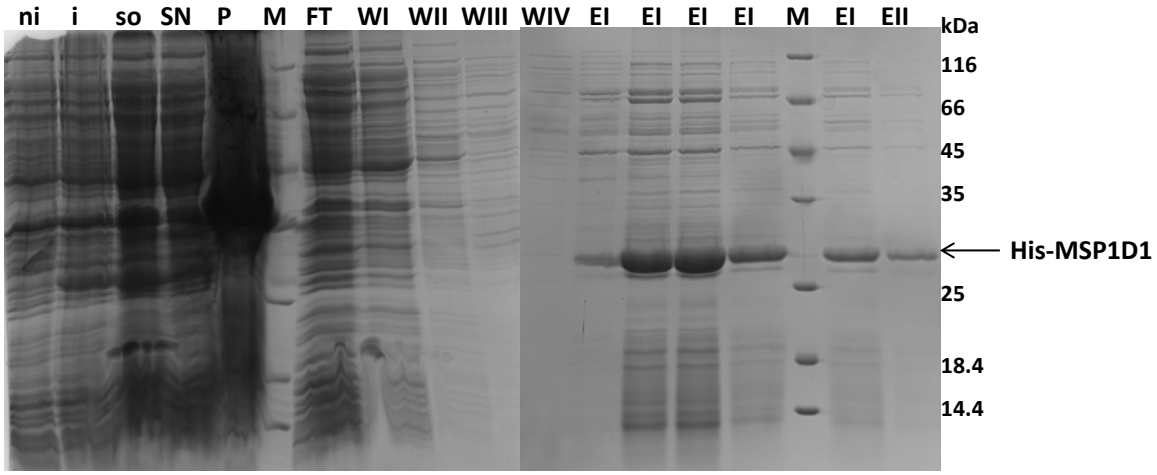

Figure 3.2: Analysis of heterologous expressed His-MSP1D1 in *E. coli* by SDS-PAGE using a 15 % polyacrylamide gel

15 % polyacrylamide gel stained with CBB. ni: crude extract taken before induction with IPTG; i: crude extract taken after induction with IPTG (final concentration 1mM); so: crude extract of sonicated cells; SN: supernatant after cell disruption and centrifugation; P: pellet after cell disruption and centrifugation; FT: flow through IMAC; WI-IV: wash fractions; EI: elution fractions (300 mM imidazole); EII: elution fraction (750 mM imidazole).

The elution fractions containing His-MSP1D1 were pooled, dialysed against TEV-cleavage buffer and the concentration was determined by measuring absorbance at 280 nm (chapter 2.2.6). The ratio of TEV protease to MSP variant was 1:100. The TEV protease cleavage was successful. The molecular weight of His-MSP1D1 and MSP1D1 as well as the other corresponding MSP variants differ in approximately 2.5 kDa, which can be detected by SDS-PAGE analysis (fig. 3.3). For the removal of the TEV protease and the His-tag a 2nd IMAC was performed. The purified MSP1D1 (fig. 3.3) was concentrated to a final concentration of 1.5 to 2.5 mg/ml, lyophylised and stored at -80°C until further use.

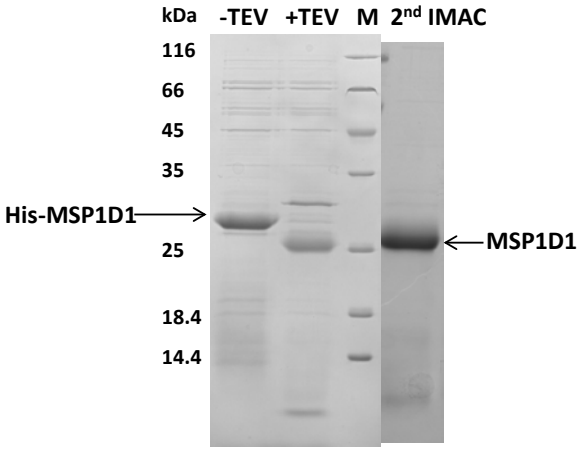

Figure 3.3: Analysis of TEV protease cleavage of His-MSP1D1

15 % polyacrylamide gel stained with CBB. –TEV: purified His-MSP1D1 before addition of TEV protease; +TEV: 46 h after addition of TEV protease to the purified His-MSP1D1; M: molecular weight marker 2nd IMAC: purified MSP1D1 after removal of TEV protease by a 2nd IMAC.

3.2 Nanodisc Assembly

Several types of nanodiscs, differing in the membrane scaffold protein (MSP) variant as well as in the lipid composition, were used for Aβ membrane interaction. For the assembly of nanodiscs the lipid to MSP ratio is crucial in order to achieve an effective transformation of the MSP into nanodiscs and to minimise aggregation of MSP with the lipids. Therefore, different MSP to lipid ratios had to be tested for new nanodisc compositions. This was done in a small-scale assembly using 100 µg MSP.

In the following section the assembly of empty nanodiscs is described exemplarily on the assembly of MSP1D1 with the lipid mixture of 40 % ganglioside GM1 (GM1), 30 % sphingomyelin (SM) and 30 % cholesterol (Chol). The mixture will be called in the following low-GM1. Table 3.2 lists all nanodiscs together with the corresponding lipid to MSP variant ratio as well as other characteristics such as stability, which varied significantly among the different types of nanodiscs.

The MSP1D1 was mixed with the detergent solubilised lipids in three different ratios. The lipid to detergent ratio was kept constant at molar ratio of 1:2. This was followed by an incubation cycle ice to 38°C 5 x for 20 minutes each. The temperature is depending on the lipid, which should be close to the melting temperature of the lipid and sometimes has to be experimentally adjusted. The detergent was removed by dialysis over 16 h, thereby leading to the self-assembly of the nanodiscs. The different assembly samples were analysed by SEC (fig. 3.4), a method for separation of molecules by their hydrodynamic radius. Visualisation of peaks is achieved by measurement of absorbance at 280 nm or in case of fluorescence labelled molecules at the respective absorption maximum of the dye. The intensity of the peak reflects the concentration. The peak with the highest intensity was in all three tested ratios the one with an elution volume of 12.25 ml (fig. 3.4, left). According to a calibration of the column with standard molecules of known hydrodynamic radii, the molecule has a hydrodynamic diameter of 9.7 nm which is consistent with the hydrodynamic radius of MSP1D1 nanodiscs in the literature (Denisov, Grinkova et al. 2004). The first peak of 7.5 ml contained

aggregates which elute in the void volume. The third peak, which reduced in hight with increasing MSP1D1 to lipid ratio, corresponded to free MSP1D1. All three peaks of all three samples were analysed by SDS-PAGE, exemplarily the CBB stained 15 % polyacrylamide gel of the 1:45 ratio is shown (fig. 3.4, right). In all three peak fractions MSP1D1 was found as expected. As the ratio 1:65 resulted in the lowest amount of free MSP1D1, this ratio was chosen for further experiments.

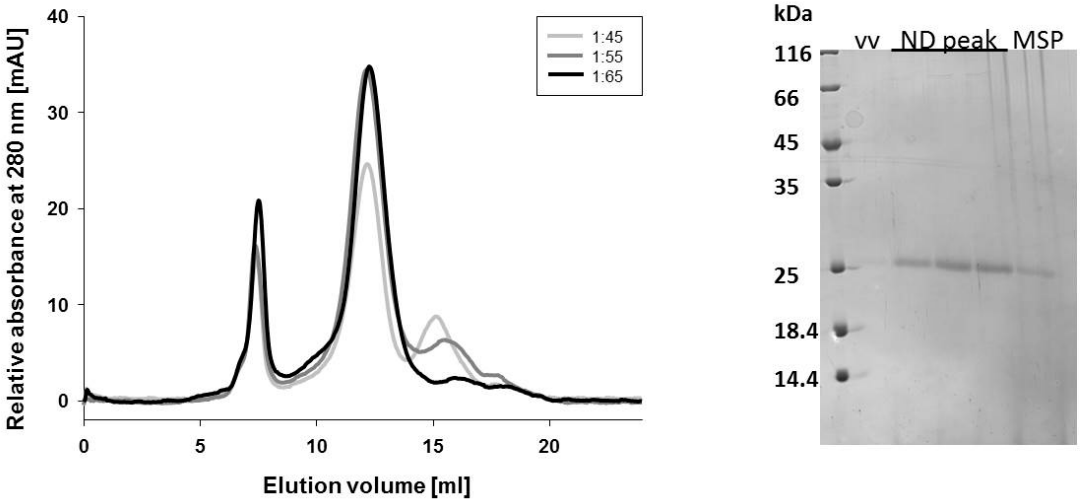

Figure 3.4: Analysis of low-GM1-MSP1D1 nanodisc test assembly by SEC and SDS-PAGE

Left: Size exclusion chromatogram of three low-GM1 to MSP1D1 ratios test assembly samples. The chromatography was performed on a Superdex 200 100/300 GL column with a flowrate of 0.5 ml/min. Visible is the monitored relative absorbance at a wavelength of 280 nm. The void volume of the column is 8 ml corresponding to the first peak. Nanodiscs elute in the second peak with a elution volume of 12.25 ml. The third peak is free MSP1D1. Right: 15 % polyacrylamide gel stained with CBB. vv: void volume peak fractions; ND peak: nanodisc peak fractions; MSP: MSP1D1 peak fractions. The band detected in all lanes is MSP1D1.

The nanodisc peak fractions of the 1:65 ratio sample were pooled and used for further analysis. This was done in order to test their stability under different conditions. The stability was checked by analytical SEC (fig. 3.5). In case of aggregation the peak shifts to an earlier elution volume.

The nanodiscs were concentrated and incubated at 25 °C up to 4.5 days. At all time points the elution volume was the same. No aggregation was detectable. Furthermore, an unconcentrated aliquot was taken and stored at -80 °C. After defrosting the sample after 4.5 days the nanodiscs were still stable and no peak shift was detected (fig. 3.5).

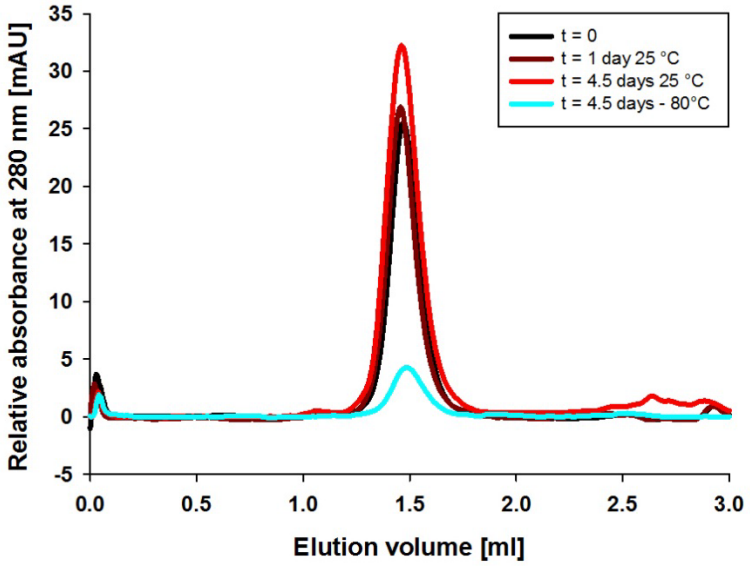

Figure 3.5: Size exclusion chromatograms of nanodiscs after incubation at 25 °C and -80 °C

Size exclusion chromatography of low-GM1-MSP1D1 nanodiscs incubated at different temperatures up to 4.5 days. The chromatography was performed on a Superdex 200 5/15 increase column with a flowrate of 0.3 ml/min. Visible is the recorded relative absorbance at a wavelength of 280 nm. Nanodiscs elute at 1.5 ml.

Table 3.1: List of used lipid mixtures and abbreviations

Lipid mixture	Abbreviation
100 % GM1	total-GM1
70 % GM1 30 % SM 30 % Chol	high-GM1
40 % GM1 30 % SM 30 % Chol	low-GM1
100 % DMPC	DMPC
45.5 % POPG 45.5 % POPG 9 % Chol	PC/PG/Chol
50 % POPC 50 % POPG	PC/PG
80 % POPC 20 % DOPS	PC/PS
Folch extract 1	Folch 1

GM1, ganglioside GM1; Chol, cholesterol; SM, sphingomyelin; DMPC, 1,2-dimyristoyl-sn-glycero-3-phosphocholine; POPG, 1-palmitoyl-2-oleoyl-sn-glycero-3-phospho-(1'-rac-glycerol); POPC, 1-palmitoyl-2-oleoyl-sn-glycero-3-phosphocholine; DOPS, 1,2-dioleoyl-*sn*-glycero-3-phospho-L-serine.

Table 3.2: List of prepared nanodiscs

MSP variant	Lipid	MSP:lipid ratio	T	Stability at -80°C	Temperature stability	R_h (nm)
MSP1D1	low-GM1	1:60	38 °C	yes	min. 4 days at 25°C	n.d.
MSP1D1	total-GM1	1:65	38 °C	yes	min. 4 days at 25°	n.d.
MSP1D1	PC/PG/Chol	1:47	4 °C	no	min. 4 days at 25	4.9
MSP1D1	DMPC	1:70	30 °C	yes	n.t.	4.8
MSP1D1	Folch1	1:47	38 °C	n.t.	n.t.	n.d.
MSP1D1	PC/PG	1:55	4 °C	yes	n.t.	4.8
MSP1D1	PC/PS	1:47	4 °C	yes	n.t	n.d.
MSP1D1ΔH5	low-GM1	1:55	38 °C	yes	min. 2 days at 25°C	n.d.
MSP1D1ΔH5	high-GM1	1:55	38 °C	no	1 day at 25°	4.3
MSP1D1ΔH5	Total-GM1	1:60	38 °C	yes	min. 2 days at 25°C	4.1

T, temperature applied during assembly procedure; n.t., not tested; Rh, hydrodynamic radius determined by dynamic light scattering (DLS); n.d., not determined.

3.3 Separating Empty Nanodiscs, Aβ Loaded Nanodiscs and Free Aβ

3.3.1 Separating Empty Nanodiscs, Aβ Loaded Nanodiscs and Free Aβ by SEC

In order to obtain protein loaded nanodiscs there are two options. The first one is to incubate preassembled empty nanodiscs with the protein of interest, which will bind to the membrane. The second one is an assembly of the nanodisc in presence of the protein of interest. In general, loaded nanodiscs are separated from empty nanodiscs and free protein of interest by SEC.

Three samples, Aβ(1-42), empty PC/PG nanodiscs, and PC/PG nanodiscs assembled with Aβ(1-42), were prepared following the protocol for nanodisc assembly. For the assembly of nanodiscs in presence of Aβ(1-42), the peptide was dried together with the lipids and resolubilised in lipid buffer. The final ratio of Aβ(1-42) to nanodisc was five Aβ(1-42) molecules per nanodisc. The ratio of MSP:lipid:Aβ(1-42) was 1:40:2.5. For Aβ(1-42) the same protocol was applied but instead of lipids and MSP the buffer was used. After the assembly and dialysis, the samples were analysed by SEC (fig. 3.6).

Regarding the low molecular weight of Aβ(1-42) (4.7 kDa), its binding to a nanodisc will not change the hydrodynamic radius of ND sufficiently from the one of an empty nanodisc (150 kDa) in order to separate the two species by SEC. Thus, a change in the elution volume of loaded nanodiscs in comparison to empty nanodiscs is not expected to be detectable. Indeed, empty nanodiscs have an elution volume of 12.5 ml as well as nanodiscs assembled in the presence of Aβ(1-42) (fig. 3.6 A/B). The subsequent analysis by SDS-PAGE and CBB staining revealed that the peak of nanodiscs assembled with Aβ(1-42) contains MSP and Aβ(1-42) (fig. 3.6 A/B). In general, an elution of the nanodisc together with the protein of interest is interpreted as the protein of interest being bound to the nanodisc, as the elution volume of the protein of interest differs from the elution volume of the nanodisc. However, Aβ(1-42) without nanodiscs eluted over the whole column volume (fig. 3.6 C). Therefore, an explicit conclusion cannot be drawn. The peak of nanodiscs assembled with Aβ(1-42) contains most likely empty nanodiscs, Aβ(1-42) loaded nanodiscs as well as free Aβ(1-42).

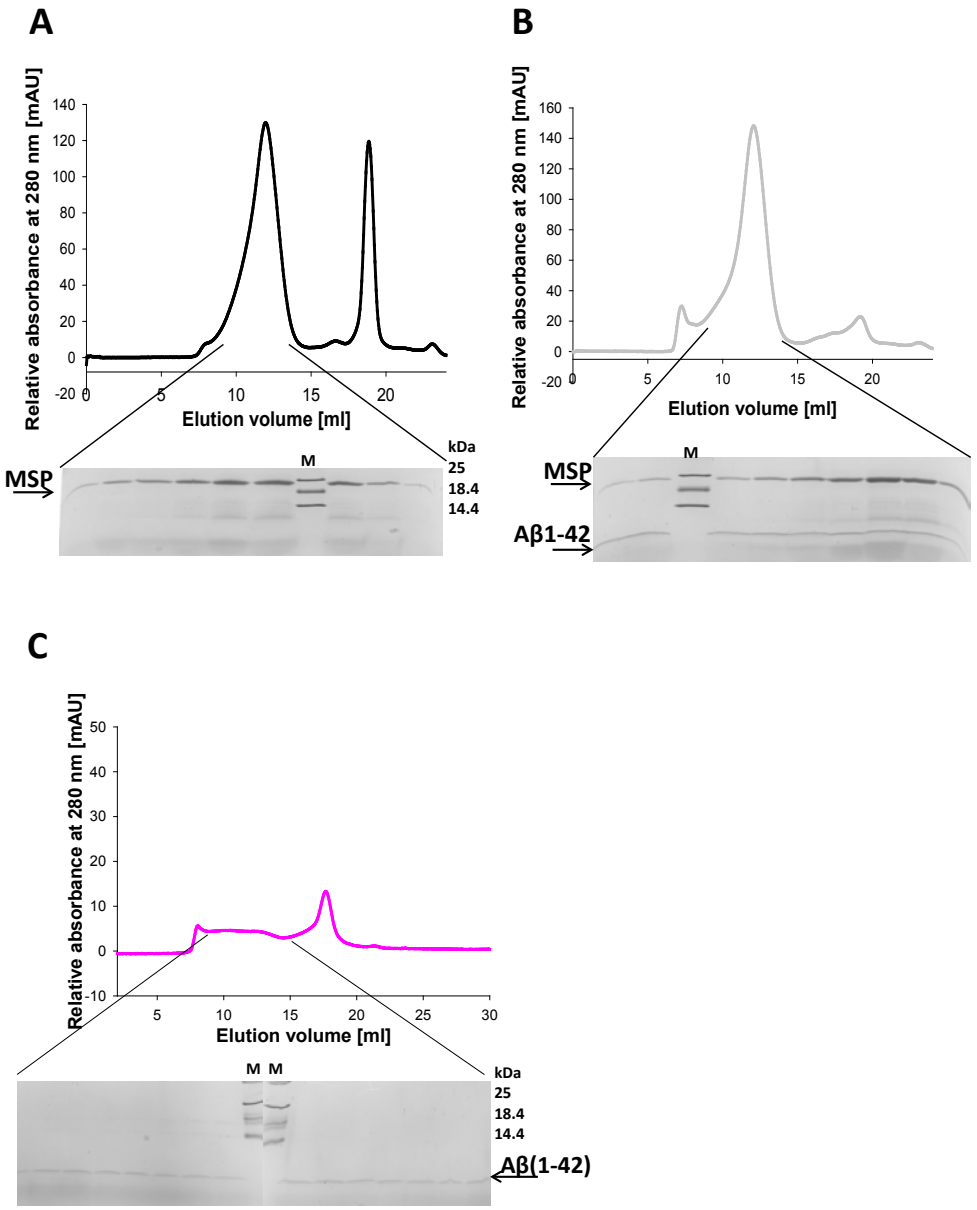

Figure 3.6: Size exclusion chromatograms of empty nanodiscs, nanodiscs assembled with Aβ(1-42) and Aβ(1-42)

The chromatography was performed on a Superdex 200 100/300 GL column with a flowrate of 0.5 ml/min. Visible is the recorded relative absorbance at a wavelength of 280 nm. The void volume of the column is 8 ml corresponding to the first peak. Nanodiscs elute in the second peak with an elution volume of 12.5 ml. Indicated peak fractions were analysed by SDS-PAGE using a 15 % polyacrylamide gel stained with CBB. lane M is the marker. A: empty nanodiscs B: nanodiscs assembled in the presence of Aβ(1-42) C: Aβ(1-42).

3.3.2 Separating Empty Nanodiscs, Aβ Loaded Nanodiscs and Free Aβ by IMAC

The His-tag of the MSP is a useful tool in separating nanodiscs from free protein of interest. Therefore, it was tested if it is possible to separate free Aβ from Aβ bound to nanodiscs by IMAC. Aβ(1-42), His-tag nanodiscs and Aβ(1-42) with His-tag nanodiscs were incubated with Ni^{2+}-NTA. The IMAC was performed as described in chapter2.2.9.4. The different fractions of IMAC were analysed by SDS-PAGE and CBB staining (fig. 3.7). His-tag nanodiscs are mainly found in the elution fractions.

Yet, Aβ(1-42) without His-tagged nanodiscs is not only detected in the flow through and wash fractions but also the elution fractions. Aβ(1-42) does bind to the Ni^{2+}-NTA matrix under the tested conditions and cannot be separated from Aβ(1-42) bound to nanodiscs.

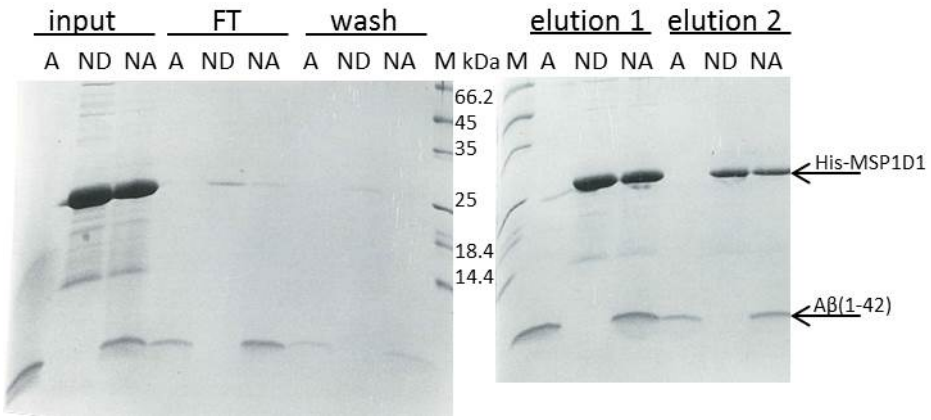

Figure 3.7: Analysis of separating Aβ from His-tag nanodiscs by IMAC

15 % polyacrylamide gels stained with CBB. A: 100 µM Aβ(1-42); ND: 50 µM His-tag nanodiscs; NA: 50 µM His-tag nanodiscs with 100 µM Aβ(1-42). Input: samples before IMAC; FT: flow through; wash: 10 mM imidazole; elution1: 300 mM imidazole; elution2: 600 mM imidazole.

As a clear separation of Aβ loaded nanodiscs from free Aβ was not possible, neither by SEC nor by IMAC, the interaction of Aβ with nanodiscs was analysed by studying the direct binding of Aβ to empty nanodiscs.

3.4 Aβ Membrane Interaction Analysed by Nuclear Magnetic Resonance Spectroscopy

Aβ(1-42) membrane interaction was analysed by nuclear magnetic resonance (NMR) spectroscopy. Therefore, [U-^{15}N]-Aβ(1-42) was prepared with different liposomes as well as different nanodiscs.

A recurring finding is the anionic lipid head group as well as cholesterol dependent interaction of Aβ(1-42) with membranes (McLaurin and Chakrabartty 1997; Terzi, Holzemann et al. 1997; Hane, Drolle et al. 2011). Therefore, the interaction of Aβ(1-42) with PC/PG/Chol liposomes, which contain the anionic phosphatidylcholine (PG) and cholesterol (Chol), and neutral DMPC liposomes was studied.

2D-[^{1}H,^{15}N]-TROSY experiments were recorded for [U-^{15}N]-Aβ(1-42) with PC/PG/Chol liposomes or DMPC liposomes as well as without liposomes. Liposomes were obtained by extrusion through a 50 nm membrane, yet resulting in large unilamellar vesicles with a hydrodynamic radius of approximately 50 nm, as revealed by dynamic light scattering. HFIP pretreated lyophylised

[U-^{15}N]-Aβ(1-42) was dissolved in the liposome solution. The experiments were performed at 25 °C and the [U-^{15}N]-Aβ(1-42) concentration was 25 µM.

The corresponding spectra are shown in figure 3.8. The spectrum of [U-^{15}N]-Aβ(1-42) without liposomes shows 27 resonance signals of the peptide backbone as well as side chain peaks (7.8 to 6.8 ^{1}H ppm; 110 to 115 ^{15}N ppm) (fig. 3.8 A). This spectrum served as reference spectrum. Yet, no significant changes in the cross peaks nor intensity changes were observed for the spectra recorded of [U-^{15}N]-Aβ(1-42) with liposomes (fig. 3.8 B and C) although a signal loss was expected upon binding of [U-^{15}N]-Aβ(1-42) to liposomes, due to their increased molecular weight.

Similar results were obtained when [U-^{15}N]-Aβ(1-42) was analysed in the presence of different MSP1D1 nanodiscs (fig. 3.9). No significant differences were observed in the spectra of [U-^{15}N]-Aβ(1-42) recorded in presence of nanodiscs in comparison to the one recorded without. Here 50 µM [U-^{15}N]-Aβ(1-42) was dissolved directly in the nanodisc solution. Again PC/PG/Chol and DMPC were used for the nanodiscs (fig. 3.9, B and C). Additionally, a lipid mixture Folch 1, containing phosphatidylinositol, phosphatidylserine and other brain lipids, was used for nanodiscs to study the interaction of Aβ with membranes (fig. 3.9, D) (Folch 1942; Folch, Lees et al. 1957). Liposomes composed of low-GM1 lipids were shown to interact with Aβ(1-40), therefore this lipid mixture was also tested (Kakio, Nishimoto et al. 2001; Kakio, Nishimoto et al. 2002) (fig. 3.9, E). The spectrum of [U-^{15}N]-Aβ(1-42) with low-GM1 MSP1D1 nanodiscs shows two additional peaks, marked by a green pentagon. These two peaks originate from the ganglioside GM1. Figure 3.12 shows in purple the spectrum of GM1 containing empty nanodiscs, these two peaks and an additional third peak are detected from the three NH-groups of ganglioside GM1.

MSP1D1 nanodiscs have a diameter of 10 nm (chapter 3.2) and upon binding of [U-^{15}N]-Aβ(1-42) to the nanodisc changes in cross peaks were expected. The only peak which is slightly shifted is the peak representing the C-terminus of [U-^{15}N]-Aβ(1-42). Yet, this can be explained by the higher flexibility of the C-terminus.

The results obtained by NMR spectroscopy are consistent with the results obtained by FT and BLI (chapter 3.5 and 3.6). No binding of DAC-Aβ(1-40) to PC/PG/Chol liposomes was detected by FT (chapter 3.5.1) nor was a binding of Aβ(1-40) or Aβ(1-42) to DMPC nanodiscs, PC/PG/Chol nanodiscs or low-GM1 nanodiscs observed by BLI (chapter 3.6.2).

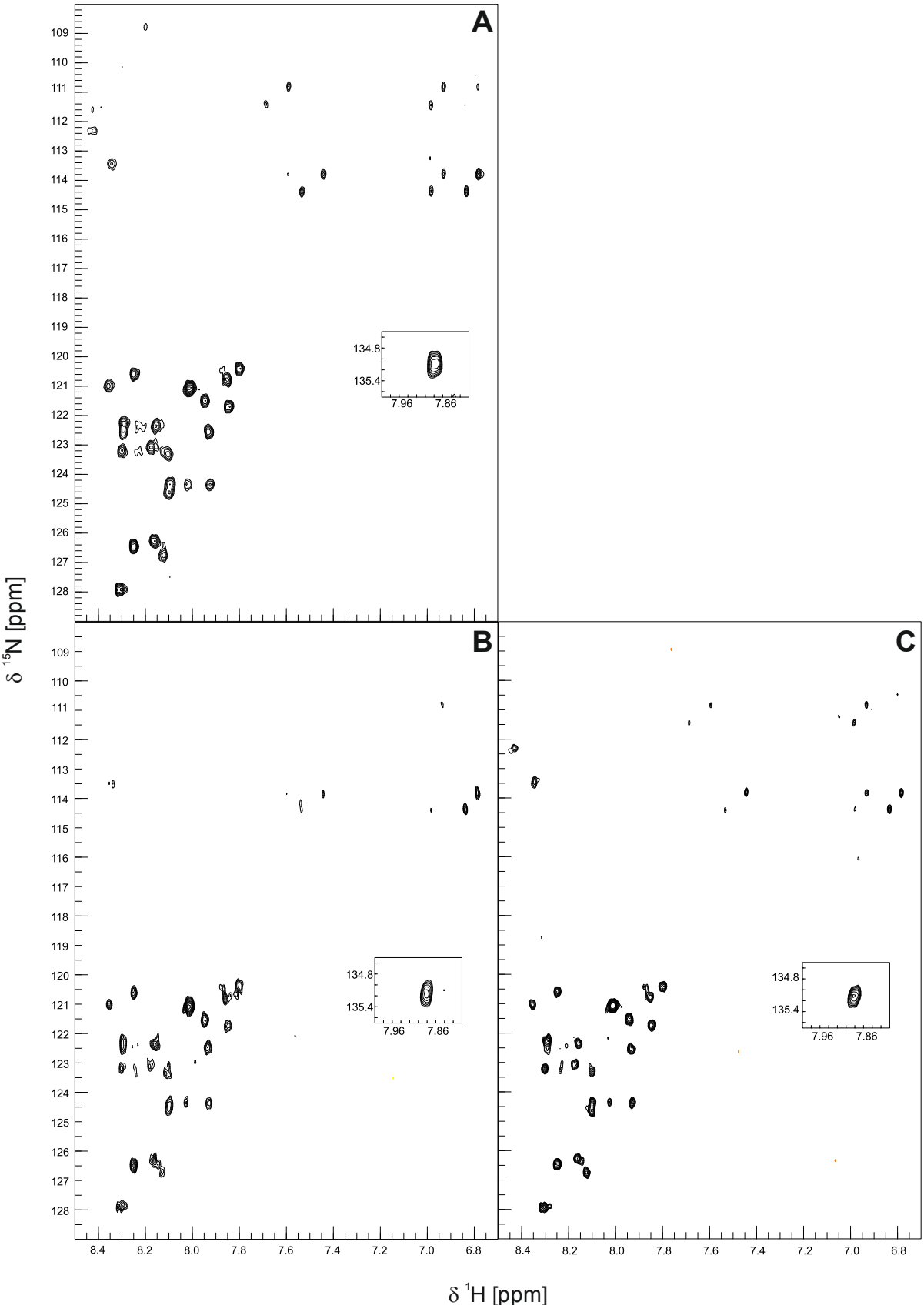

Figure 3.8: 2D-[^{1}H^{15}N]-TROSY spectra of [U-^{15}N]-Aβ(1-42) in absence or presence of liposomes

All three spectra were recorded at a magnetic field corresponding to a proton resonance frequency of 600 MHz at 25 °C in 50 mM NaCl, 10 mM NaH_2PO_4/Na_2HPO_4, pH 7.4. A) 25 µM [U-^{15}N]-Aβ(1-42) B) 25 µM [U-^{15}N]-Aβ(1-42) in the presence of DMPC liposomes C) 25 µM [U-^{15}N]-Aβ(1-42) in the presence of PC/PG/Chol liposomes.

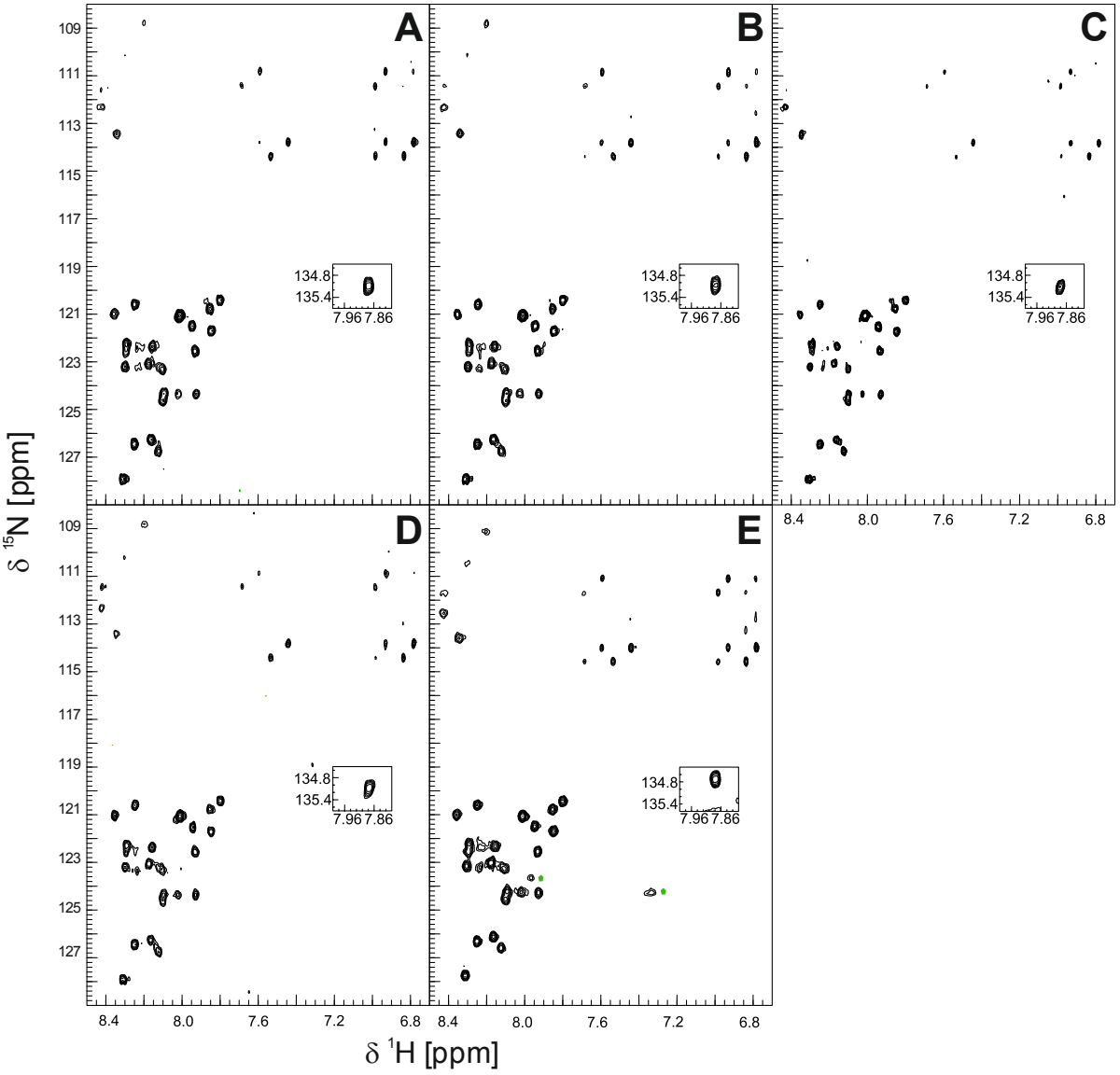

Figure 3.9: 2D-[^{1}H^{15}N]-TROSY spectra of [U-^{15}N]-Aβ(1-42) in absence or presence of nanodiscs

All five spectra were recorded at a magnetic field corresponding to a proton resonance frequency of 600 MHz at 25 °C in 50 mM NaCl, 10 mM NaH_2PO_4/Na_2HPO_4, pH 7.4. A) 25 µM [U-^{15}N]-Aβ(1-42) B) 50 µM [U-^{15}N]-Aβ(1-42) in the presence of DMPC MSP1D1 nanodiscs (28 µM) C) 50 µM [U-^{15}N]-Aβ(1-42) in the presence of PC/PG/Chol MSP1D1 nanodiscs (50 µM) D) 50 µM [U-^{15}N]-Aβ(1-42) in the presence of Folch1 MSP1D1 nanodiscs (45 µM) E) 56 µM [U-^{15}N]-Aβ(1-42) in the presence of low-GM1 MSP1D1 nanodiscs (62 µM). Green pentagons mark the peaks originating from ganglioside GM1.

Next, an experiment was set up based on findings of Kato and co-workers, who conducted NMR experiments of [U-^{15}N]-Aβ(1-40) bound to total-GM1 micelles (Utsumi, Yamaguchi et al. 2009; Yagi-Utsumi, Matsuo et al. 2010). The structure was not determined, but backbone chemical shifts indicate that the ganglioside bound region forms partial α-helices (Utsumi, Yamaguchi et al. 2009). Buffer, temperature, micelle preparation and GM1 to Aβ ratio were set as described by Utsumi *et al.*. Yet, instead of [U-^{15}N]-Aβ(1-40) [U-^{15}N]-Aβ(1-42) was used. GM1 micelles were obtained by

vortexing. DLS analysis revealed a hydrodynamic radius of 6.7 nm for the predominant species (98.8 % mass). The experiments were performed at 37 °C in 10 mM KH2PO4/K2HPO4, pH 7.2 0.5 mM EDTA.

A 2D-[^{1}H,^{15}N]-TROSY was recorded of 144 µM [U-^{15}N]-Aβ(1-42) in absence of GM1 micelles (black) and in presence of GM1 micelles (blue) (fig. 3.10). The ratio of GM1 to Aβ was 30:1. 19 out of the 41 expected backbone resonance signals were detected for [U-^{15}N]-Aβ(1-42) without GM1 micelles. These are fewer peaks than for the spectrum at lower concentrations (fig. 3.8, A). Analysis of residual sample after the experiment by density gradient centrifugation (DGC) followed by SDS-PAGE and Western Blot (fig 3.11) revealed [U-^{15}N]-Aβ(1-42) was mainly found in the pellet fraction, which indicates an aggregation of the peptide.

The spectrum of [U-^{15}N]-Aβ(1-42) with GM1 micelles shows only three peaks, of which two originate from the ganglioside GM1, marked with a green pentagon (fig. 3.11). However subsequent analysis clearly shows [U-^{15}N]-Aβ(1-42) was not aggregated. The peptide was not detected in the pellet fraction after DGC by Western blot (fig. 3.11 A). It was found in higher fractions, where soluble Aβ and micelles are found.

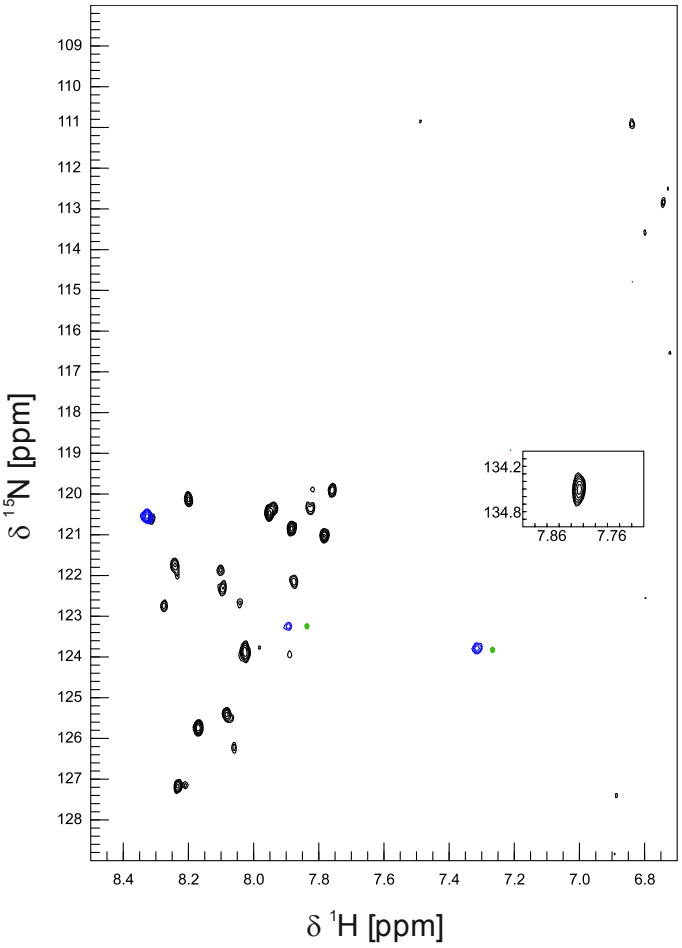

Figure 3.10: 2D-[^{1}H^{15}N]-TROSY spectra of [U-^{15}N]-Aβ(1-42) in absence or presence of GM1 micelles

The two spectra were recorded at a magnetic field corresponding to a proton resonance frequency of 900 MHz at 37 °C in 10 mM KH_2PO_4/K_2HPO_4, pH 7.2 0.5 mM EDTA. Black: 144 µM [U-15N]-Aβ(1-42); Blue: 144 µM [U-15N]-Aβ(1-42) in the presence of GM1 micelle. Green pentagons mark the peaks originating from ganglioside GM1.

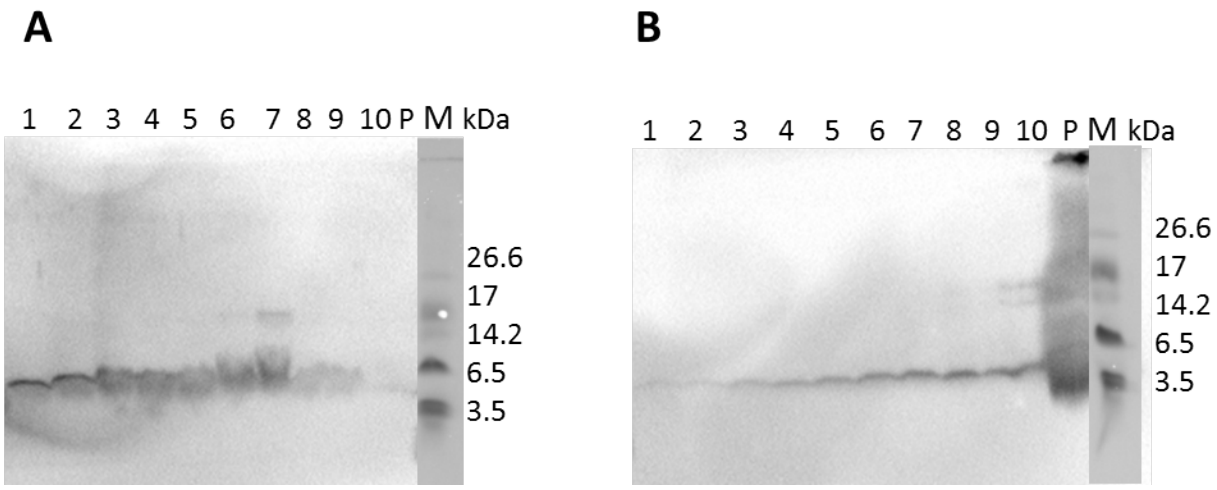

Figure 3.11: Western Blot of [U-^{15}N]-Aβ(1-42)

[U-^{15}N]-Aβ(1-42) analysed by DGC on a sucrose gradient after 2D-[^{1}H^{15}N]-TROSY. DGC Fractions (1 to 10 and pellet P) were analysed by SDS-PAGE and Western Blot. 1st antibody was 6E10. A 2nd peroxidase coupled antibody was used to detect chemiluminiscence.

Nanodiscs are surrounded by MSP, which makes them more stable than micelles or liposomes and restricts their size. Therefore, nanodiscs composed of only ganglioside GM1 (total-GM1) were used in the next set of experiments. Moreover, the temperature was reduced from 37 °C to 25 °C in order to slow down the Aβ(1-42) aggregation.

The recorded spectrum of 100 µM [U-^{15}N]-Aβ(1-42) is shown in black in figure 3.12 A. 33 resonance signals of the peptide back bone were detected. Next, a spectrum of empty total-GM1 MSP1D1ΔH5 was recorded, three peaks originating from the ganglioside GM1 were detected (fig. 3.12 A, purple spectrum). This spectrum was recorded under identical conditions and overlaid with the spectrum of total-GM1 MSP1D1ΔH5 incubated with 100 µM [U-^{15}N]-Aβ(1-42). Total-GM1 MSP1D1ΔH5 nanodiscs have a hydrodynamic radius of 4.1 nm as determined by DLS. Upon binding of [U-^{15}N]-Aβ(1-42) to the nanodiscs, a changes in the chemical shifts of the resonances signals was expected. Yet, only 10 resonance signals, of which three originated from the ganglioside GM1, were detected when [U-^{15}N]-Aβ(1-42) was analysed in the presence of total-GM1 MSP1D1ΔH5 nanodiscs (fig. 3.12 A, blue spectrum). The 7 remaining resonance signals from the peptide backbone were shifted in comparison to the signals of [U-^{15}N]-Aβ(1-42) but could not be assigned.

At higher temperatures the rotational correlation time is smaller, which can improve the spectrum of a big molecule. Yet, an increased temperature of 37 °C did not change the number of detected resonance signals. A systematic shift of the peaks, due to the increased temperature is observed (fig. 3.12 B). 2D-[^{1}H^{15}N]-TROSY of [U-^{15}N]-Aβ(1-42) in the presence of total-GM1 MSP1D1 nanodiscs resulted in very similar resonance signal distribution (fig. 3.12 C).

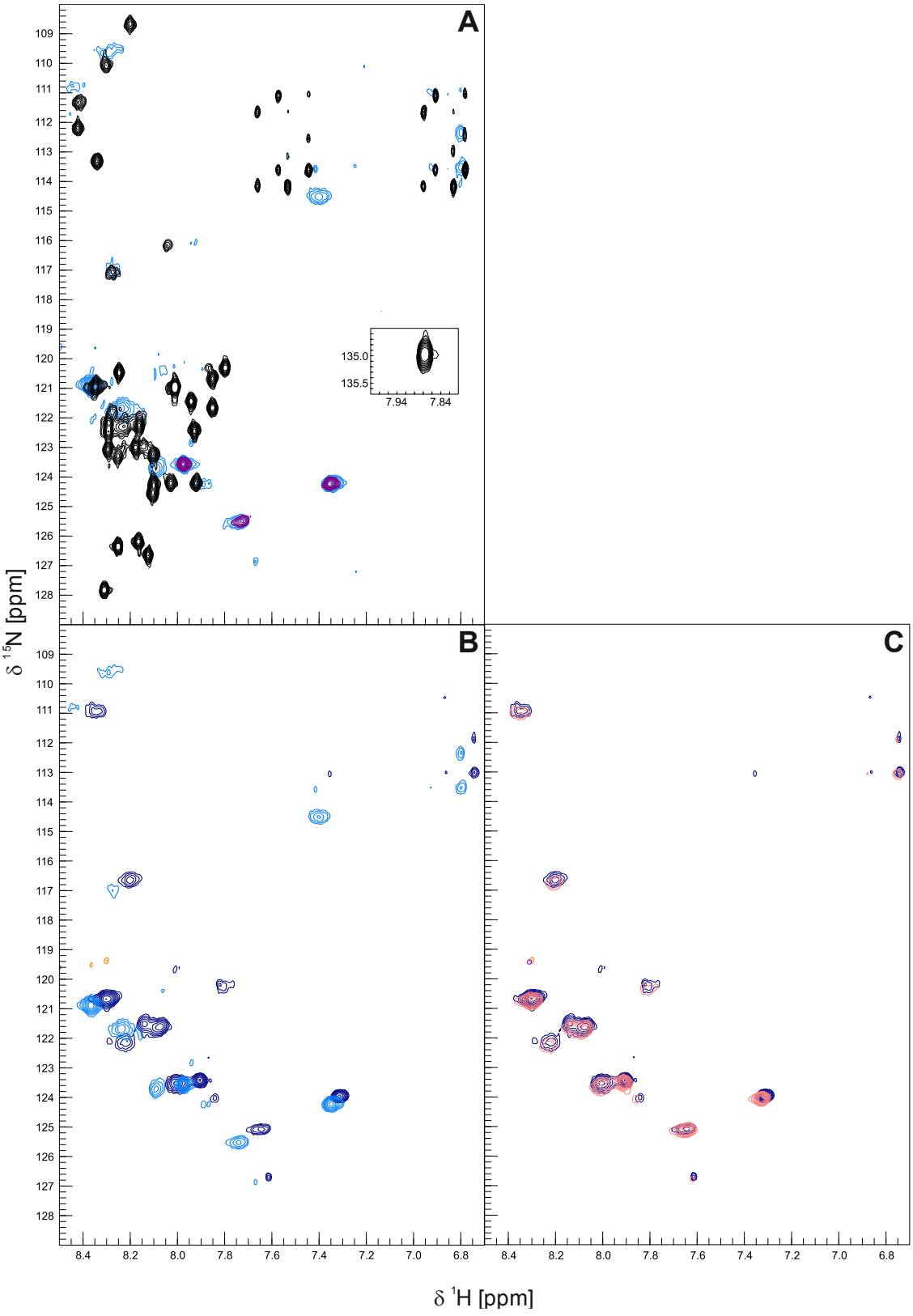

Figure 3.12: 2D-[^{1}H^{15}N]-TROSY spectra of [U-^{15}N]-Aβ(1-42)

All spectra were recorded at a magnetic field corresponding to a proton resonance frequency of 700 MHz in 10 mM KH_2PO_4/K_2HPO_4, pH 7.2 0.5 mM EDTA. A) T = 25 °C; Black: 100 µM [U-15N]-Aβ(1-42); Purple: 185 µM total-GM1 MSP1D1ΔH5 nanodiscs; Light blue: 100 µM [U-^{15}N]-Aβ(1-42) in the presence of 185 µM total-GM1 MSP1D1ΔH5 nanodiscs. B) 100 µM [U-^{15}N]-Aβ(1-42) in the presence of 185 µM total-GM1 MSP1D1ΔH5 nanodiscs. light blue: 25 °C; dark blue: 37 °C. C) T = 37 °C; dark blue: 100 µM [U-^{15}N]-Aβ(1-42) in the presence of 185 µM total-GM1 MSP1D1ΔH5 nanodiscs; pink: 100 µM [U-^{15}N]-Aβ(1-42) in the presence of 95 µM total-GM1 MSP1D1 nanodiscs.

Subsequent analysis of the residual NMR spectroscopy samples was performed. In case of the total-GM1 MSP1D1 nanodiscs the fluorescent lipid DMPE-Atto633 was introduced, one lipid per nanodisc. The fluorescently labelled lipid could be tracked using its specific absorption wavelength at 633 nm.

After DGC fractions were analysed by SDS-PAGE. [U-^{15}N]-Aβ(1-42) was not detected in the pellet, where aggregated Aβ species are found. Instead the peptide was detected in the same fractions as the MSP protein and fluorescent labelled lipid (fig. 3.13). Indicating [U-^{15}N]-Aβ(1-42) being bound to the nanodiscs. SEC revealed that the nanodiscs were aggregated after NMR spectroscopy (fig. 3.14). The elution peak of nanodiscs after the NMR spectroscopy experiments was shifted to an earlier elution volume, thus a higher molecular weight, when compared to the elution peak of nanodiscs before the NMR spectroscopy experiment. Moreover, nanodiscs did not elute as a single peak but as a double peak.

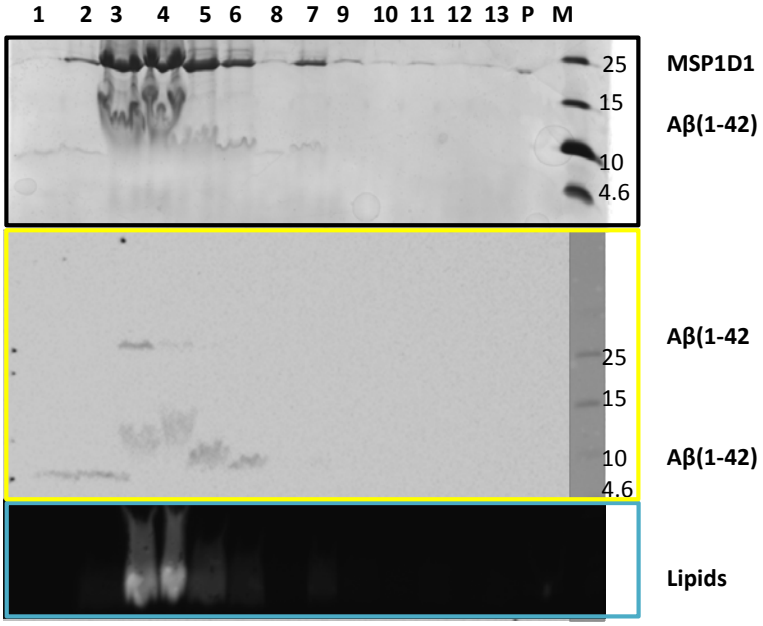

Figure 3.13: Analysis of [U-^{15}N]-Aβ(1-42) nanodisc NMR spectroscopy sample

Residiual [U-^{15}N]-Aβ(1-42) total-GM1 MSP1D1 nanodiscs, labelled with on fluorescent DMPE Atto633 lipid per nanodisc, sample was analysed by DGC. DGC fractions (1 to 13 and pellet P) were analysed by SDS-PAGE and three different detection methods. M: molecular weight marker. Black panel: silver staining; Yellow panel: Western Blot: 1st antibody was 6E10. A 2nd peroxidase coupled antibody was used to detect chemiluminiscence; Blue panel: band detection with excitation filter/bandpass 625/30 emission filter/bandpass 695/55. ATTO633-DMPE is visible.

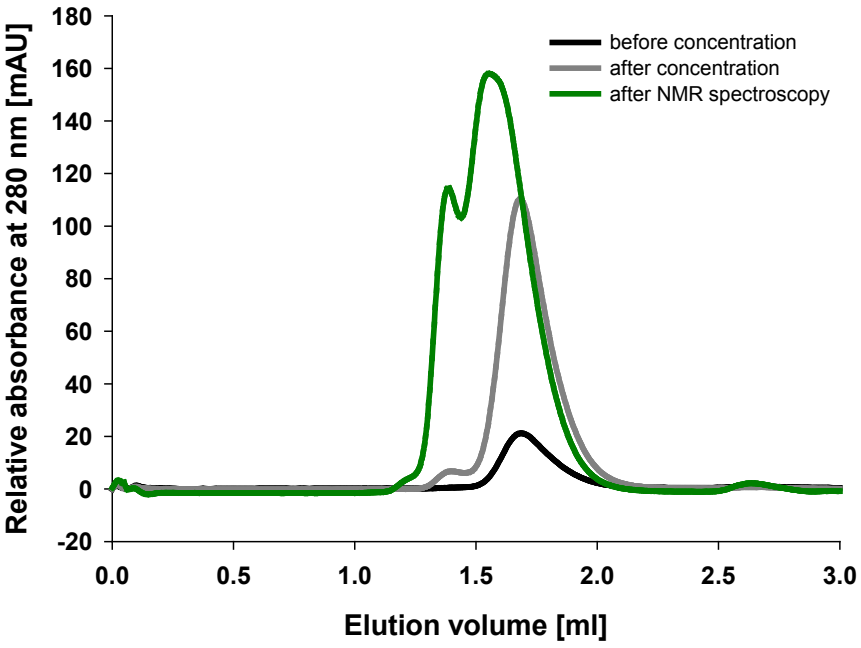

Figure 3.14: Analytical size exclusion chromatograms of nanodiscs before and after NMR spectroscopy experiments

Size exclusion chromatograms of MSP1D1ΔH5 nanodiscs before concentration (black) and after concentration (grey), but before NMR spectroscopy experiments, and after NMR spectroscopy experiments (green). The chromatography was performed on a Superdex 200 increase 5/15 column with a flowrate of 0.3 ml/min. Visible is the recorded relative absorbance at a wavelength of 280 nm. Nanodiscs eluted with an elution volume of 1.65 ml.

3.5 Aβ Membrane Interaction Analysed by Fluorescence Titration

The fluorescence changes of the (7-dimethylaminocoumarin-3yl)-carbonyl (DAC) reporter moiety of DAC-Aβ(1-40) was used to analyse binding of DAC-Aβ(1-40) to model membrane systems with different lipid compositions (fig. 3.15). DAC is a solvatochromic dye, which has a low fluorescent yield in aqueous solution but increases fluorescence intensity upon increased hydrophobicity of the surrounding environment e.g. when bound to a membrane (Demchenko, Mely et al. 2009). This effect as well as the associated blue shift, from 475 nm to 465 nm, is clearly seen in figure 3.15 and 3.16 indicating DAC-Aβ(1-40) being bound to the membrane with the dye moiety interacting with the membrane.

3.5.1 Establishment of the Fluorescence Titration Experiments

Matzusaki and co-workers revealed by fluorescence titration experiments binding of DAC-Aβ(1-40) to liposomes in a ganglioside and cholesterol dependent manner (Kakio, Nishimoto et al. 2001; Kakio, Nishimoto et al. 2002). As nanodiscs have several advantages over liposomes such as higher homogeneity, higher stability and a smaller size, it was tested if their setup also works for fluorescence titration of DAC-Aβ(1-40) and nanodiscs.

Firstly, it was tested if the findings of Matzusaki and colleagues were reproducible. Therefore, liposomes composed of the same lipid composition than in one of their setups were prepared. The lipid mixture was ganglioside GM1 (GM1), sphingomyelin (SM) and cholesterol (Chol) in a molar ratio of 4:3:3, which will be called low-GM1 in the following. Additionally, liposomes composed of the phospholipids phosphatidylglycerol (PG) and phasphatidylcholine (PC) as well as cholesterol (Chol) in a molar ratio of PG:PC:Chol 4:4:2 were used (PG/PC/Chol). Several groups found binding of Aβ to liposomes with anionic lipid head groups as well as a cholesterol dependent binding was observed by atomic force microscopy studies on supported lipid monolayers (McLaurin and Chakrabartty 1997; Hane, Drolle et al. 2011; Drolle, Gaikwad et al. 2012).

After extrusion through a 100 nm membrane, large unilamelar vesicles (LUVs) were obtained. Their size was checked by DLS. 109 nM DAC-Aβ(1-40) solution was titrated with aliquots of LUVs. The titration interval was 3 minutes in order to establish equilibrium binding, which was confirmed to be sufficient. The fluorescence emission spectra were recorded with an excitation wavelength of 430 nm. Upon titrating low-GM1-liposomes to the DAC-Aβ(1-40) an increase in fluorescence intensity as well as a blue shift from 475 nm to 465 nm of emission maximum was observed (fig. 3.15 A), indicating DAC-Aβ(1-40) interacting with the membrane. The results obtained here are consistent with findings obtained by Matzusaki and co-workers (Kakio, Nishimoto et al. 2001; Kakio, Nishimoto et al. 2002). The concentration of liposomes is displayed in the excess of ganglioside GM1 to DAC-Aβ(1-40), as shown before by Matzusaki and co-workers. However, one has to keep in mind that the concentration calculated here is based on the starting concentration of the lipid mixture used for liposome preparation. During the preparation the concentration might have changed due to losses, therefore binding constants of DAC-Aβ(1-40) to low-GM1-liposomes were not determined.

It was also tested if low-GM1-liposomes in buffer have an influence on the emission spectrum; therefore the highest titration concentration, 231 x more GM1 than DAC-Aβ(1-40), used for the titration was tested. The emission spectrum was consistent with the emission spectrum of buffer (fig. 3.15 B green and grey line). Upon titrating PG/PC/Chol-liposomes to a 109 nM DAC-Aβ(1-40) solution no increase in fluorescence nor a blue shift was detected, indicating no binding of DAC-Aβ(1-40) to those liposomes. Figure 3.15 B shows in orange the highest concentration of the PG/PC/chol-liposomes titration series, 427 x more lipid than DAC-Aβ(1-40). The fluorescence intensity was slightly lower than the starting fluorescence intensity of a DAC-Aβ(1-40) (black), which is due to dilution effects. Again the concentration of PG/PC/Chol-liposomes is given as excess of lipids to DAC-Aβ(1-40). No interaction of DAC-Aβ(1-40) with PC/PG/Chol liposomes under the here applied conditions was observed.

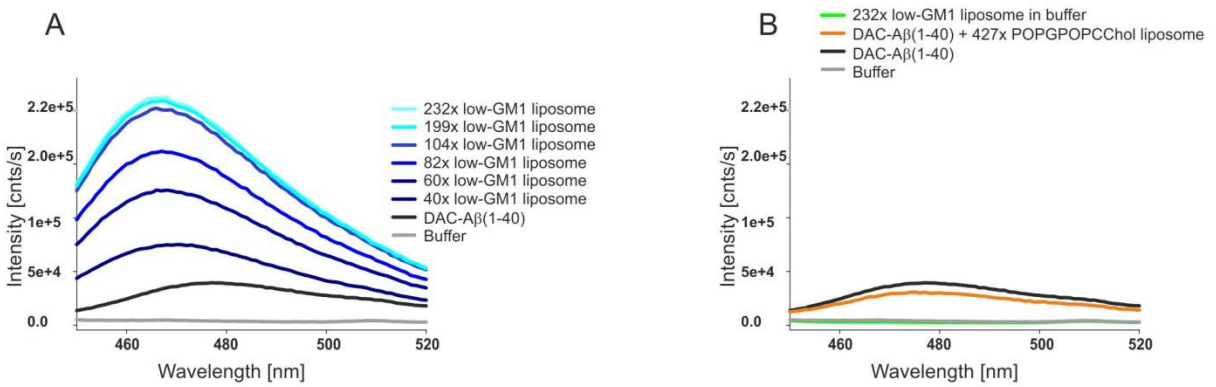

Figure 3.15: Emission spectra of DAC-Aβ(1-40) titrated with liposomes

A) Emission spectra (450-520 nm) of one representative titration series were recorded with an excitation wavelength of 430 nm at 37 °C. Grey: emission spectrum of buffer (150 mM NaCl, 2 mM $CaCl_2$, 10 mM Tris-HCl pH 7.4); black: emission spectrum of 109 nM DAC-Aβ(1-40). 109 nM DAC-Aβ(1-40) titrated with aliquots of low-GM1 liposomes. The higher the liposome concentration the lighter the blue of the emission spectrum. B) Grey: emission spectrum of buffer (150 mM NaCl, 2 mM $CaCl_2$, 10 mM Tris-HCl pH 7.4); black: emission spectrum of 109 nM DAC-Aβ(1-40) green: emission spectrum of highest concentration of low-GM1 liposome used for the titration series in buffer; orange: emission spectrum of 109 nM DAC-Aβ(1-40) in the presence of the highest PG/PC/Chol liposome concentration used for the titration series.

After successfully establishing the fluorescence titration setup with liposomes, nanodiscs composed of low-GM1 and PC/PG/Chol were tested for their interaction with DAC-Aβ(1-40). Surprisingly, upon titration of low-GM1-MSP1D1 nanodiscs to the DAC-Aβ(1-40) solution neither an increase in fluorescence nor a blue shift of the emission maximum was detected. The highest concentration, corresponding to 292 nM nanodiscs or 113 times more GM1 than DAC-Aβ(1-40), of the titration series is shown in figure 3.16 (blue), the fluorescence intensity was lower than the starting fluorescence intensity (black) due to dilution effects. The same effect was observed for PC/PG/Chol MSP1D1 nanodiscs (fig. 3.16, orange). DAC-Aβ(1-40) did neither bind to low-GM1-MSP1D1 nanodiscs nor PC/PG/Chol MSP1D1 nanodiscs.

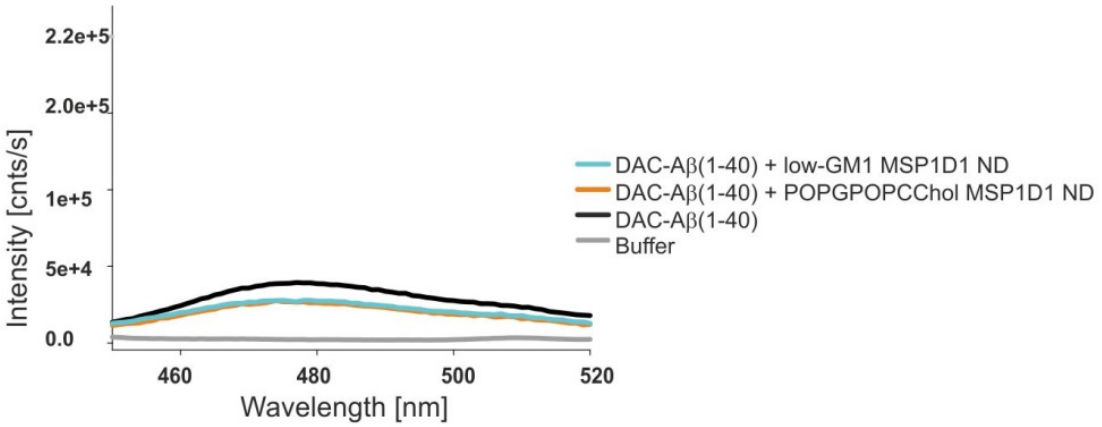

Figure 3.16: Emission spectra of DAC-Aβ(1-40) with or without nanodiscs

Emission spectra (450-520 nm) of were recorded with an excitation wavelength of 430 nm at 37°C. Grey: emission spectrum of buffer (150 mM NaCl, 2 mM $CaCl_2$, 10 mM Tris-HCl pH 7.4); black: emission spectrum of 109 nM DAC-Aβ(1-40); blue: emission spectrum of 109 nM DAC-Aβ(1-40) in the presence of the highest concentration of low-GM1 MSP1D1 nanodiscs (292 nM). orange: emission spectrum of 109 nM DAC-Aβ(1-40) in the presence of the highest PG/PC/Chol MSP1D1 nanodisc concentration (286 nM) used for the titration series.

However, titration of DAC-Aβ(1-40) with nanodiscs composed of only ganglioside GM1 (total-GM1) resulted in an increase in fluorescence and a blue shift of the emission maximum from 475 nm to 465 nm (fig. 3.17 A). DAC-Aβ(1-40) did bind to total-GM1 MSP1D1 nanodiscs. In order to determine overall equilibration dissociation constants (K_D) of DAC-Aβ(1-40) to nanodiscs, the relative fluorescence enhancement (R) was plotted against the respective nanodisc concentration, which can be easily determined by absorbance at 280 nm (fig. 3.17 B). R is determined as $(F-F_0)/F_0$. F and F_0 are the fluorescence intensities at 470 nm after buffer correction in presence and absence of nanodiscs, respectively. Data were fitted according to Langmuir´s 1:1 binding model. K_D values represent means ± SD of at least three independent experiments. The K_D determined for DAC-Aβ(1-40) to total-GM1 MSP1D1 nanodiscs was 51 nM ± 22. One representative experiment is shown in figure 3.17.

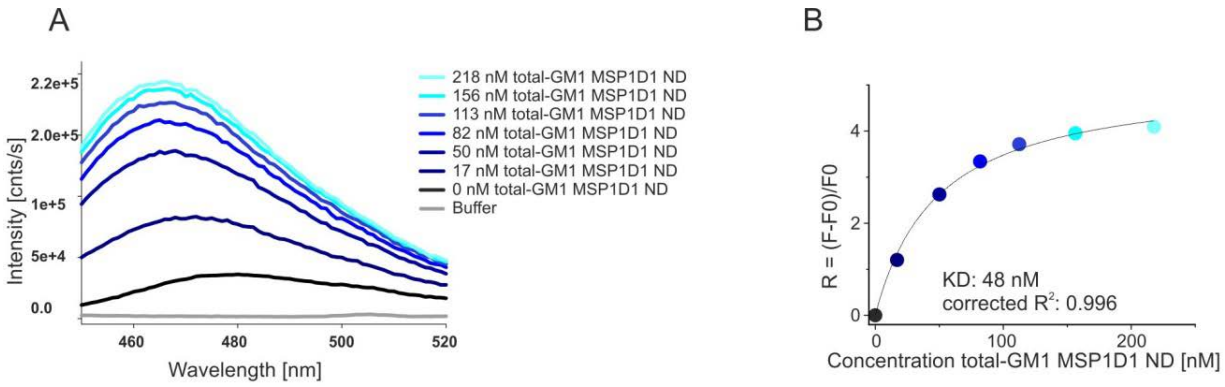

Figure 3.17: Analysis of DAC-Aβ(1-40) binding to total-GM1 MSP1D1 nanodiscs by FT

A: Fluorescence emission spectra (450-520 nm) of one representative DAC-Aβ(1-40) total-GM1 MSP1D1 nanodisc titration experiment. 109 nM DAC-Aβ(1-40) solution was prepared (black) and titrated with aliquots of concentrated nanodisc in intervals of 3 min (the lighter the blue the higher the nanodisc concentration). Grey: buffer (150°mM NaCl, 2 mM $CaCl_2$, 10 mM Tris-HCl pH 7.4). Excitation wavelength was 430 nm and the temperature 37°C B: The relative fluorescence enhancement ($R = (F-F_0)/F_0$) of each titration step was plotted against nanodisc concentrations in order to determine overall apparent equilibration dissociation constants (K_D) values. Data were fitted according to Langmuir´s 1:1 binding model.

3.5.2 Glutathione and Cys0-Aβ(1-42) Labelling with DACIA

In order to exclude that binding of DAC-Aβ(1-40) to nanodiscs is caused by an interaction of the dye itself with the nanodisc, [N-(7-dimethylamino-4-methylcoumarin-3-yl)iodoacetamide] (DACIA), a thiol reactive labelling version of the dye, was coupled to the tripeptide glutathione. The coupling of the dye to the tripeptide is required as the dye is not soluble in water. Glutathione is highly water soluble and no membrane interaction is known.

The labelling reaction was performed in darkness in the presence of 40 % DMSO in order to ensure solubility of DACIA. After 1 h at room temperature the labelling success was analysed by RP-HPLC (fig. 3.18). The reaction was monitored at an absorbance of 376 nm. The chromatogram of DACIA without glutathione is displayed in black. One peak at 16 min was detected representing the dye, a smaller peak at 15.3 min was detected, too. This is thought to be an impurity as it was also detected after 1 h of reaction time (fig. 3.18 orange chromatogram). The peak at 16 min almost disappeared after 1 h incubation time and a peak at 12.2 min appeared, which is DAC-glutathione. The peak was collected and lyophylised

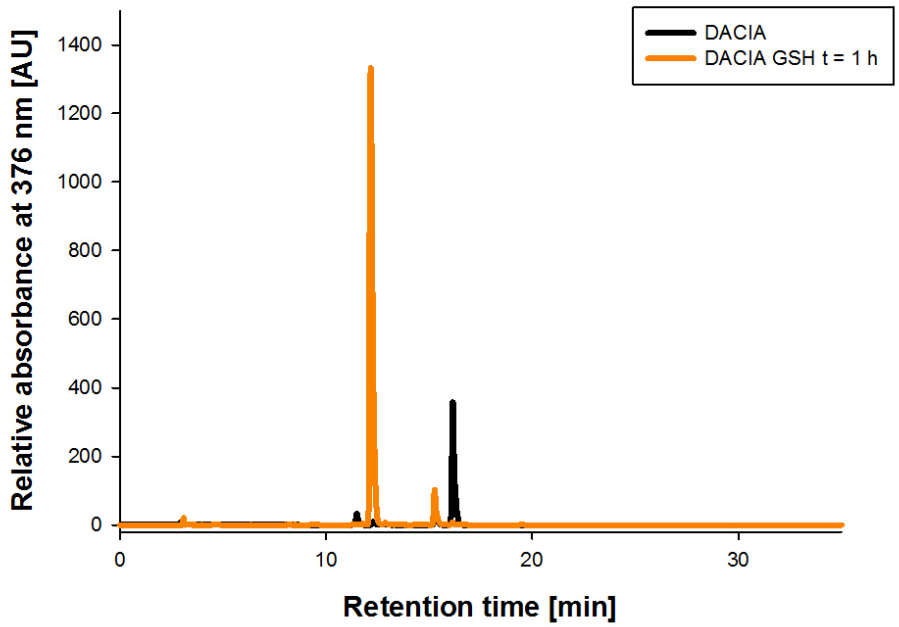

Figure 3.18: RP-HPLC chromatograms of gluthatione labelling with DACIA

The chromatography was performed with a Zorbax SB-300-C8 column with a flowrate of 1 ml/min in a gradient from aqueous 10 % (v/v) acetonitrile (AcN) 0.1 % (v/v) trifluoric acid (TCA) to 100 % (v/v) AcN 0.1 % (v/v) TCA over 35 min as mobile phase. Visible is the recorded relative absorbance at a wavelength of 376 nm. The column was tempered at 80 °C. Black: DACIA; Orange: gluthatione DACIA reaction mix after 1 h. The dye elutes after 16 min. After labelling of glutathione with DACIA the DAC-glutathion elutes at 12.2 min.

In order to extend the analysis of Aβ interaction with membranes to Aβ(1-42) recombinant Aβ(1-42) with a cysteine residue at position zero (Cys0-Aβ(1-42) was labelled with DACIA. The labelling reaction was performed in darkness in the presence of 80 % DMSO and TCEP to avoid aggregation and dimer formation of Cys0-Aβ(1-42). The ratio 20:4.5:1 DACIA:TCEP:Cys0-Aβ(1-42) was used.

After 1 h at room temperature the labelling success was analysed by RP-HPLC (fig. 3.19 A). The reaction was monitored at an absorbance of 376 nm and 214 nm. The labelling conditions were not optimal besides DAC-Cys0-Aβ(1-42) (24 min), unlabelled Cys0-Aβ(1-42) (15.8 min) and the dimer (30.2 min) were present. The DAC-Cys0-Aβ(1-42) fractions were lyophilised and confirmed by dot blot to be Aβ. The labelling conditions were not optimised as DAC-Cys0-Aβ(1-42) did not dissolve in buffer and was therefore not used in FT experiments.

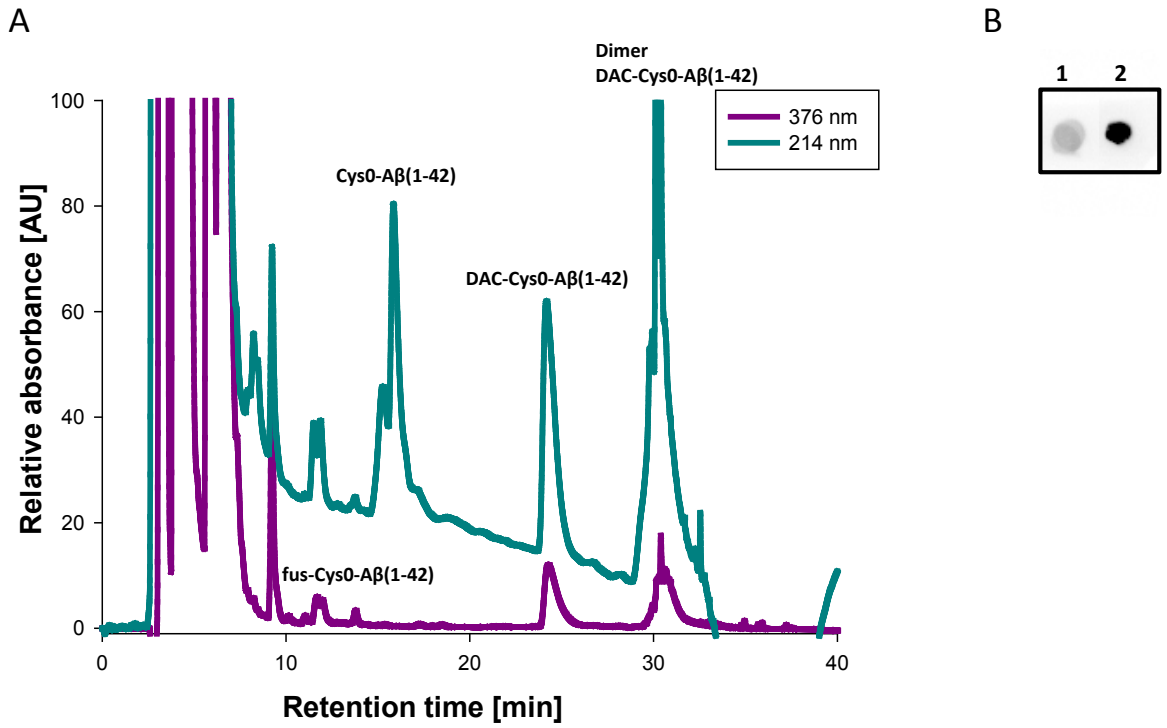

Figure 3.19: Analysis of Cys0-Aβ(1-42) labelling with DACIA

A: The chromatography was performed with a Zorbax SB-300-C8 column with a flowrate of 1 ml/min in 30 % (v/v) AcN 0.1 % (v/v) TCA for 30 min with an additional wash step from 30 % (v/v) AcN 0.1 % (v/v) TCA up to 80 % (v/v) AcN 0.1 % (v/v) TCA over 5 min and back to 30 % (v/v) AcN 0.1 % (v/v) TCA in 5 min. Visible is the recorded relative absorbance at a wavelength of 214 nm (green)and 376 nm (purple). The column was tempered at 80 °C. B: dot blot: 1st antibody was 6E10. A 2nd peroxidase coupled antibody was used to detect chemiluminiscence; 1: DAC-Cys0-Aβ(1-42) 2: synthetic Aβ(1-42).

3.5.3 Fluorescence Titration Experiments with MSP1D1ΔH5 Nanodiscs

In a next step it was tested if smaller MSP1D1ΔH5 nanodiscs are also suitable for Aβ membrane interaction. Total-GM1 MSP1D1ΔH5, high-GM1 MSP1D1ΔH5 and low-GM1 MSP1D1ΔH5 nanodiscs were prepared (fig 3.20) in a low-salt buffer and after concentration used for FT.

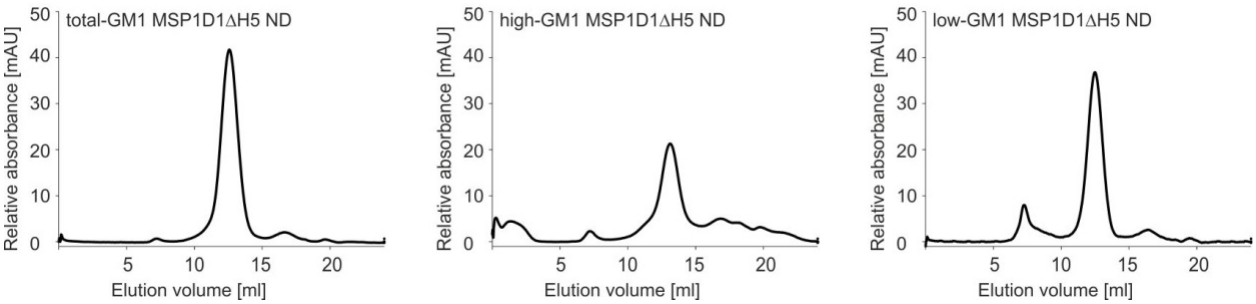

Figure 3.20: Size exclusion chromatograms of different MSP1D1ΔH5 nanodiscs

Size exclusion chromatograms of three MSP1D1ΔH5 nanodiscs. The chromatography was performed on a Superdex 200 100/300 GL column with a flowrate of 0.5 ml/min. Visible is the recorded relative absorbance at a wavelength of 280 nm. The void volume of the column is 8 ml corresponding to the first peak. Nanodiscs elute in the second peak with an elution volume of 12.25 ml.

An increase in fluorescence intensity as well as the characteristic blue shift of the emission maximum from 475 nm to 465 nm of DAC-Aβ(1-40) was observed upon titration of total-GM1 MSP1D1ΔH5 and high-GM1 MSP1D1ΔH5 nanodiscs, indicating DAC-Aβ(1-40) interacting with the membrane (fig. 3.21 A and B).

In order to determine the K_D of DAC-Aβ(1-40) to the different membranes, the relative fluorescence enhancement (R) was plotted against the respective nanodisc concentration (fig. 3.21 C/D). In figure 3.21 C/D one representative plot is shown. The overall equilibration dissociation constants were 25 ± 8.0 nM for total-GM1 MSP1D1ΔH5 nanodiscs and 41 ± 10 nM for high-GM1 MSP1D1ΔH5 nanodiscs. Both are in the same nanomolar range. In contrast, no changes in DAC fluorescence of DAC-Aβ(1-40) was detectable when low-GM1 ND (with applied final concentrations of 180 nM) were titrated on 109 nM DAC-Aβ(1-40) (fig. 3.22). This indicates that DAC-Aβ(1-40) was not interacting with low-GM1 ND, thus no K_D could be determined.

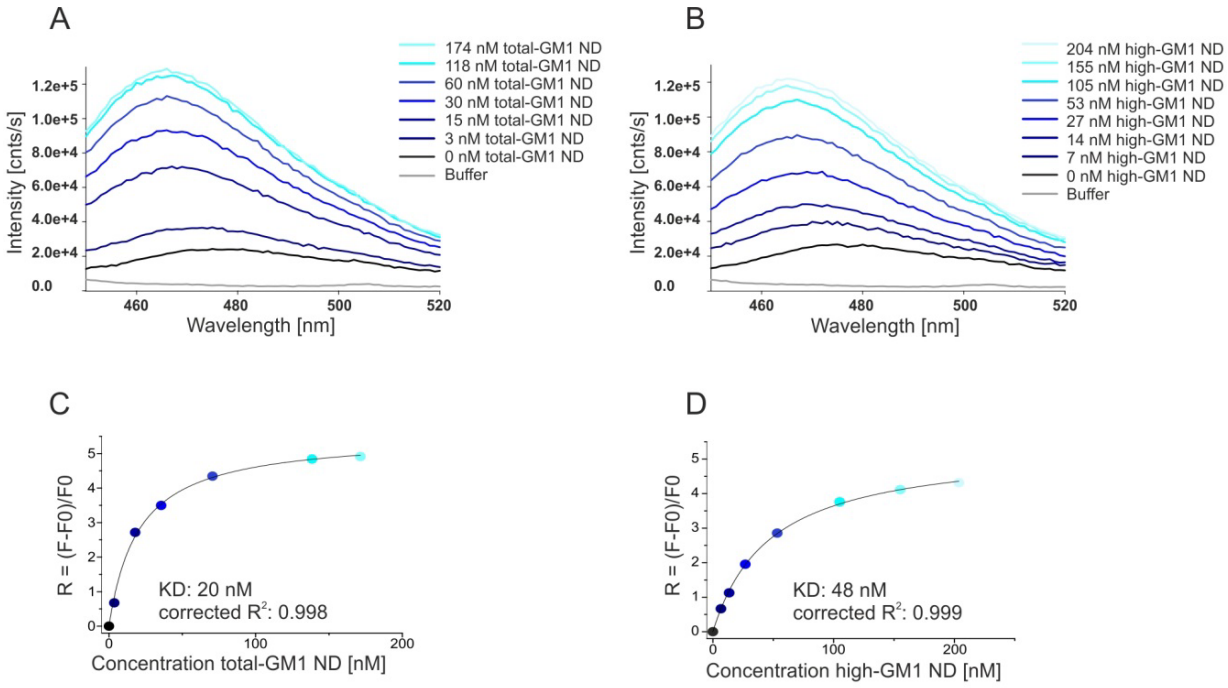

Figure 3.21: Analysis of DAC-Aβ(1-40) binding to total-GM1 and high GM1 MSP1D1ΔH5 nanodiscs by FT

Fluorescence emission spectra (450-520 nm) of one representative DAC-Aβ(1-40) MSP1D1ΔH5 nanodiscs titration experiment. 109 nM DAC-Aβ(1-40) solution was prepared and titrated with concentrated aliquots of nanodiscs. Excitation wavelength was 430 nm. A) total-GM1 nanodisc (ND) B) high-GM1 ND.
The relative fluorescence enhancement ($R = (F-F_0)/F_0$) of each titration step was plotted against nanodisc concentrations in order to determine overall apparent equilibration dissociation constants (K_D) values. Data were fitted according to Langmuir´s 1:1 binding model. C) total-GM1 ND D) high-GM1 ND.

DAC coupled to glutathione (DAC-glutathione) served as a negative control. No binding of DAC-glutathione to any of the tested nanodiscs was observed, as shown in figure 3.22 A.

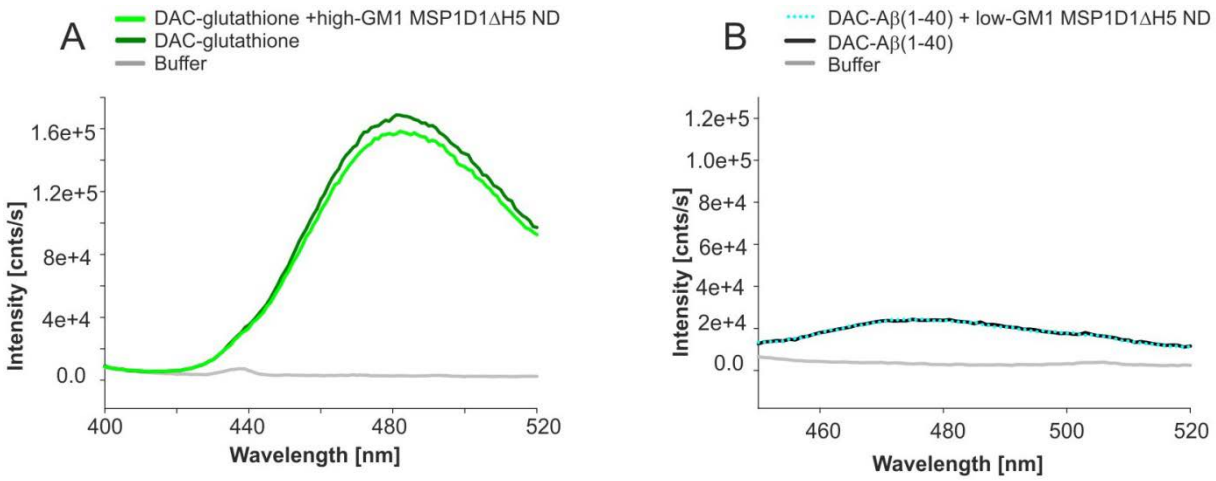

Figure 3.22: Analysis of DAC-glutathione and DAC-Aβ(1-40) binding to nanodiscs by fluorescence spectroscopy

A: Emission spectrum (400-520 nm) was recorded with an excitation wavelength of 380 nm at 37°C. Grey: emission spectrum of buffer (10 mM KH_2PO_4/K_2HPO_4, pH 7.2 0.5 mM EDTA); dark green: emission spectrum of DAC-gluthatione; light green: emission spectrum of DAC-gluthatione in presence of the highest of high-GM1 MSP1D1ΔH5 nanodiscs concentration (203 nM). B: Emission spectrum (450-520 nm) was recorded with an excitation wavelength of 430 nm at 37°C. Grey: emission spectrum of buffer (10 mM KH_2PO_4/K_2HPO_4, pH 7.2 0.5 mM EDTA); black: emission spectrum of 109 nM DAC-Aβ(1-40); blue: emission spectrum of 109 nM DAC-Aβ(1-40) in presence of the highest of low-GM1 MSP1D1ΔH5 nanodiscs concentration (180 nM).

3.6 Aβ Membrane Interaction Analysed by BioLayer Interferometry

In order to confirm the results obtained by FT with an alternative and independent method, BioLayer Interferometry (BLI) experiments were set up. Furthermore, BLI allows analysis of Aβ(1-42) binding to nanodiscs, as N-terminally biotinylated-Aβ(1-42) is commercially available.

3.6.1 Aβ Preparation for BLI

In order to analyse Aβ membrane interaction further, regarding the Aβ species binding to the membrane, monomeric as well as oligomeric Aβ species were prepared (chapter 2.2.11.1) and used for BLI. N-terminally biotinylated Aβ(1-40) as well as N-terminally biotinylated Aβ(1-42) were used.

For preparation of monomeric species, HFIP pretreated and lyophylised Aβ was dissolved in buffer and directly applied to SEC. Monomeric Aβ eluted after 14 minutes (fig. 3.23). The respective peaks were collected and immediately used for immobilisation on the BLI tip.

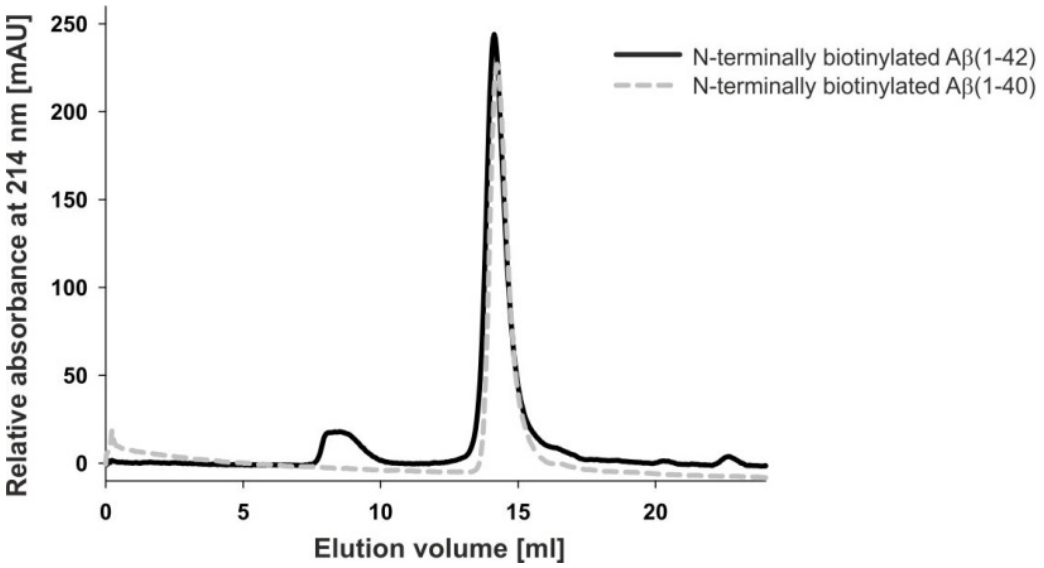

Figure 3.23: Preparation of monomeric N-terminally biotinylated Aβ species by SEC

Size exclusion chromatogram of N-terminally biotinylated Aβ (N-bio-Aβ). The chromatographies were performed on a Superdex 75 100/300 GL column with a flowrate of 0.5 ml/min. Visible is the recorded relative absorbance at a wavelength of 214 nm. The void volume of the column is 8 ml corresponding to the first peak. Monomeric N-terminally biotinylated Aβ elute at 14 ml.

For the oligomeric species preparation N-terminally biotinylated Aβ and non-biotinylated Aβ were mixed in a molar ratio of 10:1 during the HFIP pretreatment. After lyophilisation Aβ was dissolved in buffer (80 µM) and incubated at 22°C 600 rpm for 2.5 h in case of Aβ(1-42). A longer incubation over night was required for Aβ(1-40) to form oligomers, which were prepared by DGC on a iodixanol gradient. This method allows matrix-free separation and fractionation of different Aβ species according to their sedimentation coefficients which depend on particle size and shape. Directly after centrifugation, oligomeric species obtained from fraction 5 or mixed monomer and small oligomeric species from fraction 3 were used for immobilisation on the BLI tip (fig. 3.24).

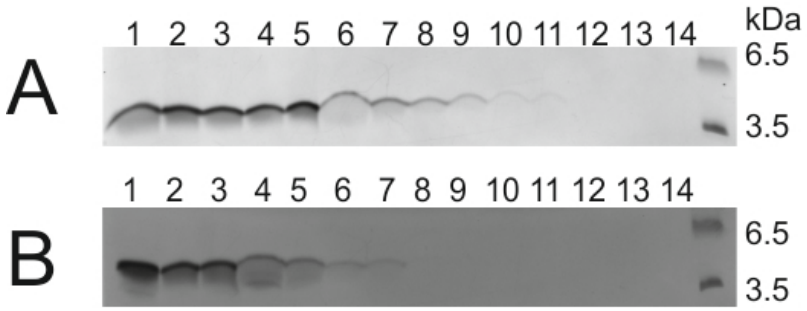

Figure 3.24: Analysis of Aβ(1-42) (A) and Aβ(1-40) (B) aggregate size distributions derived by DGC

The mixtures of oligomeric Aβ species were prepared by incubation of monomeric N-terminally biotinylated Aβ and monomeric non-biotinylated Aβ in a molar ratio of 1:10, with subsequent separation by DGC, fractionation and analysis of the fractions by were prepared by Tris-Tricine SDS-PAGE and silver staining

3.6.2 Monomeric Aβ Membrane Interaction Analysed by BLI

Initially, the binding of monomeric SEC derived N-terminally biotinylated-Aβ(1-40) and N-terminally biotinylated Aβ(1-42) to different MSP1D1ΔH5 nanodiscs was analysed. Monomeric N-terminally biotinylated Aβ was coupled on the sensor surface of Super Streptavidin biosensors (SSA) to a final level of 2 nm using an Octet RED96 instrument. The remaining free binding sites on the surface were blocked by biotin (50 µg/ml). Reference sensors were also quenched with biotin. Experiments were performed at 26 °C with 300 rpm vertical rotation.

Both monomeric Aβ(1-40) and Aβ(1-42) bound with high affinity to total-GM1 MSP1D1ΔH5 nanodiscs and high-GM1 MSP1D1ΔH5 nanodiscs (fig. 3.25) but not to low-GM1 ND, DMPC ND and PC/PG/Chol nanodiscs. No signal was detected for low-GM1 nanodiscs, DMPC nanodiscs and PC/PG/Chol nanodiscs after double referencing, using the reference biosensors and a buffer cycle. Sensorgrams of monomeric Aβ(1-40) or monomeric Aβ(1-42) binding to total-GM1 MSP1D1ΔH5 nanodiscs and high-GM1 MSP1D1ΔH5 nanodiscs are depicted in figure 3.25.

Both types of nanodiscs displayed a heterogeneous binding model to both monomeric Aβ(1-40) and monomeric Aβ(1-42). The binding behaviour was composed of two overlaying kinetics, a fast and a slow one, with a slow off rate. Therefore, monovalent steady state analyses were performed. They led to robust overall apparent equilibration dissociation constants (K_D). After double referencing the sensorgrams respective response levels were plotted against nanodisc concentration. The curves were fitted using Langmuir´s 1:1 binding model. The fitting curves are shown in figure 3.26. No binding of low-GM1 MSP1D1ΔH5 nanodiscs, DMPC MSP1D1ΔH5 nanodiscs and PC/PG/Chol MSP1D1 nanodiscs to monomeric Aβ(1-40) or monomeric Aβ(1-42) was observed in the concentration range of up to 1.0 µM. Thus no K_D values were determined.

The K_D values determined for total-GM1 MSP1D1ΔH5 nanodiscs and high-GM1 MSP1D1ΔH5 nanodiscs to monomeric Aβ(1-40) were with 24 + 13 nM and 49 ± 42 nM in the same nanomolar range. Comparing the obtained K_D values from BLI to the ones obtained from FT, 25 ± 8.0 nM for total-GM1 and 41 ± 10 nM for high-GM1 MSP1D1ΔH5 nanodiscs, showed they are consistent. No difference in binding affinity of monomeric Aβ(1-42) to total-GM1 MSP1D1ΔH5 nanodiscs and high-GM1 MSP1D1ΔH5 nanodiscs was observed as they bound with a K_D value of 30 ± 19 nM and 29 ± 26 nM, respectively. And notably, these K_D values were within the same nanomolar range than the ones for GM1 containing MSP1D1ΔH5 nanodiscs binding to monomeric Aβ(1-40).

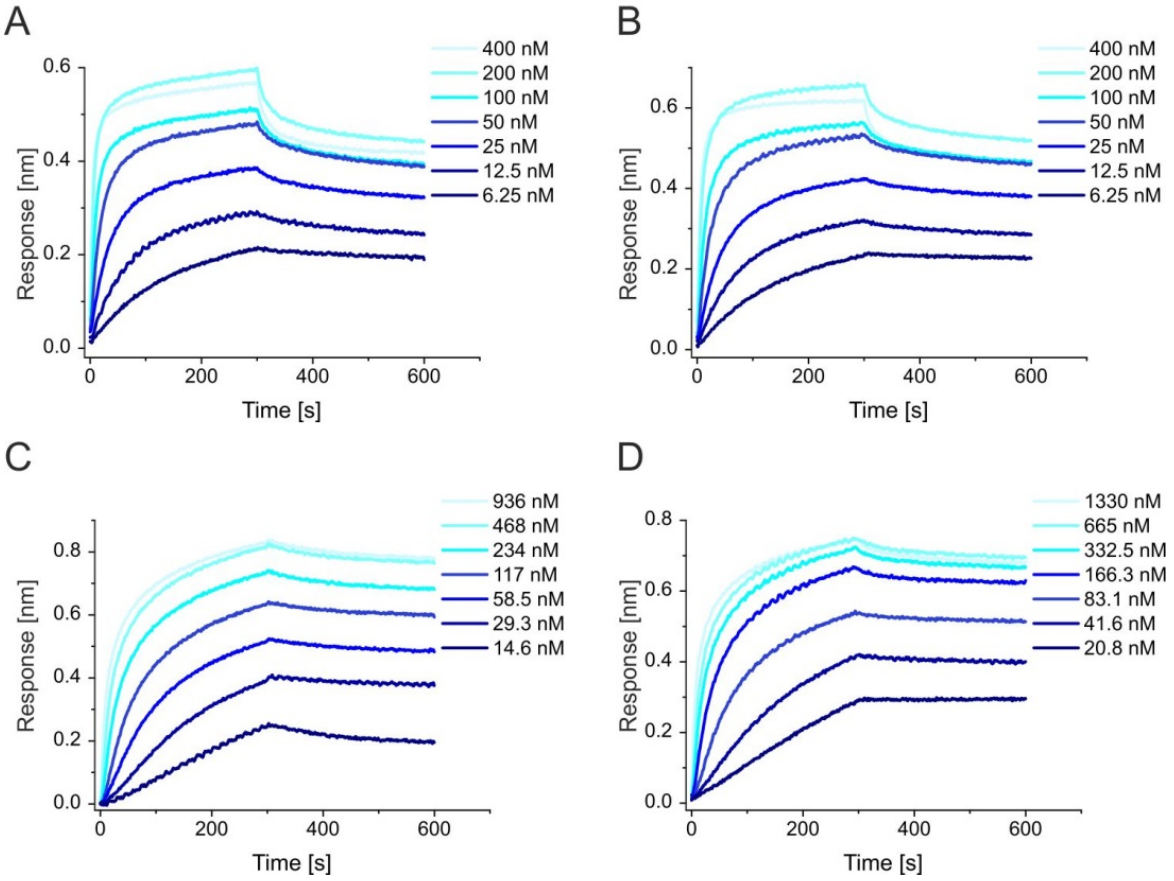

Figure 3.25: BLI sensorgrams of monomeric Aβ nanodisc interactions

Monomeric N-terminally biotinylated Aβ(1-40) (A/B) and Aβ(1-42) (C/D) was coupled to streptavidin sensor surfaces. Nanodiscs were used as analytes. The sensorgrams show one representative experiment. A) Aβ(1-40) total-GM1 MSP1D1ΔH5 nanodisc B) Aβ(1-40) high-GM1 MSP1D1ΔH5 nanodisc C) Aβ(1-42) total-GM1 MSP1D1ΔH5 nanodisc D) Aβ(1-42) high-GM1 MSP1D1ΔH5 nanodisc.

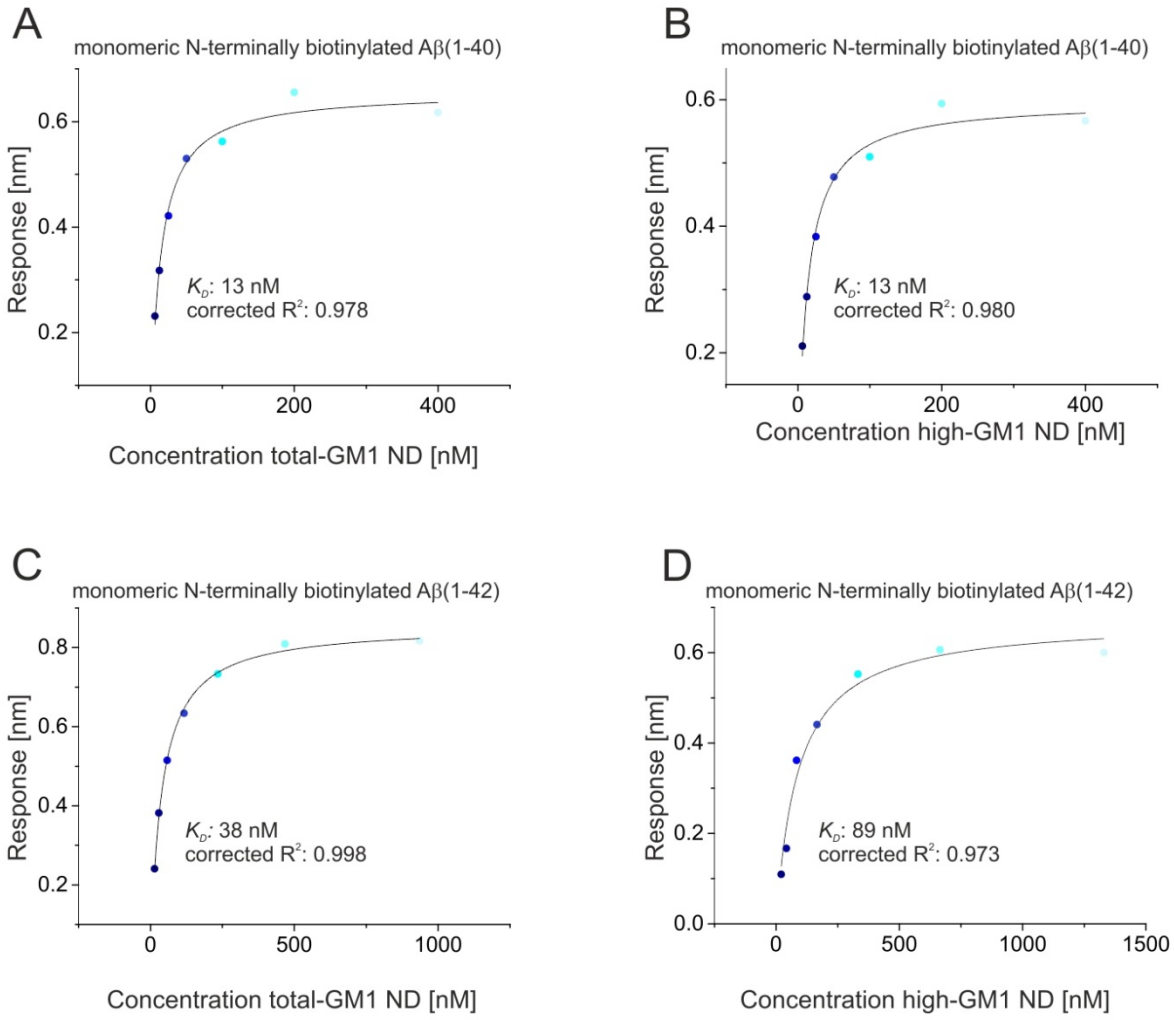

Figure 3.26: Overall apparent equilibration dissociation constants (K_D) determination of monomeric Aβ nanodisc interactions

The equilibrium response signals of each cycle were plotted against MSP1D1ΔH5 nanodiscs (ND) concentrations in order to determine overall apparent equilibration dissociation constants (K_D) values. Data were fitted according to Langmuir´s 1:1 binding model. A) Aβ(1-40) total-GM1 ND B) Aβ(1-40) high-GM1 ND C) Aβ(1-42) total-GM1 ND D) Aβ(1-42) high-GM1 ND.

3.6.3 Oligomeric Aβ Membrane Interaction Analysed by BLI

Next, binding of total-GM1 MSP1D1ΔH5 nanodiscs to oligomeric Aβ species was tested. Aβ oligomers were obtained after separation from monomeric Aβ by DGC (chapter 3.6.1 fig. 3.24). Those oligomers, which were obtained after fractionation from fraction 5, were characterised by Brener *et al*. 2015 and exhibit neurotoxcicity. No signal was detected after double referencing the sensorgrams of total-GM1 MSP1D1ΔH5 nanodiscs and oligomeric Aβ. Hence, no binding was found to neither oligomeric Aβ (1-40) nor oligomeric Aβ(1-42). Yet, binding of total-GM1 MSP1D1ΔH5 nanodisc to Aβ species from fraction 3, containing monomeric and small oligomeric Aβ species, was detected (fig. 3.27). The binding behaviour is as observed for monomeric Aβ species: two overlaying kinetics, a fast and a slow one, with a slow off rate. Again, monovalent steady state analysis was performed and led to robust overall apparent equilibration dissociation constants (K_D). The K_D values of total-GM1

MSP1D1ΔH5 nanodiscs binding to Aβ(1-40) and Aβ(1-42) were 40 ± 32 nM and 28 ± 9.4 nM, respectively.

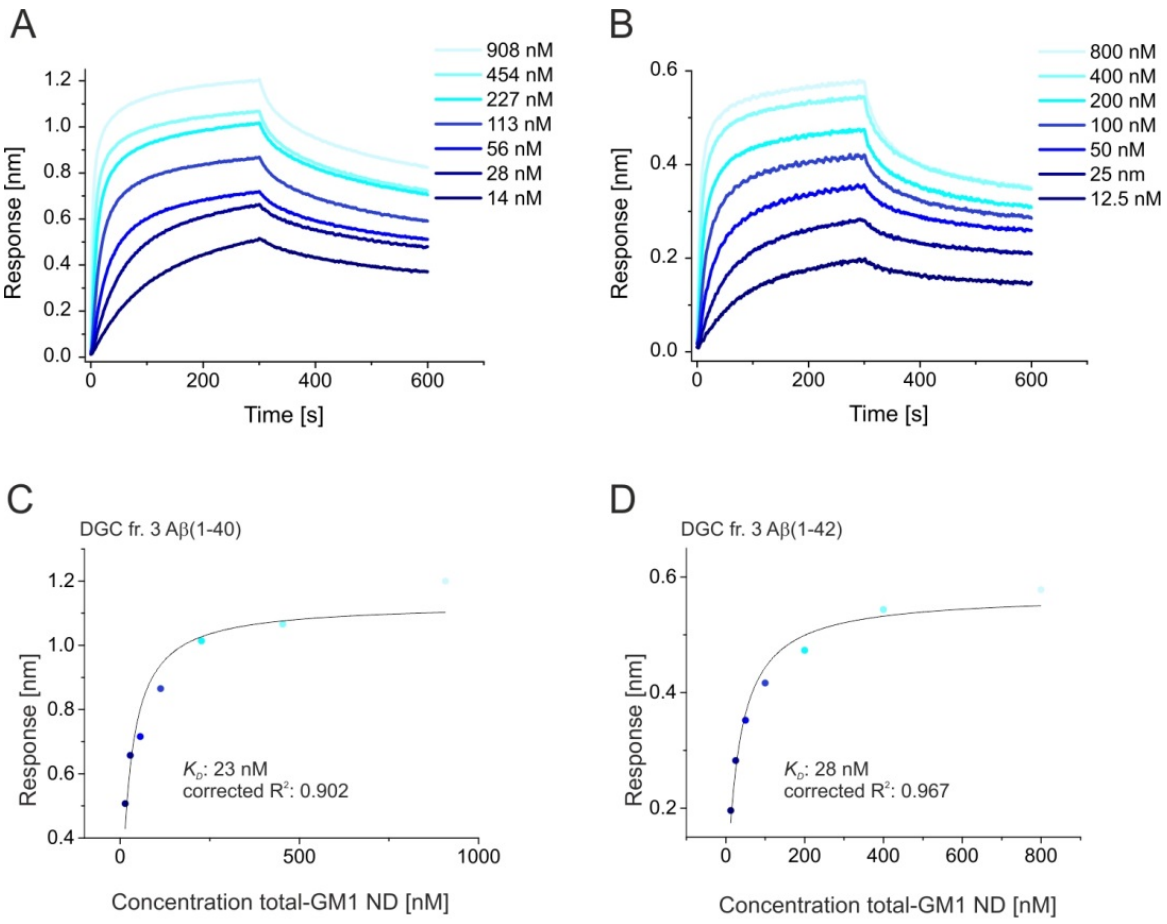

Figure 3.27: BLI sensorgrams of Aβ nanodisc interactions and overall apparent equilibration dissociation constants (K_D) determination

Sensorgrams of nanodisc Aβ interactions: Aβ(1-40) (A) and Aβ(1-42) (B) obtained from DGC fraction 3 was coupled to streptavidin sensor surfaces. Total-GM1 MSP1D1ΔH5 nanodiscs were used as analytes. The sensorgrams show one representative experiment. The equilibrium response signals of each cycle were plotted against ND concentrations in order to determine overall K_D values. Data were fitted according to Langmuir´s 1:1 binding model. C) Aβ(1-40) total-GM1ND D) Aβ(1-42) total-GM1 ND.

3.7 Concentrated Aβ Bound Nanodisc Samples Achieved by Ultracentrifugation

For further studies, high concentration of Aβ bound to nanodiscs might be crucial, therefore it was tested if it is possible to concentrate total-GM1 MSP1D1ΔH5 nanodiscs with bound Aβ(1-42) by ultracentrifugation. Aβ(1-42) incubated with total-GM1 MSP1D1ΔH5 nanodisc for 30 minutes at RT is found after centrifugation predominantly in the last three fractions, corresponding to 10 % of the total volume, together with the nanodiscs (fig. 3.28).

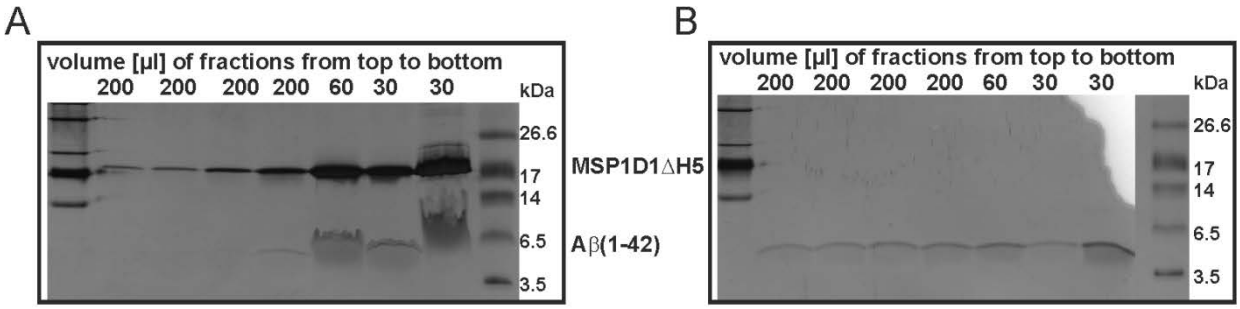

Figure 3.28: Analysis of Aβ(1-42) distribution after UC with and without nanodiscs by SDS-PAGE

Distribution of Aβ(1-42) incubated 30 min at RT with (A) and without (B) total-GM1 MSP1D1ΔH5 nanodiscs after ultracentrifugation 6 h at 160,000 g, visualised by Tris-Tricine PAGE and silver staining.

The quality of the concentrated nanodiscs was checked after concentration by analytical SEC (fig. 3.29). No shift in the elution volume of the nanodisc peak was detectable after concentration in comparison to the not concentrated sample. The concentration of nanodiscs in the last fraction was increased by a factor of 9.2, from a starting concentration of 1.2 µM to 11 µM. Concentration determination by RP-HPLC revealed that the concentration of Aβ(1-42) was increased also by a factor of 9.2 in the last fraction. In contrast, when we analysed Aβ(1-42) in the absence of total-GM1 ND is equally distributed over all fractions (fig. 3.28) and its concentration in the lower fraction was only increased by a factor of 2 in the last fraction. Hence it was possible to concentrate unlabelled Aβ(1-42) bound to total-GM1 MSP1D1ΔH5 nanodiscs by ultracentrifugation, which is a useful property for functional and structural studies such as NMR spectroscopy. The overall stoichiometry of Aβ:ND was here 1:1. Yet, this does not necessarily mean one Aβ molecule per nanodisc, as it is possible, that a mixture of empty nanodiscs as well as nanodiscs with more than one Aβ bound is present in the concentrated sample.

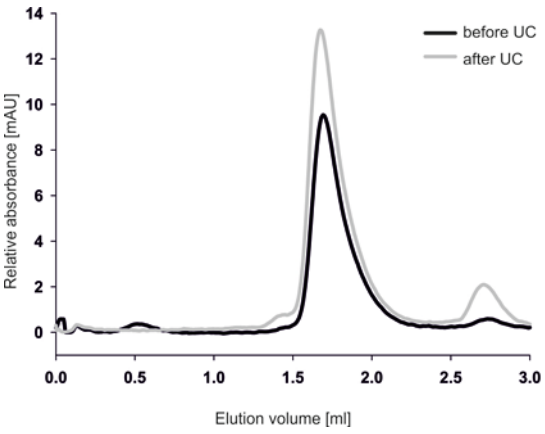

Figure 3.29: Analytical size exclusion chromatograms of nanodiscs

Size exclusion chromatograms of MSP1D1ΔH5 nanodiscs before concentration by ultracentrifugation (black) and after (grey). The chromatography was performed on a Superdex 200 increase 5/15 column with a flowrate of 0.3 ml/min. Visible is the recorded relative absorbance at a wavelength of 280 nm. Nanodiscs eluted with an elution volume of 1.65 ml.

4. Discussion

Alzheimer's disease (AD) is a progressive neurodegenerative disease and the most common form of dementia among people age 65 and older. During the progression of the disease nerve tissue is irreversibly damaged, causing loss of memory and cognitive decline. AD is characterised neuropathologically by neurofibrillar tangles, formed of hyperphosphorylated tau, and amyloid plaques, composed mainly of aggregated amyloid beta (Aβ). The aggregation of Aβ from its monomeric non-toxic form over toxic oligomeric species to amyloid fibrils and aggregates is thought to play a crucial role in AD. However, it is still unclear which mechanism causes the polymerisation process. Moreover, despite extensive research, the underlying molecular mechanism by which oligomeric Aβ species exhibit toxicity is still enigmatic.

For both mechanisms, the starting of polymerisation as well as the toxicity mechanism, Aβ interaction with neuronal cell membranes plays an important role. However, Aβ membrane interaction itself has not been completely elucidated yet. In order to gain further knowledge about the binding of Aβ to the membrane and connected structural secondary changes presumably leading to membrane insertion, high resolution structures are required. Yet, this has been hampered by the lack of an appropriate model membrane system.

Nanodiscs are model membrane systems. They are composed of two membrane scaffold proteins (MSP), surrounding a lipid bilayer. Homogeneity of nanodisc sizes can be achieved relatively easy, as the diameter of the nanodiscs is restricted by the length of the MSP, which also gives stability to nanodiscs in case of temperature changes (Denisov, McLean et al. 2005). Therefore, they exhibit several advantages over other model membrane systems such as micelles and liposomes (Timothy H. Bayburt 2009; Hagn, Etzkorn et al. 2013). Moreover, nanodiscs are easily adjustable for their lipid composition and have been shown to allow straight forward use of biophysical methods e.g. surface plasmon resonance (SPR), BioLlayer Interferometry (BLI) or nuclear magnetic resonance (NMR) spectroscopy to membrane inserted proteins (Denisov, McLean et al. 2005; Gluck, Wittlich et al. 2009; Ritchie, Grinkova et al. 2009; Timothy H. Bayburt 2009; Ma, Mohrluder et al. 2010; Hagn, Etzkorn et al. 2013).

In this work nanodiscs were tested for their suitability to investigate Aβ membrane interaction and subsequently used for studying these interactions.

4.1 Assembly of Nanodiscs with Aβ

There are two ways to obtain nanodiscs with the protein of interest (POI) inserted into the lipid bilayer. The first one is to preassemble empty nanodiscs, empty in terms of not having the protein of interest inserted. Subsequently, the empty nanodiscs are incubated with the POI, which will bind to

the membrane and possibly insert. The second option is to assemble the nanodiscs in the presence of the POI. Upon removal of the detergent, which solubilises the lipids and the POI, the nanodiscs with the POI inserted into the bilayer will form.

Atomic force microscopy (AFM) experiments and electrophysiological recordings showed that Aβ forms pores in membranes *in vitro*, therefore lipids and Aβ were mixed before forming proteoliposomes used in the experiments (Capone, Jang et al. 2012). Those pores exhibit cation selectivity and are suspected to cause a dyshomeostasis in the Ca^{2+} balance *in vivo*, supported by experiments with human fibroblasts (Rhee, Quist et al. 1998; Zhu, Lin et al. 2000). Yet, little is known about the structure of the pore. A combination of AFM and computational modelling suspects a β-sheet rich conformation, in particular a U-shaped motif found in amyloid structures (Jang, Zheng et al. 2008; Strodel, Lee et al. 2010; Connelly, Jang et al. 2012). Solid state NMR spectroscopy showed that Aβ incorporated in liposomes, by prior drying of the peptide with the lipids, led to an increased membrane fluidity is and destabilisation (Lau, Ambroggio et al. 2006).

Based on the protocols for the *in vitro* experiments, it was tested if a direct assembly of Aβ with nanodiscs is possible in order to obtain nanodiscs with Aβ incorporated in the lipid bilayer. Therefore Aβ was dried together with lipids, nanodiscs were formed and purified by size exclusion chromatography (SEC). A mixture of lipids with neutral and anionic lipid headgroups (PC/PG) was used similar to the mixture used in the above mentioned experiments (Capone, Jang et al. 2012). When nanodiscs are assembled in the presence of a protein, the lipid to MSP molar ratio needs to be adjusted in order to obtain an optimal outcome. Here the lipid to MSP molar ratio was reduced from 55:1 for empty nanodiscs to 40:1 for nanodisc assembled with Aβ, which led to a successful assembly of nanodiscs in the presence of Aβ, seen as one main peak during the purification with very little aggregation (fig. 3.6 B). The elution volume of nanodiscs assembled with Aβ was consistent with the elution volume of empty nanodiscs, which was expected. Aβ is a small peptide with a molecular weight of 4.2 kDa to 4.7 kDa depending on the respective isoform. Upon incorporation into the lipid bilayer and thereby replacing lipids, the change of the molecular weight of the 150 kDa nanodisc will not be sufficient to change the elution volume significantly. For proteins with a higher molecular weight a shift in the elution volume can be seen (Hernandez-Rocamora, Reija et al. 2012). In general, an elution of nanodiscs with the protein of interest is interpreted as an incorporation of the protein in the nanodisc, as the elution volume of the protein of interest differs from the elution volume of nanodiscs (Tsukamoto, Sinha et al. 2010). A control Aβ sample, however, revealed that the peptide, due to its propensity to aggregate, eluted over the whole column (fig. 3.6 C). Therefore the coelution of Aβ with nanodiscs cannot be interpreted as an incorporation of the peptide in the bilayer. It is likely that the sample contained a mixture of free Aβ, nanodiscs with bound Aβ and empty nanodiscs.

Nanodiscs are suitable for immobilized metal affinity chromatography (IMAC) purification. In several approaches it was shown before, that it is possible to separate empty nanodiscs from loaded ones by IMAC, when the protein of interest has an e.g. His-tag (Ritchie, Grinkova et al. 2009; Pavlidou, Hanel et al. 2013). In this work, the IMAC was performed using the His-tag of MSP in order to separate free Aβ from nanodiscs. Yet, Aβ did bind to the Ni^{2+}-NTA column and it was not possible to separate it under the tested conditions (fig.3.7). The binding of N-terminal Aβ fragments as well as full length Aβ(1-40) to nickel ions has been reported by different groups (Drochioiu, Manea et al. 2009; Jozsa, Osz et al. 2010). The binding takes place over a pH range from 5.5 to 8, harsher conditions preventing the binding of Aβ to the Ni^{2+}-NTA matrix, would also destroy the nanodiscs.

As a preparation of Aβ bound nanodiscs without free Aβ was not possible, the interaction of Aβ with nanodiscs was analysed by studying the direct binding of Aβ to empty nanodiscs.

4.2 Successful Assembly of Empty Nanodiscs

In order to study the interaction of Aβ with different membranes, empty nanodiscs, varying in their lipid composition, were assembled. Nanodiscs with single lipid compositions, DMPC or ganglioside GM1, were prepared as well as with complex mixtures, amongst others Folch 1, PC/PG/Chol and low-GM1 (table 3.2). Their lipid mixtures did not only vary in the complexity, but also in the charge of the lipid head group, cholesterol as well as GM1 content. The lipid mixtures were chosen due to earlier findings in literature (McLaurin and Chakrabartty 1997; Kakio, Nishimoto et al. 2001; Kakio, Nishimoto et al. 2002; Utsumi, Yamaguchi et al. 2009; Wong, Schauerte et al. 2009), so that the suitability of nanodiscs could be tested.

Although there are optimised protocols available for commonly used lipids such as DMPC (Ritchie, Grinkova et al. 2009), the assembly procedure had to be adjusted to the laboratory conditions in order to obtain optimal results. Ritchie *et al*. 2009 found an optimal molar ratio of 1:80 for MSP1D1 to DMPC, while in this work an optimal molar ratio of 1:70 was determined. Those marginal differnces can arise from a different assembly procedure, e.g using dialysis or Biobeads for the removal of detergents. Analysis of the MSP1D1 DMPC nanodisc by dynamic light scattering (DLS) revealed a hydrodynamic radius of 4.8 nm (table 3.2), which is consistent with the literature (Bayburt and Sligar 2010). For new lipid mixtures in general three to four different MSP to lipid molar ratios were tested. In case of MSP1D1 and high-GM1 the molar ratios of 1:45, 1:55 and 1:65 were tested (fig. 3.4). The ratio of 1:65 led to the best results as no free MSP1D1 was in contrast to the other ratios. There was still some aggregation present, which might be caused by the still not optimal MSP to lipid ratio or temperature during the assembly procedure. Since the results were satisfying the ratio was not further optimised.

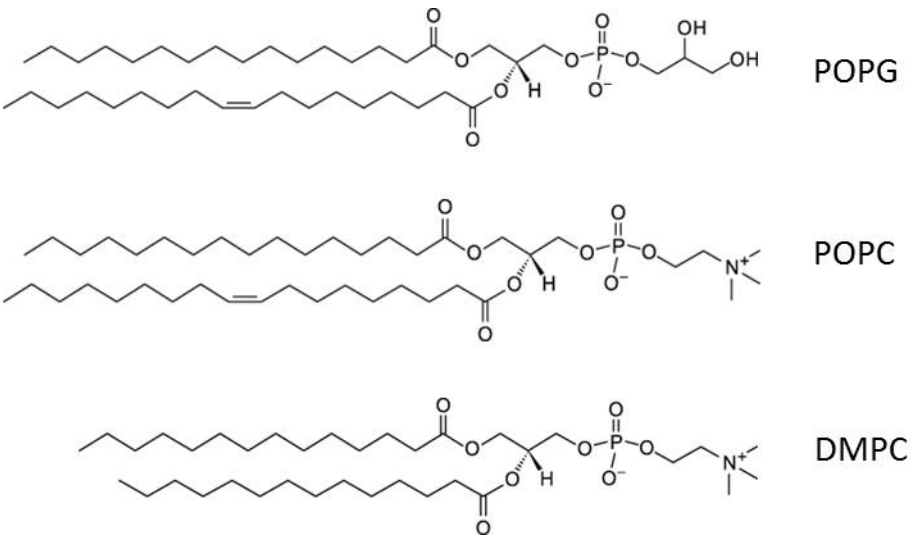

Figure 4.1: Schematic representation of the phospholipids POPG, POPC and DMPC (modified from www.avantilipids.com)

An optimal outcome of the assembly is not only dependent on the lipid to MSP molar ratio but also on the temperature during the assembly procedure. The best results are obtained when the temperature is close to the phase transition of the lipid (Bayburt and Sligar 2010). For DMPC, which has two saturated fatty acid chains (fig 4.1), a temperature of 30 °C was used during the assembly procedure. While for the mixture PG/PC, as both lipids have each one unsaturated fatty acid chain (fig. 4.1), hence a lower transition temperature, 4 °C was used. For both lipid composition references were available (http://sligarlab.life.uiuc.edu/nanodisc/protocols.html). However, for lipid mixtures, which have previously not been applied for nanodisc assembly, Folch 1 and GM1 lipid mixtures, the lipid to MSP molar ratio as well as the temperature had to be found empirically, e.g the GM1 lipid mixtures. They contain ganglioside GM1, sphingomyelin and cholesterol in varying concentrations; all three lipids are found in lipid rafts (Simons and Ikonen 1997). The phase transition temperature of sphingomyelin is, due to its long saturated acyl chains (fig. 4.2), the highest with 37 to 41 °C (Brown and London 2000). Ganglioside GM1 in turn has a transition temperature of 15 to 17.6 °C, which is a result of its large headgroup (fig.4.2) (Sonnino, Mauri et al. 2007). In combination with cholesterol, which in liquid phase bilayers leads to a higher packing of the lipids and a reduced lateral diffusion but in gel phase bilayers disturbs the packing and causes a higher mobility of the lipids (Rubenstein, Smith et al. 1979; Simons and Ikonen 1997), the optimal temperature was difficult to predict. 38 °C was found to lead to a high assembly outcome, though there was still some aggregation present. This could have been further optimised by varying the temperature further or optimising the lipid to MSP molar ratio. However, the results were satisfying therefore no further optimisation was performed. For the Folch 1 from bovine brain, which contains according to the manufacturer

phosphatidylinositol, phosphatidylserine and other brain lipids, also a temperature of 38 °C was found to lead to a satisfying assembly outcome.

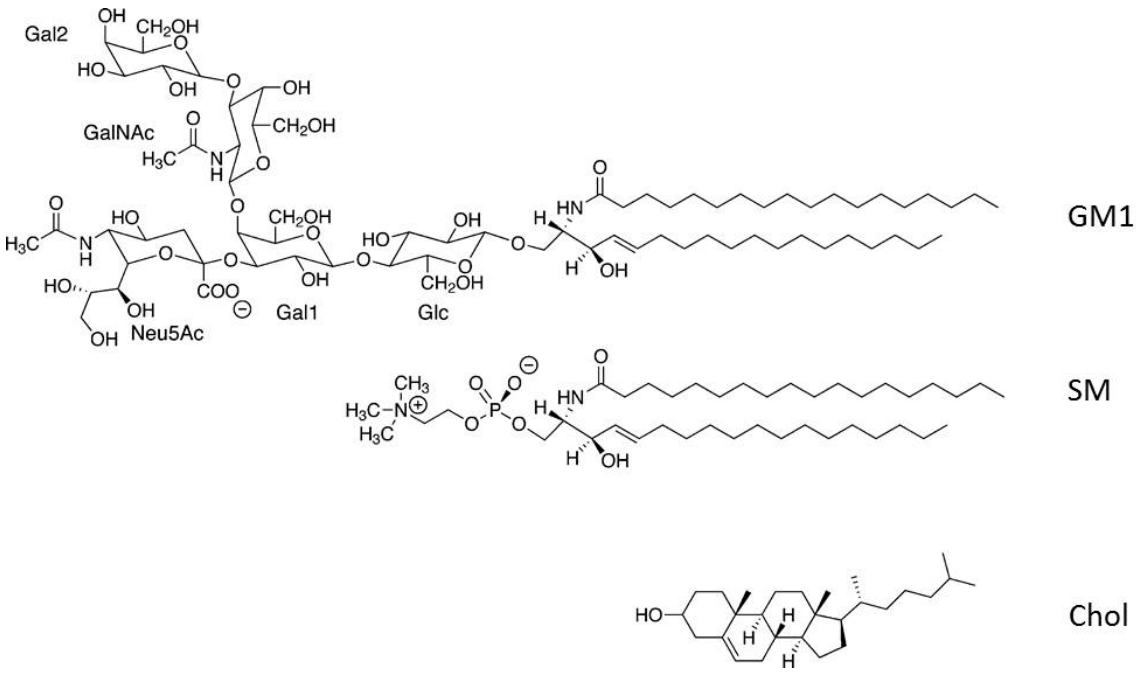

Figure 4.2: Schematic representation of ganglioside GM1, sphingomyelin (SM) and cholesterol (Chol) (modified from (Mori, Mahmood et al. 2012)

Nanodiscs obtained from the test assemblies were further analysed. The hydrodynamic radius was determined by DLS in addition to estimation from the elution volume of the calibrated column. Nanodiscs composed of the smaller MSP variant MSP1ΔH5 have a smaller hydrodynamic radius of 4.2 nm to 43 nm than nanodiscs with the bigger MSP variant MSP1D1, 4.8 nm to 4.9 nm. Those obtained values are consistent with the literature (Bayburt and Sligar 2010; Hagn, Etzkorn et al. 2013). Nanodiscs were further concentrated and their stability at different temperatures was analysed.

4.3 Nanodisc Stability

One big advantage of nanodiscs is their stability. It was for example shown, that DMPC nanodiscs are stable up to 50 days at 4 °C. The stability of the DMPC nanodiscs decreased with a reduction in size. While MSP1D1 and MSP1D1DH5 were stable for 50 days at 4 °C, two smaller variants were not (Hagn, Etzkorn et al. 2013). The herein prepared nanodiscs also showed different stabilities dependent on the size of the MSP as well as on the used lipid mixture. It was found that total-GM1 and low-GM1 MSP1D1 nanodiscs were stable for at least four days at 25 °C, while nanodiscs of the

same lipid composition surrounded by the smaller MSP variant were only stable for two days at 25 °C. Interestingly the high-GM1 MSP1D1DH5 nanodiscs were even less stable. They aggregated already after one day at 25 °C and it was not possible to store them at -80 °C. The overall reduced stability of GM1 containing nanodiscs is most likely due to different lipid dynamics when compared to phospholipid nanodiscs (Sarti, Antonini et al. 1990). Klassen and co-workers reported that assembly of nanodiscs with a concentration of GM1 higher than 15 % results in a lower yield of nanodiscs. They assume this is due to a reduced stability of the nanodiscs (Leney, Fan et al. 2014). A reduced yield was not observed for total-GM1 nanodiscs but for high-GM1 nanodiscs (fig. 3.20). Yet, the stability of nanodiscs is not only dependent on the GM1 content as low-GM1 nanodiscs and total-GM1 nanodiscs both showed a better stability than high-GM1 nanodiscs. More likely is the packing of lipids unfavourable in the high-GM1 nanodiscs than in the other two lipid mixtures. The cholesterol concentration might be important for nanodisc stability as PC/PG nanodiscs were stable during storing at -80 °C, while PC/PG/Chol nanodiscs were not. However, low-GM1 nanodiscs were stable upon storage at -80 °C.

Summarised, several nanodiscs, varying in their lipid compositions, were prepared and could be used in the following to test their suitability for the interaction of Aβ with membranes.

4.4 Aβ Membrane Interaction Analysed by NMR Spectroscopy

Aβ(1-42) membrane interaction was analysed by NMR spectroscopy, therefore hexafluoroisopropanol (HFIP) pretreated lyophilised [U-^{15}N]-Aβ(1-42) was directly dissolved in the liposome or nanodisc solution. 2D-[^{1}H,^{15}N]-TROSY experiments, which detect protons bound covalently to ^{15}N-nuclei and is optimised for larger molecules, were performed.

First the interaction of Aβ with PG/PG/Chol and DMPC liposomes was analysed. Yet, for both lipid compositions no binding was detected. It was expected, that Aβ(1-42) would bind to PG/PC/Chol liposomes as Wong *et al*. showed that Aβ(1-40) binds to POPC/POPG liposomes with 10 % cholesterol, a mixture very close to the PC/PG/Chol ND (45.5 % POPG 45.5 % POPC 9 % Cholesterol). Under the here applied conditions with a low peptide to lipid ratio, Aβ(1-40) adopted an α-helical structure (Wong, Schauerte et al. 2009). Of course, in their study Aβ(1-40) and a 10 mM NaH_2PO_4/Na_2HPO_4, pH 7.4 buffer at 22 °C was used, while in this work 50 mM NaCl added to the buffer at 25 °C was used. The salt might decrease electrostatic interactions, which are suspected to play a role in the interaction of Aβ with anionic lipid headgroups. Yet, another group showed that the interaction of pure PG liposomes Aβ(1-40) as well as Aβ(1-42) was not reduced at 150 mM NaCl (McLaurin and Chakrabartty 1997). NMR spectroscopy experiments revealed no binding of Aβ(1-42) to DMPC liposomes, which is consistent with findings of others (McLaurin, Franklin et al. 1997; Wong,

Schauerte et al. 2009). However, another group found a binding of Aβ(1-40) to neutral monolayers, therefore an interaction with DMPC liposomes was tested, too (Ege and Lee 2004).

Unsurprisingly, no binding of Aβ(1-42) to neither DMPC nor PG/PC/Chol nanodiscs was found, confirming the Aβ liposome results. As Aβ exhibits its toxicity on neuronal cell membranes, a lipid mixture from bovine brain extracts, Folch 1 was tested. To my knowledge this mixture was neither used for nanodisc assembly nor tested for Aβ interaction before. In this work no binding of Aβ(1-42) to Folch 1 nanodiscs was observed. Likewise, no binding of Aβ(1-42) to low-GM1 nanodiscs was found. This result was surprising, as binding of Aβ(1-40) to liposomes consisting of the same lipid mixture was found (Kakio, Nishimoto et al. 2001). The buffer differed, since 10 mM KH_2PO_4/K_2HPO_4, pH 7.2 with 0.5 mM EDTA was used instead of 150 mM NaCl, 2 mM CaCl, 10 mM Tris pH 7.4. Yet, the buffer used here was the same than in a study revealing a binding of Aβ(1-42) to ganglioside GM1 micelles (Utsumi, Yamaguchi et al. 2009).

To further investigate the different findings, it was tested if the results of the study from Utsumi *et al*. could be reproduced. They conducted 2D-[^{1}H,^{15}N]-TROSY experiments of Aβ bound to GM1 gangliosides in micelles a high ganglioside to Aβ molar ratio of 30:1 (Utsumi, Yamaguchi et al. 2009; Yagi-Utsumi, Matsuo et al. 2010). Although a structure of Aβ was not determined, backbone chemical shifts indicate that the ganglioside bound region of Aβ forms partial α-helices (Utsumi, Yamaguchi et al. 2009). The protocol described in the paper was used for the preparation of micelles and the same peptide to lipid ratio was used, but instead of Aβ(1-40) the longer isoform Aβ(1-42) was used. For the [U-^{15}N]-Aβ(1-42) sample without nanodiscs less signals were detected than for lower concentrations. One can explain this by aggregation of [U-^{15}N]-Aβ(1-42) to insoluble Aβ(1-42) species, which will not be detected by solution NMR spectroscopy. Analysis of residual sample after the NMR spectroscopy experiment by density gradient centrifugation (DGC) followed by sodium dodecylsulphate polyacrylamide gel electrophoresis (SDS-PAGE) and Western Blot confirmed this assumption (fig 3.10). [U-^{15}N]-Aβ(1-42) was mainly found in the pellet fraction. Aβ(1-42) is known to aggregate faster than Aβ(1-40), which can explain the different findings from Kato and co-workers (Utsumi, Yamaguchi et al. 2009).

Indeed, the spectrum of [U-^{15}N]-Aβ(1-42) with GM1 micelles indicated a binding. However, the resolution was very poor. Only three peaks, of which two originate from the ganglioside GM1 (fig. 3.10), were detected. Two possible explanations are: i) [U-^{15}N]-Aβ(1-42) did aggregate in the presence of GM1 micelles and ii) [U-^{15}N]-Aβ(1-42) did bind to GM1 micelles, yet their molecular weight was too high to allow a resonance signal detection by the 2D-[^{1}H^{15}N]-TROSY experiment. By subsequent analysis, the latter explanation is supported. [U-^{15}N]-Aβ(1-42) was not detected in the pellet fraction after DGC by Western Blot (fig. 3.11 A). It was found in higher fractions, where soluble

Aβ and micelles are found. With size the rotational correlation time of a molecule increases. This causes an increased transversal relaxation rate, which leads to line broadening of the detected resonance signal and eventually to a complete signal loss. As nanodiscs have a higher stability and homogeneity than micelles, MSP1D1 and MSP1ΔH5 nanodiscs composed of only GM1 (total-GM1) were tested next for their interaction with Aβ(1-42).

Although a binding of Aβ(1-42) to the nanodiscs was found and higher amount of cross peaks were detected than for the micelles, the resolution was still poor. Therefore no further experiments for obtaining information of the secondary structure were performed. Again, the poor resolution is due to a high molecular weight of the model membrane system. Subsequent analysis of the residual NMR spectroscopy samples by DGC, followed by SDS-PAGE and Western Blot as well as SEC lead to the conclusion, that the reduced amount of resonance signals was not caused by aggregation of [U-^{15}N]-Aβ(1-42) to insoluble species, but was due to an aggregation of the loaded nanodiscs.

In order to overcome this problem in the future, the stability of the nanodiscs must be increased. This could be achieved by different approaches. One would be to test further lipid mixtures. Introducing phospholipids most likely will increase nanodisc stability, as Klassen and co-workers found a higher stability for nanodiscs with mixed gangliosides and DMPC (Leney, Fan et al. 2014). However changing the lipid composition drastically might reduce binding of Aβ to the lipid bilayer. Another possibility would be to test different buffer conditions, which might lead to a higher stability of ganglioside GM1 nanodiscs. Of course both approaches could be combined.

4.5 Characterisation of Aβ Membrane Interaction

4.5.1 DAC-Aβ(1-40) Interaction with Nanodiscs is Dependent on the GM1 Content

Although total-GM1 nanodiscs were unstable during NMR spectroscopy, they were stable and suitable for analysing Aβ membrane interactions by fluorescence titration (FT) and BioLayer interferometry (BLI).

First a protocol from Matsuzaki and colleagues was adopted as they have used DAC-Aβ(1-40) to characterise Aβ interaction with ganglioside containing liposomes by FT, clearly showing ganglioside dependent Aβ binding to liposomes. By using circular dichroism (CD) spectroscopy, they further showed concentration dependent Aβ secondary structure changes (Kakio, Nishimoto et al. 2001; Kakio, Nishimoto et al. 2002; Kakio, Yano et al. 2004; Ikeda and Matsuzaki 2008; Ikeda, Yamaguchi et al. 2011). Their results, using the same experimental set-up regarding buffer, temperature and the lipid mix low-GM1 for liposomes, could be reproduced. A clear binding of DAC-Aβ(1-40) to the low-GM1 liposomes was observed. Additionally, PG/PC/Chol liposomes were tested for interaction with

DAC-Aβ(1-40). In accordance with the results obtained by NMR spectroscopy, no interaction of DAC-Aβ(1-40) with this lipid mixture was found.

When low-GM1 MSP1D1 nanodiscs were used with the same setup, no binding of DAC-Aβ(1-40) to the membrane was observed. This result was surprising as liposomes with the same lipid mixture and under the same applied conditions clearly revealed binding. However, when total-GM1 MSP1D1 nanodiscs were used high affinity binding was found. The K_D determined for DAC-Aβ(1-40) to total-GM1 MSP1D1 nanodiscs was 51 nM ± 22. Matsuzakis group and McLaurin *et al*. showed that a certain threshold of GM1 molecules is required for binding Aβ and that Aβ does not bind to single GM1 molecules (McLaurin, Franklin et al. 1998; Kakio, Nishimoto et al. 2001). Therefore, the discrepancy in Aβ binding to nanodiscs compared to unilamellar vesicles is likely to be due to the missing GM1 cluster in the nanodiscs caused by the low total number of lipid molecules per nanodiscs. Low-GM1 MSP1D1 nanodiscs have maximal 60 lipids per bilayer, hence 24 GM1 molecules, which might not provide the required cluster for binding (Kakio, Nishimoto et al. 2001). Furthermore, it was shown that not only the number of GM1 molecules but their packing density within the membrane plays a crucial role for Aβ binding (Matsubara, Iijima et al. 2013).

After successfully establishing the experimental setup for FT, further MSP1D1ΔH5 nanodiscs in a low salt buffer were tested. For total-GM1 as well as high-GM1 MSP1D1ΔH5 nanodiscs a binding of DAC-Aβ(1-40) with nanomolar affinity was found. Further, no binding of DAC-Aβ(1-40) to low-GM1 MSP1D1ΔH5 nanodiscs was found, which is consistent with the NMR spectroscopy results and low-GM1 MSP1D1 nanodiscs findings.

It was possible to label the tripeptide glutathione with the DACIA, a thiol reactive labelling version of the dye, as well as Cys0-Aβ(1-42). However, while labelling of glutathione resulted in a soluble negative control for the experiments which did not bind to the tested nanodiscs, the DAC-Cys0-Aβ(1-42) was insoluble. Therefore, it was not used for further experiments. Instead, Aβ(1-40) and Aβ(1-42) membrane interactions were further analysed by BLI.

4.5.2 Monomeric Aβ but not Oligomeric Aβ Bind to Total-GM1 Nanodisc

For further testing nanodisc suitability for Aβ membrane interaction BLI was used to: i) confirm FT results with an alternative and independent method, ii) analyse possible differences in Aβ(1-40) membrane interaction compared to Aβ(1-42) membrane interaction, and iii) study interaction of monomeric Aβ vs. oligomeric Aβ species with nanodisc model membrane systems. The Aβ-nanodisc interactions obtained from FT are completely confirmed by corresponding BLI analyses. No binding of monomeric Aβ(1-40) to low-GM1 nanodiscs was observed while total-GM1 and high-GM1 nanodiscs bind with nanomolar affinity to monomeric Aβ(1-40). The K_D values for monomeric Aβ(1-40) binding

to total-GM1 are with 24 nM (BLI) and 25 nM (FT) almost identical. This was also observed for monomeric Aβ(1-40) binding to high-GM1 nanodiscs with K_D values of 49 nM (BLI) and 41 nM (FT). Although the trend revealed that monomeric Aβ(1-40) binds with a higher affinity to total-GM1 nanodiscs than to high-GM1 nanodiscs, the K_D values are still in the same nanomolar range.

Additionally, DMPC nanodiscs and PC/PG/Chol nanodiscs were tested and no binding to neither monomeric Aβ(1-40) nor to monomeric Aβ(1-42) was observed. The absence of any interaction of Aβ with DMPC nanodiscs is in agreement with findings of NMR spectroscopy experiments and results from other groups, as it has been shown before that Aβ does not bind to liposomes with only zwitterionic headgroup lipids such as PC (McLaurin, Franklin et al. 1998; Wong, Schauerte et al. 2009). Yet, as mentioned above Wong *et al*. showed that Aβ(1-40) binds to and subsequently permeabilises POPC/POPG liposomes with 10 % cholesterol, a mixture very close to our PC/PG/Chol nanodisc composition (45.5 % POPG, 45.5 % POPC, 9 % Cholesterol) (Wong, Schauerte et al. 2009). In contrast to NMR spectroscopy experiments, a buffer without salt was used (30 mM KH_2PO_4/K_2HPO_4, pH 7.2, 0.5 mM EDTA) comparable to their buffer (10 mM NaH_2PO_4/Na_2HPO_4, pH 7.4) ruling out the possibility of reduced electrostatic interaction by higher salt concentrations. However, their experiments were performed with unlabelled Aβ(1-40) in solution leaving a free N-terminus, which might be important for electrostatic interaction with membranes(Williamson, Suzuki et al. 2006; Kotler, Walsh et al. 2014), while for the BLI experiments Aβ had to be coupled via a N-terminal biotin to the BLI sensor tips.

Monomeric Aβ(1-42) exhibited similar binding specificity for different nanodisc types as monomeric Aβ(1-40). Also the binding affinity of monomeric Aβ(1-42) to both total-GM1 nanodiscs and high-GM1 nanodiscs were in the same range with K_D values of 30 nM and 29 nM, respectively. Those findings are consistent with results of Ogawa *et al*., they revealed similar binding specificity and affinity for DAC-Aβ(1-40) and DAC-Aβ(1-42) to different liposomes (Ogawa, Tsukuda et al. 2011). McLaurin *et al*. further showed by density gradient centrifugation similar binding specificity for Aβ(1-40) and Aβ(1-42) to ganglioside containing liposomes and no binding to POPC vesicles (McLaurin, Franklin et al. 1998).

The binding affinity found for monomeric Aβ(1-42) to both total-GM1 nanodiscs and high-GM1 nanodiscs with K_D values of 30 nM and 29 nM is clearly lower than 520 nM, which was found by a SPR study using 20 % GM1 in DMPC (Valdes-Gonzalez, Inagawa et al. 2001). There are several explanations for the different results as their experimental set up differs considerably from the one used here. Valdes-Gonzales *et al*. immobilised the lipids on a sensor chip and used Aβ(1-42) as analyte. First, their lipid composition is 20 % GM1 80 % DMPC, which possibly leads to a lower clustering of GM1 molecules, hence to a lower binding affinity of Aβ(1-42) to GM1 (Vyas, Patel et al.

2001; Kakio, Nishimoto et al. 2002; Lozano, Liu et al. 2013; Matsubara, Iijima et al. 2013). Second, they do not comment on the Aβ(1-42) species used, which makes a mixture of monomeric as well as oligomeric species possible, thus explaining different results. Third, a 150 mM NaCl buffer was used. The higher salt concentration might reduce putative electrostatic interactions, leading to a lower binding affinity.

So far, monomeric Aβ interaction with nanodiscs was tested, which clearly bound to GM1 containing nanodiscs. Next, the question was asked and addressed if oligomeric Aβ species are also able to bind to nanodiscs. Aβ oligomers are thought to be the most toxic species causing damage in synaptic plasticity, oxidative stress, disturbances in calcium homeostasis and chronic inflammation (McLean, Cherny et al. 1999; Walsh, Klyubin et al. 2002; Shankar, Li et al. 2008). Furthermore, Williams *et al*. found permeation of ganglioside GM1 containing liposomes by oligomeric Aβ species (Williams, Day et al. 2010). Yet, the trouble is that a wide range of different Aβ oligomers has been described and shown to be neurotoxic (Ono, Condron et al. 2009; Kotler, Walsh et al. 2014). Here, an Aβ oligomeric species, which has been characterised in a recent study (Brener, Dunkelmann et al. 2015), was used. The oligomers are obtained by DGC and exhibit neurotoxicity, contain β-sheet dominated structures, but are Thioflavin-T negative (Brener, Dunkelmann et al. 2015). Interestingly, there was no nanodisc binding of either Aβ(1-40) or Aβ(1-42) oligomers detectable, even to total-GM1 nanodiscs, meaning that the GM1-membrane binding regions of the Aβ monomers are masked in the Aβ oligomers. To my knowledge this is the first observation that describes the loss of the membrane binding ability of Aβ upon forming a certain oligomeric Aβ species (Brener, Dunkelmann et al. 2015). In order to exclude that the density gradient forming agent iodixanol used for the preparation of Aβ oligomers interferes with the binding to nanodiscs, gradient fractions that contain smaller Aβ species including monomeric Aβ were tested. For both Aβ(1-40) and Aβ(1-42) monomeric species derived from iodixanol DGC a clear binding to total-GM1 nanodiscs is observed and the K_D values are in the same range as the K_D values obtained from SEC derived monomeric Aβ. The results obtained in this work do not necessarily contradict the finding of Williams *et al*. small oligomers binding to GM1 containing membrane (Williams, Day et al. 2010). Since their Aβ oligomers, which range from 10 to 70 nm in diameter, differ from the ones (8.7 nm) used here in addition to using large unilamellar vesicles with a DMPC/cholesterol/GM1 molar ratio of 62:30:2 (Williams, Day et al. 2010).

Finally, it was shown that concentration of unlabelled Aβ(1-42) bound to total-GM1 nanodisc by ultracentrifugation is possible. The Aβ(1-42) bound to total-GM1 nanodiscs cosedimented and nanodisc integrity was confirmed. Ding *et al*. showed that with this method nanodiscss containing outer membrane protein Ail from *Yersina pestis* can be sedimented and used for solid state as well as solution NMR spectroscopy (Ding, Fujimoto et al. 2015). It is promising that Aβ(1-42) bound to total-

GM1 nanodiscs can be concentrated by this method. As NMR spectroscopy can help to unravel the molecular mechanism of Aβ membrane binding in more detail and reveal the structure of Aβ bound to the membrane, the approach to achieve concentrated samples will be of great importance for such studies.

4.6 Relevance

The herein presented data clearly show that nanodiscs are suitable for studying Aβ membrane interaction. It was shown that both monomeric Aβ(1-40) and monomeric Aβ(1-42), but not oligomeric Aβ species, bound with high affinity to nanodiscs in a ganglioside GM1 concentration dependent manner. Interestingly, low-GM1 liposomes provided the specific GM1 cluster required for Aβ binding to membranes while nanodiscs also composed of low-GM1 did not. This is an interesting finding and raises the question whether the total number of GM1 molecules in low-GM1 nanodiscs was too little or the packing of the GM1 molecules within the nanodiscs was not dense enough to provide a specific GM1 cluster. As not only the total number of GM1 molecules but also their packing density is crucial for GM1 clustering and Aβ interaction (Kakio, Nishimoto et al. 2002; Matsubara, Iijima et al. 2013). Using the fluorescence dye BODIPY for labelling GM1 could resolve the question as the dye forms excimer (exited dimer), when locally concentrated and emits fluorescence 100 nm shifted from the monomer. The monomer to dimer concentration is a measure for clustering (Forster 1969; Kakio, Nishimoto et al. 2002). Moreover, using BODIPY-GM1 with different GM1/SM/Chol ratios could possibly determine the minimal number of GM1 molecules required for the binding of Aβ.

To my knowledge this is the first study using nanodiscs with lipid mixtures of ganglioside GM1, sphingomyelin and cholesterol. All three lipids are found in lipid rafts (Simons and Ikonen 1997) and the clustering of GM1 in cell membranes is crucial for physiological and pathological processes (Michel and Bakovic 2007), therefore the nanodiscs presented in here could be used for further studies e.g for characterisation of α-synuclein interaction with lipid raft membranes. α-synuclein plays an important role in Parkinson´s disease and has been recently shown to bind to GM1 containing liposomes yet without SM and Chol (Bartels, Kim et al. 2014).

Physicochemical methods such as imaging mass spectroscopy (Lozano, Liu et al. 2013) and Foerster resonance energy transfer (Vyas, Patel et al. 2001) showed that GM1 forms specific clusters and is preferentially colocalised with cholesterol. Molecular dynamic simulations supported those findings and revealed that the GM1 clustering is facilitated by interaction of GM1 with cholesterol (Mori, Mahmood et al. 2012; Fantini, Yahi et al. 2013). Several hydrogen bonds are formed between the hydroxyl group of cholesterol and GM1 as well as SM, keeping the sphingolipid moieties of GM1

close to each other, thereby stabilising the GM1 cluster (Mori, Mahmood et al. 2012). This cluster is important for Aβ GM1 interaction (Fantini, Yahi et al. 2013). However, the characterisation of carbohydrate-protein interactions on an experimental atomistic level is little explored, which is mainly due to the absence of suitable model systems for such a complicated diverse system of glycolipids, cholesterol and proteins. So far, there have been first results by using isotropic fast tumbling bicelles of DMPC/CHAPS/gangliosides, whereby the detergent CHAPS (3-[(3-cholamidopropyl)dimethylammonio]-1-propanesulfonate) is a cholesterol mimetic, for neuropeptide interaction and in addition to bicelles composed of DMPC, gangliosides and the short fatty acid chain DHPC (1,2-diheptanoyl-*sn*-glycero-3-phosphocholine) (Yamaguchi, Uno et al. 2013). The nanodiscs used in this study could provide, after an optimisation for a higher stability, an excellent model system, as they are detergent free and their lipid bilayer is composed of cholesterol as well as gangliosides. Moreover nanodiscs have been shown to have a more native like lipid environment than other membrane model systems (Shaw, McLean et al. 2004).

5. Summary

Alzheimer's disease is a progressive neurodegenerative disease and the most common form of dementia. During the progression of the disease, neuronal nerve tissue is irreversibly damaged causing loss of memory and cognitive decline. The aggregation of amyloid β (Aβ) peptide from its monomeric non-toxic form over toxic oligomeric species to amyloid fibrils and aggregates is thought to play an important role in the disease. However, it is still unclear which mechanism causes the polymerisation process. Moreover, despite extensive research, the underlying molecular mechanism by which oligomeric Aβ species exhibit toxicity is still enigmatic. For both mechanisms, Aβ interaction with neuronal cell membranes is crucial. However, Aβ interaction with membranes has not been completely elucidated yet.

In this work, nanodiscs were firstly used to study the interactions of Aβ with membranes. Nanodiscs are composed of two copies of the membrane scaffold protein surrounding a lipid bilayer. They are excellent model membrane systems for studying protein-membrane interactions, e.g. they have been shown to allow straight forward use of biophysical methods e.g. surface plasmon resonance, BioLlayer Interferometry (BLI) or nuclear magnetic resonance (NMR) spectroscopy to membrane inserted proteins. In this work their suitability to investigate the membrane interaction of Aβ is shown. Protocols for the assembly of nanodiscs with new lipid mixtures found in lipid rafts of neuronal cell membranes were established and the stability of nanodiscs was assessed by analytical size exclusion chromatography.

In order to gain further knowledge about the binding of Aβ to the membrane and connected structural secondary changes presumably leading to membrane insertion, high resolution structures are required. Yet, this has been hampered by the lack of an appropriate model membrane system. In this work, first NMR spectroscopy results revealed a binding of Aβ to GM1 containing nanodiscs. By further optimisation nanodiscs could serve as an excellent model membrane system to study Aβ in a membrane environment.

To analyse the molecular requirements of Aβ membrane binding, different nanodiscs varying in their lipid composition, regarding the charge of the head group as well as ganglioside GM1 concentration, were tested for membrane interaction with Aβ. Therefore fluorescence titration experiments were established and a high affinity binding of DAC-Aβ(1-40) to GM1 containing nanodiscs in a GM1 concentration dependent manner was found. BLI experiments confirmed completely binding of Aβ(1-40) to ganglioside GM1 containing nanodiscs. BLI allowed to extend binding studies to Aβ(1-42), which also bound with high affinity to GM1 nanodiscs in the same nanomolar range than Aβ(1-40). Interestingly, neither oligomeric Aβ(1-40) nor oligomeric Aβ(1-42) did bind to GM1 containing

nanodiscs, indicating GM1-membrane binding regions of the Aβ monomers are masked in the Aβ oligomers. Thus nanodiscs are suitable model membrane systems to analyse and characterise Aβ membrane binding and interaction revealing new insights.

6. Zusammenfassung

Alzheimer-Demenz ist eine neurodegenerative Krankheit und die häufigste Form der Demenz. Im Verlauf der Krankheit werden Nervenzellen im Gehirn irreversibel geschädigt, was zu Gedächtnisverlust und Wahrnehmungsstörungen führt. Die Aggregation des Amyloid-β (Aβ) Peptides von seiner monomeren nicht toxischen Form über toxische Oligomere hin zu amyloiden Fibrillen und Aggregaten spielt eine entscheidende Rolle in der Krankheit. Es ist jedoch noch nicht geklärt, welcher Mechanismus zum Polymerisationsprozess führt. Ebenfalls sind trotz intensiver Forschung, die zugrunde liegenden molekularen Mechanismen, welche zur Toxizität der Oligomere führen, noch ungeklärt. Für beide Mechanismen ist die Interaktion von Aβ mit neuronalen Zellen entscheidend, die jedoch noch nicht aufgeklärt ist.

In dieser Arbeit wurden erstmalig Nanodisks verwendet, um die Interaktion von Aβ mit Membranen zu untersuchen. Nanodisks bestehen aus zwei Kopien des Proteins MSP (membrane scaffold protein), die eine Lipiddoppelschicht umgeben. Sie sind exzellente Modelmembransysteme um Protein Membran Interaktionen zu analysieren. Hier konnte gezeigt werden, dass sie sich für die Untersuchung von Aβ mit Membranen eignen. Protokolle für die Assemblierung mit neuen Lipidmischungen aus Lipiden, die sich in Lipid-Rafts von neuronalen Zellmembranen befinden, wurden etabliert und die Stabilität der Nanodiscs wurde mittels analytischer Größenausschlusschromatographie untersucht.

Um Information über die Bindung von Aβ an Membranen und die damit verbundenen strukturellen Änderungen zu gewinnen, welche wahrscheinlich zur Membraninsertion führen, sind hochaufgelöste Strukturen erforderlich. Dies war bisher nicht möglich, da die geeigneten Modelmembransysteme fehlten. In der vorliegenden Arbeit zeigten erste NMR spektroskopische Untersuchungen, dass Aβ an Gangliosid GM1 haltige Nanodisks bindet und mit weiteren Optimierungen könnten Nanodisks als hervorragende Model Membran Systeme für die Untersuchung von Aβ in Membranumgebung dienen.

Um die molekularen Voraussetzungen der Aβ-Membran-Bindung zu untersuchen wurden verschiedene Nanodisks mit variierenden Lipiden, bezüglich der Ladung der Kopfgruppe wie auch der GM1 Konzentration, eingesetzt. Fluoreszenz Titrations Experimente wurden etabliert und eine hoch affine Bindung von DAC-Aβ(1-40) an GM1 Nanodiscs in GM1 Konzentrationsabhängigkeit wurde entdeckt und charakterisiert. BioLayer Interferometrie (BLI) Experimente bestätigten die Bindung von Aβ(1-40) an GM1 Nanodisks. Mittels BLI wurde zusätzlich die Bindung von Aβ(1-42) an Nanodisks untersucht. Es bindet ebenfalls mit hoher Affinität an GM1 enthaltende Nanodisks und auch im gleichen nanomolaren Bereich wie Aβ(1-40). Interessanterweise banden weder Aβ(1-40) Oligomere

noch Aβ(1-42) Oligomere an GM1 enthaltende Nanodisks, was darauf hinweist, dass die GM1-Membran-bindenden Regionen in Aβ-Monomeren in Aβ-Oligomeren verdeckt sind. Nanodisks sind somit geeignete Modelmembransysteme um die Bindung und Interaktion von Aβ an und mit Membranen zu analysieren und charakterisieren.

7. References

Allen, J. A., R. A. Halverson-Tamboli, et al. (2007). "Lipid raft microdomains and neurotransmitter signalling." Nature Reviews Neuroscience **8**(2): 128-140.

Alzheimer, A. (1911). "Concerning unsual medical cases in old age." Zeitschrift Fur Die Gesamte Neurologie Und Psychiatrie **4**: 356-385.

Arispe, N., E. Rojas, et al. (1993). "Alzheimer-Disease Amyloid Beta-Protein Forms Calcium Channels in Bilayer-Membranes - Blockade by Tromethamine and Aluminum." Proceedings of the National Academy of Sciences of the United States of America **90**(2): 567-571.

Assoc, A. (2015). "Alzheimer's Association Report 2015 Alzheimer's disease facts and figures." Alzheimers & Dementia **11**(3): 332-384.

Aue, W. P., E. Bartholdi, et al. (1976). "2-Dimensional Spectroscopy - Application to Nuclear Magnetic-Resonance." Journal of Chemical Physics **64**(5): 2229-2246.

Bailey, J. A., B. Maloney, et al. (2011). "Functional activity of the novel Alzheimer's amyloid beta-peptide interacting domain (AbetaID) in the APP and BACE1 promoter sequences and implications in activating apoptotic genes and in amyloidogenesis." Gene **488**(1-2): 13-22.

Barrow, C. J. and M. G. Zagorski (1991). "Solution Structures of Beta Peptide and Its Constituent Fragments - Relation to Amyloid Deposition." Science **253**(5016): 179-182.

Bartels, T., N. C. Kim, et al. (2014). "N-Alpha-Acetylation of alpha-Synuclein Increases Its Helical Folding Propensity, GM1 Binding Specificity and Resistance to Aggregation." Plos One **9**(7).

Barucker, C., A. Harmeier, et al. (2014). "Nuclear Translocation Uncovers the Amyloid Peptide A beta 42 as a Regulator of Gene Transcription." Journal of Biological Chemistry **289**(29): 20182-20191.

Bayburt, T. H., J. W. Carlson, et al. (1998). "Reconstitution and imaging of a membrane protein in a nanometer-size phospholipid bilayer." J Struct Biol **123**(1): 37-44.

Bayburt, T. H., Y. V. Grinkova, et al. (2002). "Self-assembly of discoidal phospholipid bilayer nanoparticles with membrane scaffold proteins." Nano Letters **2**(8): 853-856.

Bayburt, T. H. and S. G. Sligar (2002). "Single-molecule height measurements on microsomal cytochrome P450 in nanometer-scale phospholipid bilayer disks." Proc Natl Acad Sci U S A **99**(10): 6725-6730.

Bayburt, T. H. and S. G. Sligar (2010). "Membrane protein assembly into Nanodiscs." FEBS Lett **584**(9): 1721-1727.

Blennow, K., M. J. de Leon, et al. (2006). "Alzheimer's disease." Lancet **368**(9533): 387-403.

Blennow, K., H. Hampel, et al. (2010). "Cerebrospinal fluid and plasma biomarkers in Alzheimer disease." Nature Reviews Neurology **6**(3): 131-144.

Bloch, F., W. W. Hansen, et al. (1946). "Nuclear Induction." Physical Review **69**(3-4): 127-127.

Bobby, R., K. Medini, et al. (2013). "Structure and dynamics of human Nedd4-1 WW3 in complex with the alphaENaC PY motif." Biochim Biophys Acta **1834**(8): 1632-1641.

Borch, J. and T. Hamann (2009). "The nanodisc: a novel tool for membrane protein studies." Biol Chem **390**(8): 805-814.

Braak, H., K. Del Tredici, et al. (2000). "Vulnerability of select neuronal types to Alzheimer's disease." Alzeheimer's Disease: A Compendium of Current Theories **924**: 53-61.

Brener, O., T. Dunkelmann, et al. (2015). "QIAD assay for quantitating a compound's efficacy in elimination of toxic Abeta oligomers." Sci Rep **5**: 13222.

Brown, D. A. and E. London (2000). "Structure and function of sphingolipid- and cholesterol-rich membrane rafts." Journal of Biological Chemistry **275**(23): 17221-17224.

Bruggink, K. A., M. Muller, et al. (2012). "Methods for analysis of amyloid-beta aggregates." Journal of Alzheimers Disease **28**(4): 735-758.

Butterfield, S. M. and H. A. Lashuel (2010). "Amyloidogenic Protein Membrane Interactions: Mechanistic Insight from Model Systems." Angewandte Chemie-International Edition **49**(33): 5628-5654.

Capone, R., H. Jang, et al. (2012). "All-D-Enantiomer of beta-Amyloid Peptide Forms Ion Channels in Lipid Bilayers." Journal of Chemical Theory and Computation **8**(3): 1143-1152.
Chan, Y. H. M. and S. G. Boxer (2007). "Model membrane systems and their applications." Current Opinion in Chemical Biology **11**(6): 581-587.
Chi, E. Y., C. Ege, et al. (2008). "Lipid membrane templates the ordering and induces the fibrillogenesis of Alzheimer's disease amyloid-beta peptide." Proteins-Structure Function and Bioinformatics **72**(1): 1-24.
Cleary, J. P., D. M. Walsh, et al. (2005). "Natural oligomers of the amyloid-protein specifically disrupt cognitive function." Nature Neuroscience **8**(1): 79-84.
Connelly, L., H. Jang, et al. (2012). "Atomic Force Microscopy and MD Simulations Reveal Pore-Like Structures of All-D-Enantiomer of Alzheimer's beta-Amyloid Peptide: Relevance to the Ion Channel Mechanism of AD Pathology." Journal of Physical Chemistry B **116**(5): 1728-1735.
Crescenzi, O., S. Tomaselli, et al. (2002). "Solution structure of the Alzheimer amyloid beta-peptide (1-42) in an apolar microenvironment - Similarity with a virus fusion domain." European Journal of Biochemistry **269**(22): 5642-5648.
Dammers, C., L. Gremer, et al. (2015). "Purification and Characterization of Recombinant N-Terminally Pyroglutamate-Modified Amyloid-beta Variants and Structural Analysis by Solution NMR Spectroscopy." Plos One **10**(10): e0139710.
Dammers, C., L. Gremer, et al. (2015). "Structural Analysis and Aggregation Propensity of Pyroglutamate Abeta(3-40) in Aqueous Trifluoroethanol." Plos One **10**(11): e0143647.
Delaglio, F., S. Grzesiek, et al. (1995). "Nmrpipe - a Multidimensional Spectral Processing System Based on Unix Pipes." J Biomol NMR **6**(3): 277-293.
Demchenko, A. P., Y. Mely, et al. (2009). "Monitoring biophysical properties of lipid membranes by environment-sensitive fluorescent probes." Biophysical Journal **96**(9): 3461-3470.
Denisov, I. G., Y. V. Grinkova, et al. (2004). "Directed self-assembly of monodisperse phospholipid bilayer nanodiscs with controlled size." J Am Chem Soc **126**(11): 3477-3487.
Denisov, I. G., M. A. McLean, et al. (2005). "Thermotropic phase transition in soluble nanoscale lipid bilayers." Journal of Physical Chemistry B **109**(32): 15580-15588.
Ding, Y., L. M. Fujimoto, et al. (2015). "Solid-state NMR of the Yersinia pestis outer membrane protein Ail in lipid bilayer nanodiscs sedimented by ultracentrifugation." J Biomol NMR **61**(3-4): 275-286.
Dislich, B. and S. F. Lichtenthaler (2012). "The membrane-bound aspartyl protease BACE1: molecular and functional properties in Alzheimer's disease and beyond." Front Physiol **3**.
Drochioiu, G., M. Manea, et al. (2009). "Interaction of beta-amyloid (1-40) peptide with pairs of metal ions: An electrospray ion trap mass spectrometric model study." Biophys Chem **144**(1-2): 9-20.
Drolle, E., R. M. Gaikwad, et al. (2012). "Nanoscale Electrostatic Domains in Cholesterol-Laden Lipid Membranes Create a Target for Amyloid Binding." Biophysical Journal **103**(4): L27-L29.
Edbauer, D., E. Winkler, et al. (2003). "Reconstitution of gamma-secretase activity." Nature Cell Biology **5**(5): 486-488.
Ege, C. and K. Y. C. Lee (2004). "Insertion of Alzheimer's A beta 40 peptide into lipid monolayers." Biophysical Journal **87**(3): 1732-1740.
El-Agnaf, O. M., D. S. Mahil, et al. (2000). "Oligomerization and toxicity of beta-amyloid-42 implicated in Alzheimer's disease." Biochem Biophys Res Commun **273**(3): 1003-1007.
Esch, F. S., P. S. Keim, et al. (1990). "Cleavage of Amyloid-Beta Peptide during Constitutive Processing of Its Precursor." Science **248**(4959): 1122-1124.
Fantini, J., N. Yahi, et al. (2013). "Cholesterol accelerates the binding of Alzheimer's beta-amyloid peptide to ganglioside GM1 through a universal hydrogen-bond-dependent sterol tuning of glycolipid conformation." Front Physiol **4**: 120.
Finder, V. H. and R. Glockshuber (2007). "Amyloid-beta aggregation." Neurodegenerative Diseases **4**(1): 13-27.

Folch, J. (1942). "Brain cephalin, a mixture of phosphatides. Separation from it of phosphatidyl serine, phosphatidyl ethanolamine, and a fraction containing an inositol phosphatide." Journal of Biological Chemistry **146**(1): 35-44.

Folch, J., M. Lees, et al. (1957). "A Simple Method for the Isolation and Purification of Total Lipides from Animal Tissues." Journal of Biological Chemistry **226**(1): 497-509.

Forster, T. (1969). "Excimers." Angewandte Chemie-International Edition **8**(5): 333-&.

Fotuhi, M., V. Hachinski, et al. (2009). "Changing perspectives regarding late-life dementia." Nature Reviews Neurology **5**(12): 649-658.

Fox, N. C., S. Cousens, et al. (2000). "Using serial registered brain magnetic resonance imaging to measure disease progression in Alzheimer disease - Power calculations and estimates of sample size to detect treatment effects." Arch Neurol **57**(3): 339-344.

Frenzel, D., J. M. Gluck, et al. (2014). "Immobilization of homogeneous monomeric, oligomeric and fibrillar Abeta species for reliable SPR measurements." Plos One **9**(3): e89490.

Georgieva, E. R., T. F. Ramlall, et al. (2008). "Membrane-bound alpha-synuclein forms an extended helix: long-distance pulsed ESR measurements using vesicles, bicelles, and rodlike micelles." J Am Chem Soc **130**(39): 12856-12857.

Gerlach, W. and O. Stern (1922). "The experimental evidence of direction quantistion in the magnetic field." Zeitschrift Fur Physik **9**: 349-352.

Gerlach, W. and O. Stern (1922). "The magnetic moment of silver atoms." Zeitschrift Fur Physik **9**: 353-355.

Glenner, G. G. and C. W. Wong (1984). "Alzheimers-Disease - Initial Report of the Purification and Characterization of a Novel Cerebrovascular Amyloid Protein." Biochem Biophys Res Commun **120**(3): 885-890.

Gluck, J. M., B. W. Koenig, et al. (2011). "Nanodiscs allow the use of integral membrane proteins as analytes in surface plasmon resonance studies." Anal Biochem **408**(1): 46-52.

Gluck, J. M., M. Wittlich, et al. (2009). "Integral membrane proteins in nanodiscs can be studied by solution NMR spectroscopy." J Am Chem Soc **131**(34): 12060-12061.

Grinkova, Y. V., I. G. Denisov, et al. (2010). "Engineering extended membrane scaffold proteins for self-assembly of soluble nanoscale lipid bilayers." Protein Engineering Design & Selection **23**(11): 843-848.

Haass, C., M. G. Schlossmacher, et al. (1992). "Amyloid Beta-Peptide Is Produced by Cultured-Cells during Normal Metabolism." Nature **359**(6393): 322-325.

Hagn, F., M. Etzkorn, et al. (2013). "Optimized Phospholipid Bilayer Nanodiscs Facilitate High-Resolution Structure Determination of Membrane Proteins." J Am Chem Soc **135**(5): 1919-1925.

Hane, F., E. Drolle, et al. (2011). "Amyloid-beta Aggregation on Model Lipid Membranes: An Atomic Force Microscopy Study." Journal of Alzheimers Disease **26**(3): 485-494.

Hardy, J. and D. J. Selkoe (2002). "Medicine - The amyloid hypothesis of Alzheimer's disease: Progress and problems on the road to therapeutics." Science **297**(5580): 353-356.

Hardy, J. A. and G. A. Higgins (1992). "Alzheimers-Disease - the Amyloid Cascade Hypothesis." Science **256**(5054): 184-185.

Harper, J. D. and P. T. Lansbury (1997). "Models of amyloid seeding in Alzheimier's disease and scrapie: Mechanistic truths and physiological consequences of the time-dependent solubility of amyloid proteins." Annual Review of Biochemistry **66**: 385-407.

Harper, J. D., S. S. Wong, et al. (1997). "Observation of metastable A beta amyloid protofibrils by atomic force microscopy." Chemistry & Biology **4**(2): 119-125.

Hayashi, H., N. Kimura, et al. (2004). "A seed for Alzheimer amyloid in the brain." Journal of Neuroscience **24**(20): 4894-4902.

Helzner, E. P. (2009). "Survival in Alzheimer disease: A multiethnic, population-based study of incident cases (vol 71, pg 1489, 2008)." Neurology **72**(9): 861-861.

Hernandez-Rocamora, V. M., B. Reija, et al. (2012). "Dynamic Interaction of the Escherichia coli Cell Division ZipA and FtsZ Proteins Evidenced in Nanodiscs." Journal of Biological Chemistry **287**(36): 30097-30104.

Hilbich, C., B. Kisterswoike, et al. (1992). "Substitutions of Hydrophobic Amino-Acids Reduce the Amyloidogenicity of Alzheimers-Disease Beta-A4 Peptides." J Mol Biol **228**(2): 460-473.

Igbavboa, U., G. Y. Sun, et al. (2009). "Amyloid beta-protein stimulates trafficking of cholesterol and caveolin-1 from the plasma membrane to the Golgi complex in mouse primary astrocytes." Neuroscience **162**(2): 328-338.

Ikeda, K. and K. Matsuzaki (2008). "Driving force of binding of amyloid beta-protein to lipid bilayers." Biochem Biophys Res Commun **370**(3): 525-529.

Ikeda, K., T. Yamaguchi, et al. (2011). "Mechanism of amyloid beta-protein aggregation mediated by GM1 ganglioside clusters." Biochemistry **50**(29): 6433-6440.

Jahn, H. (2013). "Memory loss in Alzheimer's disease." Dialogues Clin Neurosci **15**(4): 445-454.

Jan, A., O. Adolfsson, et al. (2011). "Abeta42 neurotoxicity is mediated by ongoing nucleated polymerization process rather than by discrete Abeta42 species." Journal of Biological Chemistry **286**(10): 8585-8596.

Jang, H., J. Zheng, et al. (2008). "New structures help the modeling of toxic amyloidbeta ion channels." Trends Biochem Sci **33**(2): 91-100.

Jao, C. C., B. G. Hegde, et al. (2008). "Structure of membrane-bound alpha-synuclein from site-directed spin labeling and computational refinement." Proceedings of the National Academy of Sciences of the United States of America **105**(50): 19666-19671.

Jozsa, E., K. Osz, et al. (2010). "Nickel(II) and mixed metal complexes of amyloid-beta N-terminus." Dalton Transactions **39**(30): 7046-7053.

Kakio, A., S. Nishimoto, et al. (2002). "Interactions of amyloid beta-protein with various gangliosides in raft-like membranes: Importance of GM1 ganglioside-bound form as an endogenous seed for Alzheimer amyloid." Biochemistry **41**(23): 7385-7390.

Kakio, A., S. I. Nishimoto, et al. (2001). "Cholesterol-dependent formation of GM1 ganglioside-bound amyloid beta-protein, an endogenous seed for Alzheimer amyloid." Journal of Biological Chemistry **276**(27): 24985-24990.

Kakio, A., Y. Yano, et al. (2004). "Interaction between amyloid beta-protein aggregates and membranes." J Pept Sci **10**(10): 612-621.

Kang, J., H. G. Lemaire, et al. (1987). "The Precursor of Alzheimers-Disease Amyloid-A4 Protein Resembles a Cell-Surface Receptor." Nature **325**(6106): 733-736.

Kapust, R. B., J. Tozser, et al. (2001). "Tobacco etch virus protease: mechanism of autolysis and rational design of stable mutants with wild-type catalytic proficiency." Protein Engineering **14**(12): 993-1000.

Katz, M. J., R. B. Lipton, et al. (2012). "Age-specific and Sex-specific Prevalence and Incidence of Mild Cognitive Impairment, Dementia, and Alzheimer Dementia in Blacks and Whites A Report From the Einstein Aging Study." Alzheimer Disease & Associated Disorders **26**(4): 335-343.

King, M. E., H. M. Kan, et al. (2006). "Tau-dependent microtubule disassembly initiated by prefibrillar beta-amyloid." J Cell Biol **175**(4): 541-546.

Kirschner, D. A., H. Inouye, et al. (1987). "Synthetic Peptide Homologous to Beta-Protein from Alzheimer-Disease Forms Amyloid-Like Fibrils Invitro." Proceedings of the National Academy of Sciences of the United States of America **84**(19): 6953-6957.

Klein, W. L. (2002). "Abeta toxicity in Alzheimer's disease: globular oligomers (ADDLs) as new vaccine and drug targets." Neurochemistry International **41**(5): 345-352.

Klein, W. L. (2002). "A beta toxicity in Alzheimer's disease: globular oligomers (ADDLs) as new vaccine and drug targets." Neurochemistry International **41**(5): 345-352.

Knowles, R. B., C. Wyart, et al. (1999). "Plaque-induced neurite abnormalities: implications for disruption of neural networks in Alzheimer's disease." Proc Natl Acad Sci U S A **96**(9): 5274-5279.

Kotler, S. A., P. Walsh, et al. (2014). "Differences between amyloid-beta aggregation in solution and on the membrane: insights into elucidation of the mechanistic details of Alzheimer's disease." Chem Soc Rev **43**(19): 6692-6700.

Kremer, J. J., D. J. Sklansky, et al. (2001). "Profile of changes in lipid bilayer structure caused by beta-amyloid peptide." Biochemistry **40**(29): 8563-8571.

Kril, J. J., J. Hodges, et al. (2004). "Relationship between hippocampal volume and CA1 neuron loss in brains of humans with and without Alzheimer's disease." Neuroscience Letters **361**(1-3): 9-12.

Kumar, S. and J. Walter (2011). "Phosphorylation of amyloid beta (A beta) peptides - A trigger for formation of toxic aggregates in Alzheimer's disease." Aging-Us **3**(8): 803-812.

Kummer, M. P. and M. T. Heneka (2014). "Truncated and modified amyloid-beta species." Alzheimers Research & Therapy **6**(3): 28.

Laemmli, U. K. (1970). "Cleavage of Structural Proteins during Assembly of Head of Bacteriophage-T4." Nature **227**(5259): 680-&.

Lau, T. L., E. E. Ambroggio, et al. (2006). "Amyloid-beta peptide disruption of lipid membranes and the effect of metal ions." J Mol Biol **356**(3): 759-770.

Leissring, M. A., A. Lu, et al. (2003). "Kinetics of amyloid beta-protein degradation determined by novel fluorescence- and fluorescence polarization-based assays." Journal of Biological Chemistry **278**(39): 37314-37320.

Leney, A. C., X. X. Fan, et al. (2014). "Nanodiscs and Electrospray Ionization Mass Spectrometry: A Tool for Screening Glycolipids Against Proteins." Anal Chem **86**(11): 5271-5277.

Lin, H., R. Bhatia, et al. (2001). "Amyloid beta protein forms ion channels: implications for Alzheimer's disease pathophysiology." Faseb Journal **15**(13): 2433-2444.

Lin, H. and Y. W. J. Zhu (1999). "Amyloid beta protein (1-40) (A beta P) reconstituted in lipid vesicles forms calcium-permeable channels." Biophysical Journal **76**(1): A146-A146.

Lin, H., Y. W. J. Zhu, et al. (1999). "Amyloid beta protein (1-40) forms calcium-permeable, Zn2+-sensitive channel in reconstituted lipid vesicles." Biochemistry **38**(34): 11189-11196.

Lozano, M. M., Z. Liu, et al. (2013). "Colocalization of the Ganglioside G(M1) and Cholesterol Detected by Secondary Ion Mass Spectrometry." J Am Chem Soc **135**(15): 5620-5630.

Ma, P. X., J. Mohrluder, et al. (2010). "Preparation of a Functional GABARAP-Lipid Conjugate in Nanodiscs and its Investigation by Solution NMR Spectroscopy." Chembiochem **11**(14): 1967-1970.

Masters, C. L., G. Simms, et al. (1985). "Amyloid Plaque Core Protein in Alzheimer-Disease and down Syndrome." Proceedings of the National Academy of Sciences of the United States of America **82**(12): 4245-4249.

Matsubara, T., K. Iijima, et al. (2013). "Density of GM1 in nanoclusters is a critical factor in the formation of a spherical assembly of amyloid beta-protein on synaptic plasma membranes." Langmuir **29**(7): 2258-2264.

McLaurin, J. and A. Chakrabartty (1997). "Characterization of the interactions of Alzheimer beta-amyloid peptides with phospholipid membranes." European Journal of Biochemistry **245**(2): 355-363.

McLaurin, J., T. Franklin, et al. (1997). "Characterization of the interactions of Alzheimer beta-amyloid peptides with gangliosides." Society for Neuroscience Abstracts **23**(1-2): 535-535.

McLaurin, J., T. Franklin, et al. (1998). "Structural transitions associated with the interaction of Alzheimer beta-amyloid peptides with gangliosides." Journal of Biological Chemistry **273**(8): 4506-4515.

McLean, C. A., R. A. Cherny, et al. (1999). "Soluble pool of Abeta amyloid as a determinant of severity of neurodegeneration in Alzheimer's disease." Ann Neurol **46**(6): 860-866.

Michel, V. and M. Bakovic (2007). "Lipid rafts in health and disease." Biology of the Cell **99**(3): 129-140.

Mori, K., M. I. Mahmood, et al. (2012). "Formation of GM1 Ganglioside Clusters on the Lipid Membrane Containing Sphingomyeline and Cholesterol." Journal of Physical Chemistry B **116**(17): 5111-5121.

Nath, A., W. M. Atkins, et al. (2007). "Applications of phospholipid bilayer nanodiscs in the study of membranes and membrane proteins." Biochemistry **46**(8): 2059-2069.

Nussbaum, J. M., S. Schilling, et al. (2012). "Prion-like behaviour and tau-dependent cytotoxicity of pyroglutamylated amyloid-beta." Nature **485**(7400): 651-655.

Ogawa, M., M. Tsukuda, et al. (2011). "Ganglioside-mediated aggregation of amyloid beta-proteins (Abeta): comparison between Abeta-(1-42) and Abeta-(1-40)." J Neurochem **116**(5): 851-857.

Ohashi, R., H. Mu, et al. (2005). "Reverse cholesterol transport and cholesterol efflux in atherosclerosis." Qjm-an International Journal of Medicine **98**(12): 845-856.

Ono, K., M. M. Condron, et al. (2009). "Structure-neurotoxicity relationships of amyloid beta-protein oligomers." Proceedings of the National Academy of Sciences of the United States of America **106**(35): 14745-14750.

Pavlidou, M., K. Hanel, et al. (2013). "Nanodiscs Allow Phage Display Selection for Ligands to Non-Linear Epitopes on Membrane Proteins." Plos One **8**(9).

Perl, D. P. (2010). "Neuropathology of Alzheimer's disease." Mt Sinai J Med **77**(1): 32-42.

Pervushin, K., R. Riek, et al. (1997). "Attenuated T2 relaxation by mutual cancellation of dipole-dipole coupling and chemical shift anisotropy indicates an avenue to NMR structures of very large biological macromolecules in solution." Proc Natl Acad Sci U S A **94**(23): 12366-12371.

Petkova, A. T., R. D. Leapman, et al. (2005). "Self-propagating, molecular-level polymorphism in Alzheimer's beta-amyloid fibrils." Science **307**(5707): 262-265.

Porath, J., J. Carlsson, et al. (1975). "Metal Chelate Affinity Chromatography, a New Approach to Protein Fractionation." Nature **258**(5536): 598-599.

Portelius, E., N. Bogdanovic, et al. (2010). "Mass spectrometric characterization of brain amyloid beta isoform signatures in familial and sporadic Alzheimer's disease." Acta Neuropathologica **120**(2): 185-193.

Price, J. L. and J. C. Morris (1999). "Tangles and plaques in nondemented aging and "preclinical" Alzheimer's disease." Annals of Neurology **45**(3): 358-368.

Prince, M., R. Bryce, et al. (2013). "The global prevalence of dementia: A systematic review and metaanalysis." Alzheimers & Dementia **9**(1): 63-75.

Prosser, R. S., F. Evanics, et al. (2006). "Current applications of bicelles in NMR studies of membrane-associated amphiphiles and proteins." Biochemistry **45**(28): 8453-8465.

Purcell, E. M., H. C. Torrey, et al. (1946). "Resonance Absorption by Nuclear Magnetic Moments in a Solid." Physical Review **69**(1-2): 37-38.

Quist, A., L. Doudevski, et al. (2005). "Amyloid ion channels: A common structural link for protein-misfolding disease." Proceedings of the National Academy of Sciences of the United States of America **102**(30): 10427-10432.

Raschle, T., S. Hiller, et al. (2010). "Nonmicellar systems for solution NMR spectroscopy of membrane proteins." Current Opinion in Structural Biology **20**(4): 471-479.

Rhee, S. K., A. P. Quist, et al. (1998). "Amyloid beta protein-(1-42) forms calcium-permeable, Zn2+-sensitive channel." Journal of Biological Chemistry **273**(22): 13379-13382.

Ritchie, T. K., Y. V. Grinkova, et al. (2009). "Chapter 11 - Reconstitution of membrane proteins in phospholipid bilayer nanodiscs." Methods Enzymol **464**: 211-231.

Ross, C. A. and M. A. Poirier (2005). "What is the role of protein aggregation in neurodegeneration?" Nature Reviews Molecular Cell Biology **6**(11): 891-898.

Rountree, S. D., W. Chan, et al. (2012). "Factors that influence survival in a probable Alzheimer disease cohort." Alzheimers Research & Therapy **4**(3).

Rubenstein, J. R., B. A. Smith, et al. (1979). "Lateral Diffusion in Binary-Mixtures of Cholesterol and Phosphatidylcholines." Proceedings of the National Academy of Sciences of the United States of America **76**(1): 15-18.

Sarti, P., G. Antonini, et al. (1990). "Effect of gangliosides on membrane permeability studied by enzymic and fluorescence-spectroscopy techniques." Biochemical Journal **267**(2): 413-416.
Schagger, H. (2006). "Tricine-SDS-PAGE." Nat Protoc **1**(1): 16-22.
Schlenzig, D., S. Manhart, et al. (2009). "Pyroglutamate Formation Influences Solubility and Amyloidogenicity of Amyloid Peptides." Biochemistry **48**(29): 7072-7078.
Sciacca, M. F., S. A. Kotler, et al. (2012). "Two-step mechanism of membrane disruption by Abeta through membrane fragmentation and pore formation." Biophysical Journal **103**(4): 702-710.
Selkoe, D. J. (1998). "The cell biology of beta-amyloid precursor protein and presenilin in Alzheimer's disease." Trends in Cell Biology **8**(11): 447-453.
Serrano-Pozo, A., M. P. Frosch, et al. (2011). "Neuropathological alterations in Alzheimer disease." Cold Spring Harb Perspect Med **1**(1): a006189.
Shankar, G. M., S. M. Li, et al. (2008). "Amyloid-beta protein dimers isolated directly from Alzheimer's brains impair synaptic plasticity and memory." Nat Med **14**(8): 837-842.
Shao, H. Y., S. C. Jao, et al. (1999). "Solution structures of micelle-bound amyloid beta-(1-40) and beta-(1-42) peptides of Alzheimer's disease." J Mol Biol **285**(2): 755-773.
Shaw, A. W., M. A. McLean, et al. (2004). "Phospholipid phase transitions in homogeneous nanometer scale bilayer discs." FEBS Lett **556**(1-3): 260-264.
Shoji, M., E. Matsubara, et al. (1998). "Combination assay of CSF Tau, A beta 1-40 and A beta 1-42(43) as a biochemical marker of Alzheimer's disease." J Neurol Sci **158**(2): 134-140.
Simons, K. and E. Ikonen (1997). "Functional rafts in cell membranes." Nature **387**(6633): 569-572.
Singer, S. J. and G. L. Nicolson (1972). "The fluid mosaic model of the structure of cell membranes." Science **175**(4023): 720-731.
Sonnino, S., L. Mauri, et al. (2007). "Gangliosides as components of lipid membrane domains." Glycobiology **17**(1): 1R-13R.
Soscia, S. J., J. E. Kirby, et al. (2010). "The Alzheimer's Disease-Associated Amyloid beta-Protein Is an Antimicrobial Peptide." Plos One **5**(3).
Stine, W. B., K. N. Dahlgren, et al. (2003). "In vitro characterization of conditions for amyloid-beta peptide oligomerization and fibrillogenesis." Journal of Biological Chemistry **278**(13): 11612-11622.
Stoothoff, W. H. and G. V. Johnson (2005). "Tau phosphorylation: physiological and pathological consequences." Biochim Biophys Acta **1739**(2-3): 280-297.
Strodel, B., J. W. L. Lee, et al. (2010). "Transmembrane Structures for Alzheimer's A beta(1-42) Oligomers." J Am Chem Soc **132**(38): 13300-13312.
Takami, M., Y. Nagashima, et al. (2009). "gamma-Secretase: Successive Tripeptide and Tetrapeptide Release from the Transmembrane Domain of beta-Carboxyl Terminal Fragment." Journal of Neuroscience **29**(41): 13042-13052.
Tamai, Y., Matsukaw.S, et al. (1971). "Lipid Composition of Nerve Cell Perikarya." Brain Res **26**(1): 149-&.
Terry, R. D., N. K. Gonatas, et al. (1964). "Ultrastructural Studies in Alzheimer's Presenile Dementia." Am J Pathol **44**: 269-297.
Terzi, E., G. Holzemann, et al. (1995). "Self-Association of Beta-Amyloid Peptide(1-40) in Solution and Binding to Lipid-Membranes." J Mol Biol **252**(5): 633-642.
Terzi, E., G. Holzemann, et al. (1997). "Interaction of Alzheimer beta-amyloid peptide(1-40) with lipid membranes." Biochemistry **36**(48): 14845-14852.
Timothy H. Bayburt, S. G. S. (2009). "Membrane protein assembly into Nanodiscs." FEBSLetters **584**(2010): 6.
Trexler, A. J. and E. Rhoades (2009). "alpha-Synuclein Binds Large Unilamellar Vesicles as an Extended Helix." Biochemistry **48**(11): 2304-2306.
Tsukamoto, H., A. Sinha, et al. (2010). "Monomeric Rhodopsin Is the Minimal Functional Unit Required for Arrestin Binding." J Mol Biol **399**(3): 501-511.
Ulmer, T. S., A. Bax, et al. (2005). "Structure and dynamics of micelle-bound human alpha-synuclein." Journal of Biological Chemistry **280**(10): 9595-9603.

Utsumi, M., Y. Yamaguchi, et al. (2009). "Up-and-down topological mode of amyloid beta-peptide lying on hydrophilic/hydrophobic interface of ganglioside clusters." Glycoconj J **26**(8): 999-1006.

Valdes-Gonzalez, T., J. Inagawa, et al. (2001). "Neuropeptides interact with glycolipid receptors - A surface plasmon resonance study." Peptides **22**(7): 1099-1106.

Vranken, W. F., W. Boucher, et al. (2005). "The CCPN data model for NMR spectroscopy: Development of a software pipeline." Proteins-Structure Function and Bioinformatics **59**(4): 687-696.

Vyas, K. A., H. V. Patel, et al. (2001). "Segregation of gangliosides GM1 and GD3 on cell membranes, isolated membrane rafts, and defined supported lipid monolayers." Biol Chem **382**(2): 241-250.

Walsh, D. M., D. M. Hartley, et al. (1999). "Amyloid beta-protein fibrillogenesis - Structure and biological activity of protofibrillar intermediates." Journal of Biological Chemistry **274**(36): 25945-25952.

Walsh, D. M., I. Klyubin, et al. (2002). "Naturally secreted oligomers of amyloid beta protein potently inhibit hippocampal long-term potentiation in vivo." Nature **416**(6880): 535-539.

Walsh, D. M., B. P. Tseng, et al. (2000). "The oligomerization of amyloid beta-protein begins intracellularly in cells derived from human brain." Biochemistry **39**(35): 10831-10839.

Weingarten, M. D., A. H. Lockwood, et al. (1975). "A protein factor essential for microtubule assembly." Proc Natl Acad Sci U S A **72**(5): 1858-1862.

Williams, T. L., I. J. Day, et al. (2010). "The Effect of Alzheimer's A beta Aggregation State on the Permeation of Biomimetic Lipid Vesicles." Langmuir **26**(22): 17260-17268.

Williamson, M. P., Y. Suzuki, et al. (2006). "Binding of amyloid beta-peptide to ganglioside micelles is dependent on histidine-13." Biochemical Journal **397**(3): 483-490.

Wong, P. T., J. A. Schauerte, et al. (2009). "Amyloid-beta Membrane Binding and Permeabilization are Distinct Processes Influenced Separately by Membrane Charge and Fluidity." J Mol Biol **386**(1): 81-96.

Yagi-Utsumi, M., K. Matsuo, et al. (2010). "Spectroscopic Characterization of Intermolecular Interaction of Amyloid beta Promoted on GM1 Micelles." Int J Alzheimers Dis **2011**: 925073.

Yamaguchi, T., T. Uno, et al. (2013). "Ganglioside-embedding small bicelles for probing membrane-landing processes of intrinsically disordered proteins." Chem Commun (Camb) **49**(12): 1235-1237.

Yanagisawa, K. (2015). "GM1 ganglioside and Alzheimer's disease." Glycoconj J **32**(3-4): 87-91.

Yanagisawa, K., A. Odaka, et al. (1995). "GM1 ganglioside-bound amyloid beta-protein (A beta): a possible form of preamyloid in Alzheimer's disease." Nat Med **1**(10): 1062-1066.

Zhu, Y. J., H. Lin, et al. (2000). "Fresh and nonfibrillar amyloid beta protein(1-40) induces rapid cellular degeneration in aged human fibroblasts: evidence for A beta P-channel-mediated cellular toxicity." Faseb Journal **14**(9): 1244-1254.

8. Appendix

8.1 List of Abbreviations

$A_{280\ nm}$	Absorbance at 280 nm
AD	Alzheimer´s Disease
APP	Amyloid precursor protein
APS	Ammonium persulfate
BLI	BioLayer interferometry
BSA	Bovine serum albumin
CBB	Coomassie Briliant Blue
Chol	Cholesterol
cmc	Critical micelle concentration
CV	Column volume
DAC	7-dimethyl-aminocoumarin-3yl-carboxylic acid
DACIA	N-(7-dimethylamino-4-methylcoumarin-3-yl)iodoacetamide
DGC	Density gradient centrifugation
DLS	Dynamic light scattering
DMPC	1,2-dimyristoyl-sn-glycero-3-phosphocholine
DMSO	Dimethylsulfoxid
DOPS	1,2-dioleoyl-*sn*-glycero-3-phospho-L-serine
DTT	Dithiothreitol
E. coli	*Escherichia coli*
EDTA	Ethylenediaminetetraacetic acid
ESR	Electron spin resonance
FAD	Familiar Alzheimer´s disease
FT	Fluorescence Titration
g	Gravitational rotation
GM1	Ganglioside GM1
GSH	Gluthatione
h	hour
HDL	High density lipoprotein
His-tag	Oligohistidine tag
HRP	Horse radish peroxidase
IMAC	Imobilzed metal affinity chromatography
IPTG	Isopropyl β-D-1-thiogalactopyranoside
K_D	Overall apparent equilibration dissociation constant
kDA	Kilo dalton
LB	Lysogeny broth
LTP	Long term potentiation
LUV	Large unilamellar vesicle
mAU	Milli absorbance units
min	minutes
MSP	Membrane scaffold protein
MW	Molecular weight
MWCO	Molecular weight cut off
NFT	Neuro fibrillary tangles
nm	Nano meter
NMR	Nuclear magnetic resonance
NTA	Nitrilotriacetic acid
OD	Optical density
PAGE	Polyacrylamide gel electrophoresis
POI	Protein of interest
POPC	1-palmitoyl-2-oleoyl-sn-glycero-3-phosphocholine
POPG	1-palmitoyl-2-oleoyl-sn-glycero-3-phospho-(1'-rac-glycerol)
RP-HPLC	Reversed phase high performance liquid chromatography
RT	Room temperature
SDS	Sodium dodecyl sulfate
s	second
SEC	Size exclusion chromatography
SM	sphingomyelin
SN	supernatant
SPR	Surface plasmon resonance
SUV	Small unilamellar vesicle
TBS	Tris-buffered saline
TEMED	Tetramethylethylenediamine
TEV	Tobacco etch virus
Tris	Tris(hydroxymethyl)aminomethane
UC	Ultracentrifugation
UV	Ultraviolet
v/v	Volume per volume
w/v	Weight per volume
w/w	Weight per weight

8.2 Publication and Poster Presentation

M. Thomaier, J. Fabig, L. Gremer and D. Willbold-High affinity binding of monomeric, but not oligomeric amyloid-ß to ganglioside GM1 containing nanodisc-submitted

M. Thomaier, J. Fabig, L. Gremer and D. Willbold-Nanodiscs as a suitable tool for amyloid beta membrane interaction

1st Jülich-Düsseldorf symposium for neurodegenerative diseases-October 2015, Düsseldorf

8.3 Acknowledgement

I would firstly like to thank Prof. Dr. Dieter Willbold for giving me the opportunity to work in his group and complete this interesting project around Alzheimer's disease. It's been a great learning experience for me, and for this I am truly grateful.

I want to thank Prof. Dr. Karl-Erich Jäger for being my mentor and second examiner as well as for reviewing my dissertation.

I want to thank the graduate school iGRASPseed for funding and the iGRASPseed team for their support.

I would like to thank my supervisor Dr. Lothar Gremer for his constant guidance and support.

Furthermore, I would like to thank all the members of the ICS-6, ICS-5 and Physikalische Biologie for professional and personal support as well as a friendly work environment. I furthermore would like to thank the service team.

Especially, I would like to thank my office colleagues Kateryna, Christina and Volker for their suggestions, chats and help concerning all sorts of things.

I want to thank very much all my friends and family for their support. A special thanks goes to Stephan for his everlasting patience and support.

8.4 Eidesstattliche Erklärung

Hiermit erkläre ich an Eides statt, dass ich die vorliegende Promotionsarbeit selbständig angefertigt habe. Es wurden nur die in der Arbeit ausdrücklich benannten Quellen und Hilfsmittel benutzt. Wörtlich oder sinngemäß übernommenes Gedankengut habe ich als solches kenntlich gemacht. Diese Arbeit hat in gleicher oder ähnlicher Form noch keiner Prüfungsbehörde vorgelegen.

Jülich, Januar 2016

Maren Thomaier